Nonlinear Beam Physics

Folsom, Benjamin

2019

Document Version:
Other version

Nonlinear Beam Physics

by Benjamin Tyler Folsom

LUND
UNIVERSITY

Thesis for the degree of Doctorate of Philosophy
Thesis advisors: Dr. Emanuele Laface, Prof. Mats Lindroos,
Prof. Torsten Åkeson
Faculty opponent: Prof. Stephen Peggs

Supplemental Illustrations by Dirk Nordt

Organization
LUND UNIVERSITY

Department of Physics
Particle Physics Division
Box 118
SE–221 00 Lund, Sweden

Author(s)
Benjamin Tyler Folsom

Document name
DOCTORAL DISSERTATION

Sponsoring organization
European Spallation Source, ERIC
Box 176
SE-221 00 Lund, Sweden

Title and subtitle
Nonlinear Beam Physics

Abstract
A condensed treatment of conventional beam physics (both linear and nonlinear) is given for the non-expert; this constitutes a minimum knowhow for constructing simulations of rudimentary beamlines. The criteria for an ideal nonlinear charged-particle simulation algorithm are then presented, leading to the derivation of a symplectic, explicit, Lorentz-covariant integrator.

Space charge (inter-particle interaction) is addressed next, with a first-principles approach based on the Liénard—Weichert potentials. A cumulative chapter follows, applying the developed simulation methods to multipole magnets (sextupoles, octupoles, and higher-order) which have inherently nonlinear potentials.

A concluding chapter proposes applications for nonlinear simulation of neutron particle dynamics in terms of magnetic dipole moment steering.

Classification system and/or index terms (if any)

Supplementary bibliographical information

Language
English

ISBN
978-91-7895-012-6 (print)
978-91-7895-013-3 (pdf)

Recipient's notes

Number of pages
128

Price

Security classification

Signature _____ Date _____

Contents

Popular Summary

A review of elementary accelerator physics is given, including both the commonly taught linear formalism and the more complicated nonlinear methods. With this basis, a theoretical groundwork is developed for simulating the dynamics of accelerated particles with fewest possible approximations. This entails incorporating a relativistic extension of the static Coulomb potential into an algorithm which must remain accurate for extended periods (as in a storage ring) or under extreme conditions (to better understand beam losses). Applications of such an approach are addressed in the final chapters: with particular attention given to types electromagnets consisting of more than four poles, and the steering of neutrons by their magnetic dipole moment; both of which are well-suited to such a nonlinear framework.

Populärvetenskaplig sammanfattning

Detta arbete börjar med en översikt över grundläggande acceleratorfysik, vilket inkluderar både den sedvanliga linjära formalismen och mer avancerade icke-linjära metoder. Med dessa som grund utvecklas ett teoretiskt ramverk för att simulera dynamiken hos accelererade partiklar med så få approximationer som möjligt. Detta inkluderar en relativistisk utvidgning av den statiska Coulombpotentialen till en algoritm som förblir noggrann för långa tidsintervall (som i en lagringsring) eller under extrema förhållanden (för att bättre förstå strålförluster). I de avslutande kaptitlen anges tillämpningar av denna metod. Speciellt betraktas fallen med magnetfält som har mer än fyra poler och avlänkning av neutrala partiklar genom växelverkan med deras dipolmoment, vilka båda lämpar sig väl för beskrivning inom detta ramverk.

Preface

This thesis is primarily concerned with the improvement of particle accelerators, with simulation as the *de facto* proving ground for new technologies. It will forgo a thorough theoretical introduction, instead proceeding from electrodynamics first principles where possible, and referring to conventional accelerator physics theory as succinctly as possible. The intent of this approach is accessibility and reproducibility for the non-specialist, with the target audience being any physicist or physics student who has taken graduate-level electrodynamics coursework.† That said, the foundational Courant–Snyder[1] (optical) formalism and the complementary Lie-operator formalism (Heisenberg-picture or Dyson-series-like)[2] will be used for benchmarking throughout. While many texts are available on the former, the latter theory primarily stems from the works of Dragt–Finn,[3] and Forest.[4] Wolski's book[5] is also an excellent reference which unifies these subjects. The brief introductory chapter covers these concepts for non-expert readers.‡

This is followed by a short chapter which introduces first-principles simulation of charged-particles using a Lorentz-covariant integrator. We do so as an attempt at best-possible accuracy, with covariant Hamiltonian dynamics as a basis.[6]

†In this same spirit, running condensed citations are provided as footnotes, with an alphabetized bibliography at the end of each chapter. Consecutive citations of a single source will omit its title, while retaining page numbers where applicable.

[1]Courant, Livingston, and Snyder, "The strong-focusing synchroton—A new high energy accelerator".

[2]Dragt, *Lie Methods for Nonlinear Dynamics with Applications to Accelerator Physics*, p929.

[3]Dragt and Finn, "Lie series and invariant functions for analytic symplectic maps".

[4]Forest and Ruth, "Fourth-order symplectic integration"; Forest, *Beam dynamics: A New Attitude and Framework*.

[5]Wolski, *Beam dynamics: In High Energy Particle Accelerators*.

‡The remaining chapters are original work from the author.

[6]Wang, Liu, and Qin, "Lorentz covariant canonical symplectic algorithms for dynamics of charged particles".

Specifically, a derivation is shown for an explicit integrator (which requires no stepwise numerical solver) that is symplectic (having long-term stability) and covariant (frame-independent, energy conserving). This will constitute the core tracking algorithm to be implemented throughout the remainder of the text.

The next chapter addresses inter-particle interaction (space charge) and velocity/acceleration dependent emission using the Liénard–Wiechert potentials. Since such effects are inherently nonlinear and require pairwise summing of all constituents, they are extremely demanding in terms of calculation time, and generally simulated with coarse approximations. In light of this, the chapter concludes with a proposed technique for compromising accuracy with scalable precision. This involves adaptating the conventional particle-in-cell (PIC) method from the usual rectilinear mesh to a coordinate system based on a 3D-projected Archimedian spiral.

The following chapter deals with beam dynamics through multipole magnets as a primary test case (particle bunches passing through external potentials with no explicit time-dependence). While the intent throughout is a first-principles approach, performance considerations are taken into account. With, for example, the explicit integrator offering significant performance gains over the conventional nonlinear (Lie) method.

The brief final chapter then discusses neutral-particle dynamics, particularly in terms of beam focusing and steering via magnetic dipole moment.[7]

A selection of detailed derivations and discussions of more tangential topics are then given as a set of appendices.

[7] McChesney, "Neutron accelerator physics".

References

Courant, E. D., M. S. Livingston, and H. S. Snyder. "The strong-focusing synchroton—a new high energy accelerator". In: *Physical Review* 88.5 (1952), p. 1190.

Dragt, A. J. *Lie Methods for Nonlinear Dynamics with Applications to Accelerator Physics*. College Park, MD, USA: University of Maryland, Forthcoming, 2019. URL: https://www.physics.umd.edu/dsat/dsatliemethods.html.

Dragt, A. J. and J. M. Finn. "Lie series and invariant functions for analytic symplectic maps". In: *Journal of Mathematical Physics* 17.12 (1976), pp. 2215–2227. DOI: 10.1063/1.522868.

Forest, E and R. D. Ruth. "Fourth-order symplectic integration". In: *Physica D* 43.LBL-27662 (1989), p. 105. URL: http://cds.cern.ch/record/201901.

Forest, E. *Beam dynamics: A New Attitude and Framework*. Phys. Technol. Part. Phot. Beams. Sidney: Harwood, 1998. URL: http://cds.cern.ch/record/367626.

McChesney, P. "Neutron accelerator physics". English. PhD thesis. Indiana University, 2015, p. 203.

Wang, Y., J. Liu, and H. Qin. "Lorentz covariant canonical symplectic algorithms for dynamics of charged particles". In: *Physics of Plasmas* 23.12 (Dec. 2016). arXiv: 1609.07019, p. 122513. DOI: 10.1063/1.4972824.

Wolski, A. *Beam dynamics: In High Energy Particle Accelerators*. London, UK: Imperial College Press, 2014. URL: http://cds.cern.ch/record/1622200.

Chapter 1

Conventional Beam Physics

A brief, informal glossary of essential terms may be helpful for the non-specialist:

"Beam" is conventionally used for either a sequence of charged particles that are divided into discrete "bunches" longitudinally (along the direction of propagation) with a length comparable to their mean transverse spread; or it can refer to an unbunched stream of particles in what are referred to as continuous-wave or DC accelerators, where the latter has no RF modulation. This work is exclusively concerned with bunched beams. (Continuous beams can, in fact, be treated with relatively simplistic longitudinal dynamics thanks to the longitudinal symmetry of an infinitely long beam.)[1]

"Phase space" refers to the position and momentum components of a particle or several particles' trajectories treated as interdependent quantities. These are often plotted for a single spatial direction of motion with momentum as the vertical and position as the horizontal axis; which amounts to 2D phase space. Care must be taken to distinguish whether a single particle's phase-space evolution is being plotted over several cycles through a periodic structure (as in a storage ring), or whether a multiparticle distribution is being plotted (i.e. a bunch or a cross-section of its components).

"Emittance" (ϵ) is an inherently conserved quantity of any Hamiltonian system, which consequently defines its area in phase space ($A = \pi\epsilon$). A single particle in a periodic beam line (i.e. a circular accelerator) traces a path along an ellipse in phase space encompassing this area. From the resulting ellipse equation, one can derive the "Twiss" or "Courant–Snyder" parameters, which are often

[1] Wolski, *Beam dynamics: In High Energy Particle Accelerators*, p403 ff.

convenient for characterizing a beam throughout an accelerator, and can be tracked independently of phase-space coordinates. The most prominent of these parameters is the "beta function" (β_t), which describes the amplitude of a particle's oscillation around the central (longitudinal) axis of the accelerator.

The derivation of ϵ and the Twiss parameters in terms of *single-particle* dynamics is fairly involved and will be presented later in this chapter. For a simple qualitative picture, a *distribution's* emittance can be defined as the root-mean-square (rms) deviation of position–momentum coupling:[2]

$$\epsilon_{RMS} = \sqrt{\langle (xp_x)^2 \rangle - \langle xp_x \rangle^2}. \tag{1.1}$$

In terms of distributions, the Twiss parameters allow for beam tracking solely by their root-mean-squared (rms) deviation values (σ's), provided all forces acting on (and within) the beam are treated as linear.

"Space charge" refers to the inter-particle charge-dependent forces (which are derived from a relativistic extension of the Coulomb potential). This topic will be addressed extensively in Chapter 3.

In terms of hardware, "beam line" or "lattice" refers to the longitudinal sequence of "machine elements" and "beam instrumentation" used for, respectively, manipulating and monitoring the beam. Vacuum piping connects machine elements and instrumentation which are not flanged directly. When discussing machines in their entirety, the two main categories are linear accelerators ("linacs") in which bunches pass each machine element only once; and circular accelerators ("rings"), where bunches can be accelerated though several million periods before reaching nominal energy. These can be interdependent: circular accelerators use relatively small "injector" linacs, while the proposed International Linear Collider integrates "damping" rings.

"Dipole" typically refers to a fixture of two electromagnets with opposing poles aligned transversely to the beamline, which has the effect of displacing any charged particle along a chosen transverse axis. A short series of dipole magnets specifically designed for extracting particles from one beamline to another (i.e. from a linear proton accelerator to a storage ring) is referred to as a "kicker". Dipoles typically consist of iron yokes wound with normal-conducting or superconducting wire (although single-element magnets which have dipole-equivalent fields are a topic of active research).[3] Dipoles are most commonly used to bend

[2] Wolski, p151.

[3] Caspi et al., "Design, Fabrication, and Test of a Superconducting Dipole Magnet Based on Tilted Solenoids"; Caspi et al., "Canted cosine theta magnet CCT);A concept for high field accelerator magnets"; Godeke et al., "Bi-2212 Canted-Cosine-Theta Coils for High-Field

beams in circular accelerators. A "steerer" refers to a short dipole to correct a beam's trajectory.

"Quadrupole" refers to a similar type of magnet, but with four evenly spaced poles alternating N–S. These are used primarily to squeeze or "focus" the beam along a single transverse axis. By nature of the field distribution, this simultaneously stretches or "defocuses" the beam along the other transverse axis. However, pairs of quadrupoles with opposite alignments can be shown, using elementary optics, to have an overall focusing effect. This is the acting principle for a technique referred to "strong focusing"; which has been leveraged heavily for several decades for the confinement of highly energetic beams. (Its predecessor, "weak focusing" is an effect related to the curved trajectory of charged particles through a uniform dipole field.)[4] Such a sequence along the beamline of focusing–vacuum–defocusing–vacuum is known as a "FODO" cell, with vacuum sections often referred to as "drifts".

This family of electromagnets can be referred to as "multipoles". The next two higher-order multipole magnets, "sextupoles" and "octupoles", are similar in design to lower-order multipoles; these typically have more specialized uses, but their characteristic nonlinear behavior will be studied in depth in the later chapters of this work. In general, dynamics in transverse regime falls under the heading "confinement" (with longitudinal dynamics as the "acceleration" regime).

Figure 1.1 is a schematic of the relevant fields and displacement effects of quadrupole magnets, along with dipoles and sextupoles. Note how a "normal" quadrupole alignment acts along the defined transverse axes, while a "skew" alignment acts along the diagonals.

For all types of multipoles, the sign and amplitude of the "field gradient" is determined by the current, number of coils, and distance between pole-tips. There is no standard for field-gradient definitions, as they require rescaling unless using a covariant Hamiltonian formalism. Thus, care is needed when defining field gradients, as tracking codes and textbooks often use incompatible rescaling factors.

The most fundamental longitudinal technology are "cavities"; these are hollow metallic structures which, in the typical case, have a dumbbell-like appearance

Accelerator Magnets"; Wan et al., "Alternating-Gradient Canted Cosine Theta Superconducting Magnets for Future Compact Proton Gantries".

[4] Veksler, "A new method of relativistic particle acceleration"; Sokolov and Ternov, "Synchrotron radiation"; Burshtein et al., "Application of the principle of automatic correction of the magnetic field in cyclic superhigh-energy accelerators".

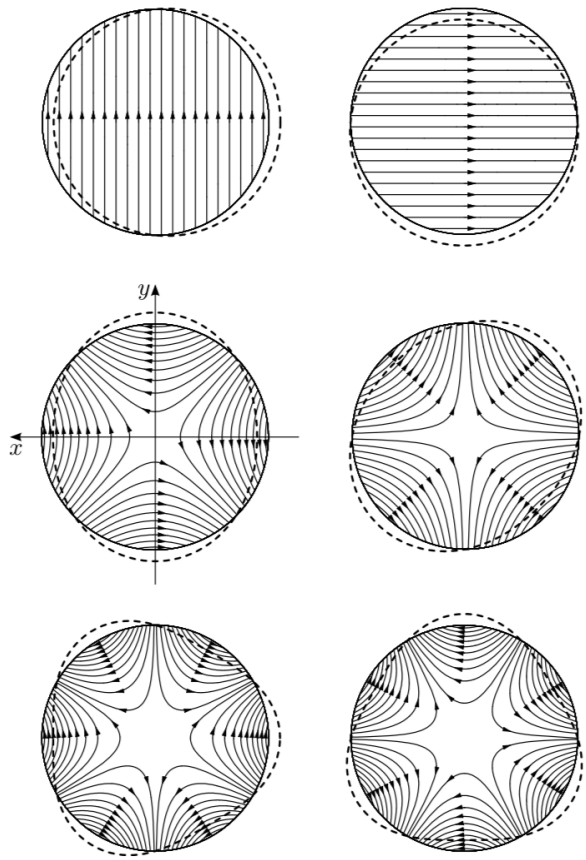

Figure 1.1: Fields of a dipole (top), quadrupole (middle), and sextupole magnet (bottom) with normal and skew orientations shown in the left and right columns, respectively. The dotted lines represent the current distribution near the origin; for a beam traveling out of the page ($-\mathbf{z}$), this is synonymous with the observed deflection/focusing of a uniform bunch. Image reprinted with publisher permission: *Beam Dynamics in High Energy Particle Accelerators*, Andrzej Wolski, ©2014 Imperial College Press

and have electromagnetic radiofrequency (RF) waves input via waveguides. When synchronized for acceleration, an incoming bunch witnesses an attractive potential which peaks at the center of each cavity.

A notable device which has become a mainstay for low-energy injection into RF-cavity based linacs is the radiofrequency quadrupole ("RFQ"); which provides focusing, acceleration, and bunching to a DC beam within a single four-vaned cavity.[5] In modern accelerators, ultrarelativistic energies are achieved using superconducting cavities and magnets which are housed in "cryomodules" that manage supercooled helium throughput. Although this thesis will not focus

[5]Wangler, *RF Linear Accelerators*, p9.

directly on cavities or other longitudinal devices and their underlying physics, the simulation techniques presented in later chapters are intended to be fully compatible with them.

1.1 Focusing Primer

This short section gives an example of transverse dynamics in terms familiar from elementary optics. The forthcoming sections will derive in detail the approximations used. For now, the intent is to justify the use of strong focusing while establishing a sense of scale for the required field strengths.

Although weak focusing by dipole magnets is the actual historical antecedent to strong focusing with quadrupoles, a solenoid oriented axially along the beam line can in principle be used for focusing, with the focal length approximation[6]

$$\frac{1}{f} \approx \frac{\pi}{16} \frac{q^2}{m} \frac{\ell}{2} \frac{\mathcal{B}_0^2}{E_0} \tag{1.2}$$

where ℓ is solenoid length; B_0 is the maximum magnetic field strength; and E_0 is a test particle's kinetic energy, with q and m as its respective charge and mass.

This thin-lens approximation is nonrelativistic, geometrically simplistic, and only accurate to within $\sim$10%. What is interesting here is that such a device *only* works for focusing (there is no diverging/defocusing lens equivalent) and is less effective for high-energy or high-mass particles.

The quadrupole magnet improves upon this, with

$$\frac{1}{f} \approx \pm \kappa \ell \tag{1.3}$$

for respective electric and magnetic field gradients

$$\kappa_E \approx \frac{q\mathcal{E}_0}{\gamma m r_0 (\beta c)^2} \quad ; \quad \kappa_{\mathcal{M}} \approx \frac{qB_0}{\gamma m r_0 \beta c} \tag{1.4}$$

where r_0 is aperture radius (formed between the tips of facing poles), γ is the relativistic Lorentz factor for a reference particle, $\mathcal{E}_0$ is electric field strength, and v is particle velocity.[7] The inverse v^2 dependence for electric quadrupoles implies

[6] Egerton, *Physical Principles of Electron Microscopy*, p39.

[7] Reiser, *Theory and Design of Charged Particle Beams*, p 88–101.

that magnetic quadrupoles are more appropriate for high-energy applications.[†] Here, the Lorentz force $F = q\left(\vec{\mathcal{E}} + \vec{v} \times \vec{B}\right)$ is inherent.

As mentioned earlier, the caveat with quadrupole magnets is that focusing along one transverse axis causes defocusing along the other. However, pairs of quadrupoles with opposite-sign gradients can be combined for a net strong focusing in both directions, which is evident in the elementary-optics expression for a thin-lens doublet:[8]

$$\frac{1}{\mathcal{F}} = \frac{1}{f_1} + \frac{1}{f_2} - \frac{s}{f_1 f_2} \tag{1.5}$$

where s is the distance between magnets. Then, if $f_1 = -f_2$

$$F = \frac{f_1^2}{s}. \tag{1.6}$$

Reiser notes that for $\ell \approx 10\, r_0$ such a quadrupole doublet is 50 times stronger than a solenoid of equivalent pole-tip strength B_0.[9] This makes it no surprise that FODO cells are the mainstay for transverse focusing of beams in high-energy machines. Considering longitudinal dynamics, an earlier discovery of G. Ising's was of equal weight: RF modulated electromagnetic fields are crucial for accelerating into the MeV scale; this is known as resonant acceleration.[10,11] The physics in this case has no simple optical analog.

As we begin to discuss single and multiparticle dynamics in the next few sections, we will prioritize such transverse dynamics (which are more straightforward than, and can serve as a basis for, longitudinal dynamics).

1.2 Liouville's Theorem, Symplecticity, and Linear Transforms

The historical approach to simulating beam dynamics through an accelerator approximates the forces acting on the beam as linear, meaning that the potentials within the governing Hamiltonian are dependent on position and momentum terms of no greater than quadratic-order. The next few sections will demonstrate how, given linear forces acting on a beam, the matrix computation of its transverse

[†]However, electric quadrupoles can be made mass-independent, and are thus commonly used for controlling slow radioactive ions.

[8]Hecht, *Optics*, p246.

[9]Reiser, p103.

[10]Bryant, "A brief history and review of accelerators".

[11]Wolski, p44.

single-particle dynamics can be extrapolated to determining its deviation (σ) values per timestep. Afterwards, the formalism introduced in this section will be extended to Hamiltonians which produce nonlinear forces.

We begin with Liouville's theorem, which states that[†,12] for some region in phase-space D wherein a function obeying Hamilton's equations $M(t, \vec{s})$ transforms a particle at $\vec{s}_0 = (\vec{x}_0, \vec{p}_0)$ to $\vec{s}_t = (\vec{x}_t, \vec{p}_t)$, the volume of D is conserved.[13] Abbreviating $M(t, \vec{s})$ as M, we have

$$\begin{aligned} M &= \vec{s} + f(\vec{s})t + \mathcal{O}(t^2) \\ \vec{s}_t &= M\vec{s}_0 \end{aligned} \tag{1.7}$$

where

$$\vec{f} = \dot{\vec{s}} \tag{1.8}$$

and, by the change of variable method

$$\begin{aligned} V_0 &= \int_{D_0} d\vec{s} \\ V_t &= \int_{D_0} \det \frac{\partial M}{\partial \vec{s}} d\vec{s} \end{aligned} \tag{1.9}$$

where $\det \frac{\partial M}{\partial \vec{s}}$ is also known the determinant of the Jacobian matrix, which we abbreviate as $|J|$. We can then take the series

$$|J| = 1 + t \cdot \mathrm{tr} \frac{\partial \vec{f}}{\partial \vec{s}} + \mathcal{O}(t^2) \tag{1.10}$$

where the trace reduces as

$$\mathrm{tr} \frac{\partial \vec{f}}{\partial \vec{s}} = \sum_{i=1}^{n} \frac{\partial f_i}{\partial s_i} = \nabla \cdot \vec{f} \tag{1.11}$$

then, for the Hamiltonian case

$$\nabla \cdot \vec{f} = \frac{\partial}{\partial \vec{p}} \left(-\frac{\partial H}{\partial \vec{x}} \right) + \frac{\partial}{\partial \vec{x}} \left(\frac{\partial H}{\partial \vec{p}} \right) = 0 \tag{1.12}$$

thus, to first order, $|J| = 1$ and $V_t = V_0$. Note that by introducing approximations in t we have linearized M and $|J|$, but only in the temporal domain (i.e. for

[†]In fact, the working version of Liouville's theorem in terms of Hamiltonian dynamics is also attributable to Jacobi, Boltzmann, and Gibbs.

[12]Nolte, "The tangled tale of phase space".

[13]Arnol'd, Kozlov, and Neishtadt, *Mathematical Aspects of Classical and Celestial Mechanics. Dynamical systems III; 3rd rev.* pp68-70.

infinitesimal changes).[14] So, for $t \to 0$, Eq. (1.12) will still hold for nonlinear Hamiltonians with $\vec{x}$ and $\vec{p}$ dependent terms of cubic or higher order.

Qualitatively, Liouville's theorem implies that focusing a bunch to a very narrow spot size inherently increases its momentum density, such that it will more rapidly diverge (and vice-versa).[15] In terms of 2D phase-space, this trait is equivalent to conservation of rms emittance (which, recall, is defined as $\epsilon = A/\pi$, where A is phase-space area).

This conservation proves useful in both linear and nonlinear tracking; to examine it further, we first need to define a more general property of Hamiltonian systems known as symplecticity.

First, recall the familiar Hamiltonian equations of motion

$$\dot{x_i} = \frac{\partial H}{\partial p_i} \quad ; \quad \dot{p_i} = -\frac{\partial H}{\partial x_i} \tag{1.13}$$

These can be, in a sense, *detected* in any system with the following conditions: if we concatenate x_i and p_i as before

$$\begin{aligned} \vec{s} &= (x_1, x_2, \ldots, x_n; p_1, p_2, \ldots, p_n)^T \\ \vec{\partial} &= \left(\frac{\partial}{\partial x_1}, \frac{\partial}{\partial x_2}, \ldots, \frac{\partial}{\partial x_n}, \frac{\partial}{\partial p_1}, \frac{\partial}{\partial p_2}, \ldots, \frac{\partial}{\partial p_n} \right)^T \end{aligned} \tag{1.14}$$

then we have the compact form[16]

$$\dot{\vec{s}} = S \cdot \vec{\partial} H = S \cdot W \vec{s} \quad ; \quad S = \begin{pmatrix} 0 & \mathbb{I} \\ -\mathbb{I} & 0 \end{pmatrix} \tag{1.15}$$

where S is an example of a symplectic matrix. The symplectic property then states that if M is a solution to Hamilton's equations, then

$$J^T S J = S \tag{1.16}$$

This is an alternative means for demonstrating $|J| = 1$, and will also be helpful in deriving the Twiss parameters and predicting error in nonlinear cases. Its proof is lengthy and can be found in Appendix A. Note that *any* matrix S satisfying Eq. (1.16) fits the definition of a symplectic matrix, although the one shown here is the most common choice.

[14] Wolski, p77–78.
[15] Ibid., p80.
[16] Laface, *Four Lectures in Particle Dynamics*.

What we are still lacking is a method for finding M. The simplest approach comes from examining Eq. (1.15), where we can predict that for quadratic Hamiltonians (which yield linear forces). To satisfy $\dot{\vec{s}} = S \cdot W\vec{s}$, where W is a matrix, we can choose the solution

$$\begin{aligned} M &= e^{tS\cdot W} \\ \vec{s}(t) &= M\vec{s}_0 \end{aligned} \tag{1.17}$$

We can then refer to M as a transfer matrix,[17] and we now have an operational example of linear dynamics. It also will be shown in the next chapter that

$$M^T S M = S \tag{1.18}$$

Thus, explicitly calculating $\dot{\vec{s}}$ is not necessary to ensure symplecticity—so long as Eq. (1.18) is satisfied.

We now have a means of predicting a particle's motion through phase space based solely on the Hamiltonian. This should be stressed, since Liouville's theorem is often introduced in terms of phase-space density[18,19]

$$\frac{d\rho}{dt} = \frac{\partial\rho}{\partial t} + \sum_{i=1}^{n}\left(\frac{\partial\rho}{\partial x_i}\dot{x}_i + \frac{\partial\rho}{\partial p_i}\dot{p}_i\right) = 0 \tag{1.19}$$

Here it follows that ρ is constant over any phase-space trajectory.

This form grounds the concept of phase-space volume in tangible terms, and we will return to it later when discussing covariant-Hamiltonian tracking). However, it is the underlying principle of symplecticity that enables tracking via Eqs. (1.17) *without* any defined density.

Nevertheless, for distributions, symplecticity also implies that any system with n degrees of freedom has n conserved quantities; these are the rms emittances in each spatial direction as mentioned earlier. Single-particle emittance is also an invariant quantity that can be tracked linearly at any point in a periodic beamline using the Twiss parameters, which will be introduced shortly. However, for non-periodic cases, its designation becomes arbitrary, and a defining it in terms of a distribution's σ_x and σ_p becomes a necessity.[20]

Equation 1.19 can also be stated in terms of the Poisson bracket and Hamiltonian

$$\frac{\partial\rho}{\partial t} = -\{\rho, H\} \tag{1.20}$$

[17] Rosenzweig, *Fundamentals of Beam Physics*, p56.
[18] Tolman, *The Principles of Statistical Mechanics*, p48 ff.
[19] Gibbs, *Elementary Principles in Statistical Mechanics*, p5 ff.
[20] Wolski, p80,150.

where ρ is phase-space density. This relation proves true for any analytical function $f(\vec{s})$ and applies for both linear and nonlinear cases

$$\frac{\partial f}{\partial t} = -\{f, H\} \tag{1.21}$$

which implies that *any* such f (any function of both $\vec{x}$ and $\vec{p}$ obeying Hamilton's equations) is a phase-space density or a contour of a phase-space density.

The notion of symplecticity is particularly important for long-term tracking, as with storage rings or circular colliders. For such cases, non-symplectic beam tracking codes can become grossly inaccurate over millions of revolutions.[21] In the past few decades, the use of symplectic integrators is now common for physics simulation in many disciplines,[22] with the seminal work attributable to Yoshida.[23]

1.3 The Thin-Lens and Paraxial Approximations

We have shown that a transfer matrix M can represent any linear element such as a solenoid, dipole, or quadrupole magnet. To find an explicit expression for M we can scale B_0 from Eq. (1.4) as $\frac{q}{p_0}$ where p_0 is a reference particle momentum. This also entails a rescaling of p_x and p_y:

$$\begin{aligned} p_x &= \frac{\gamma m\dot{x} + qA_x}{p_0} \\ p_y &= \frac{\gamma m\dot{y} + qA_y}{p_0} \end{aligned} \tag{1.22}$$

where $A_x = A_y = 0$ for transversely acting machine elements (i.e. A_z is the only nonzero potential component for multipoles and solenoids).

Taking a quadrupole as an example, a simple Hamiltonian can then be derived using the paraxial (small-angle) approximation—that is, expanding about $p_x =$

[21] Kleiss et al., "On the Feasibility of Tracking with Differential Algebra Maps in Long Term Stability Studies for Large Hadron Colliders".

[22] Phillips et al., "Scalable molecular dynamics with NAMD"; Chambers, "A hybrid symplectic integrator that permits close encounters between massive bodies".

[23] Yoshida, "Construction of Higher Order Symplectic Integrators".

$p_y = 0$ to second order:[24]

$$\begin{aligned} H &= \frac{p_x^2}{2} + \frac{p_y^2}{2} + \frac{\delta^2}{2\beta^2\gamma^2} + \frac{A_z q}{p_0} \\ &= \frac{p_x^2}{2} + \frac{p_y^2}{2} + \frac{\delta^2}{2\beta^2\gamma^2} + \frac{\kappa}{2}(x^2 - y^2) \end{aligned} \tag{1.23}$$

where β and γ are the reference-particle Lorentz factors, and δ is the conventional longitudinal momentum value, defined as energy deviation and treated in this context as a constant. (The expansion here is about $\delta = 0$.) Because of this rescaling, the field gradient κ is *not* equivalent to that shown in Eq. (1.4)—more thorough definitions for A_z and κ will follow in Chapter 3.†

From here we adopt the more conventional formalism for the paraxial approximation. That is

$$\begin{aligned} x' &= \frac{\partial x(\ell)}{\partial x(0)} \approx p_x \\ y' &= \frac{\partial y(\ell)}{\partial y(0)} \approx p_y \end{aligned} \tag{1.24}$$

is the change in trajectory *angle*, which can be seen as a secondary rescaling of the momentum parameters into radians. This is only valid in the paraxial approximation: trajectories with minor deviations from that of a reference particle's, which follows the ideal beam-line axis.

By first solving Eq. (1.23) for its equations of motion, Eqs. (1.17) becomes

$$\begin{aligned} \begin{pmatrix} x_\ell \\ x'_\ell \end{pmatrix} &= \begin{pmatrix} \cos(\sqrt{\kappa}\ell) & \frac{\sin(\sqrt{\kappa}\ell)}{\sqrt{\kappa}} \\ -\sqrt{\kappa}\sin(\sqrt{\kappa}\ell) & \cos(\sqrt{\kappa}\ell) \end{pmatrix} \begin{pmatrix} x_0 \\ x'_0 \end{pmatrix} \\ \begin{pmatrix} y_\ell \\ y'_\ell \end{pmatrix} &= \begin{pmatrix} \cosh(\sqrt{\kappa}\ell) & \frac{\sinh(\sqrt{\kappa}\ell)}{\sqrt{\kappa}} \\ \sqrt{\kappa}\sinh(\sqrt{\kappa}\ell) & \cosh(\sqrt{\kappa}\ell) \end{pmatrix} \begin{pmatrix} y_0 \\ y'_0 \end{pmatrix} \\ \begin{pmatrix} z_\ell \\ \delta_\ell \end{pmatrix} &= \begin{pmatrix} 1 & \frac{\ell}{\beta^2\gamma^2} \\ 0 & 1 \end{pmatrix} \begin{pmatrix} z_0 \\ \delta_0 \end{pmatrix} \end{aligned} \tag{1.25}$$

where the transfer matrix M has been written out explicitly for each spatial axis. What we now have is a basis for 6D linear tracking through the length of a quadrupole for low p_i and x_i values. Given that most accelerators are designed to minimize transverse momentum, the paraxial approximation is useful in many cases, at least as a starting point for coarse-tuning of machine parameters.

[24] Wolski, pp75,82,102.

† Where we will show that a fully covariant Hamiltonian has terms dependent on $\vec{A}^2$.

We can then apply the thin-lens approximation (i.e. letting $\ell \to 0$ but keeping $\sqrt{\kappa}\ell$ finite). This brings us back to the optical analogy from Section 1.1, where we now have the matrix equivalent of Eq. (1.3):

$$\begin{aligned}
\begin{pmatrix} x_\ell \\ x'_\ell \end{pmatrix} &= \begin{pmatrix} 1 & 0 \\ -\frac{1}{f} & 1 \end{pmatrix} \begin{pmatrix} x_0 \\ x'_0 \end{pmatrix} \\
\begin{pmatrix} y_\ell \\ y'_\ell \end{pmatrix} &= \begin{pmatrix} 1 & 0 \\ \frac{1}{f} & 1 \end{pmatrix} \begin{pmatrix} y_0 \\ y'_0 \end{pmatrix} \\
\begin{pmatrix} z_\ell \\ \delta_\ell \end{pmatrix} &= \begin{pmatrix} 1 & 0 \\ 0 & 1 \end{pmatrix} \begin{pmatrix} z_0 \\ \delta_0 \end{pmatrix}
\end{aligned} \tag{1.26}$$

Linear transfer maps such as these can be devised for most common accelerator elements, (see Wolski, Chapter 3).[25] The thin-lens approximation greatly simplifies analysis and makes for extremely fast simulations. With the help of the Twiss parameters to be introduced shortly, such simplified forms can be used to characterize and monitor beam lines (especially periodic ones) without any specific knowledge of a bunch's coordinates (aside from its proximity to the beam axis).

Similar methods for longitudinal tracking can be also be devised by treating an accelerating RF structure as a series of drift spaces (vacuum with a null external potential) with thin separating gaps wherein forces are applied.[26] However, this involves careful rescaling at each timestep, as the Hamiltonian is no longer constant.

To clarify this point: it is apparent that Eq. (1.26) does not permit longitudinal tracking. This means that simulations involving thin longitudinal kicks, such as accelerating RF cavities, entail carefully resetting δ to zero at each timestep by increasing the reference momentum. Such ad hoc momentum shifting means that a bunch's phase-space area is no longer conserved (Liouville's theorem no longer applies). This can be taken as evidence that phase space shrinks adiabatically throughout acceleration.[27] However, the Lovertz-covariant tracking method developed over the next two chapters challenges this assertion[28] (or rather, it inherently tracks $\beta\gamma\epsilon$, known as *normalized* emittance, which is conserved throughout acceleration). Generalized linear methods for longitudinal–transverse-coupled dynamics are also well-developed.[29]

[25] Ibid., p83 ff.

[26] Wangler, p177.

[27] Wolski, p154.

[28] Wang, Liu, and Qin, "Lorentz covariant canonical symplectic algorithms for dynamics of charged particles"; Folsom and Laface, "Beam dynamics with covariant hamiltonians".

[29] Edwards and Teng, "Parametrization of Linear Coupled Motion in Periodic Systems";

In most practical cases, particles are not relativistic in both the bunch frame and the lab frame, allowing longitudinal and transverse dynamics to be decoupled, which makes for simplified tracking codes.† However, any effect involving a bunch losing its uniform phase-space density is nonlinear (e.g. emittance growth, halo formation, and particle loss);[30] and longitudinal dynamics remain clumsy for linear tracking in general. Thus, the use of longitudinal elements is a strong motivation for improving nonlinear tracking. This is especially true for elements which manipulate the longitudinal phase space of the beam, such as bunch compressors.[31]

We will defer further discussion of nonlinear dynamics and longitudinal effects until after the next section, in which the remaining fundamentals of linear dynamics are presented.

1.4 Twiss Parameters and Multiparticle Tracking

The tendency of a single particle to trace an elliptical phase-space envelope is illustrated in Fig. 1.2. For an arbitrary beam line of several identical FODO cells, its constituent particles will trace differently shaped elliptical envelopes depending on their starting trajectories,[32] while for a ring, all particles will eventually populate an envelope defined by ϵ_{rms}. For a single particle, it is important to note that it will only paint such a phase-space ellipse for periodic lattices (e.g. repeated FODO cells or rings).

The single-particle and multiparticle formalism can often be complementary. For example, bunches that are Gaussian, uniform, or having ellipsoidal symmetry are often used in simulation or desired in practice. In such cases, if the rms emittance is known and if space charge is treated as linear, the bunch's trajectory through a drift space can be shown to be solely dependent on its σ values[33] (in other words, bunches with such symmetry have linear dynamics that are not dependent on its shape function—only its deviations). In fact, irregularly shaped

Sagan and Rubin, "Linear Analysis of Coupled Lattices"; Wolski, "Alternative Approach to General Coupled Linear Optics".

†In fact, space charge introduces a coupling in all spatial dimensions, even at low β, and its effect and is typically calculated separately and interpolated into the external-force based dynamics; it can, however be treated with a series expansion for small distances from the ideal design path (i.e. akin to the paraxial approximation, but in 3D.)

[30]Reiser, p273, 334, 522.

[31]Wolski, p265.

[32]Ibid., p132.

[33]Sacherer, "RMS Envelope Equations with Space Charge".

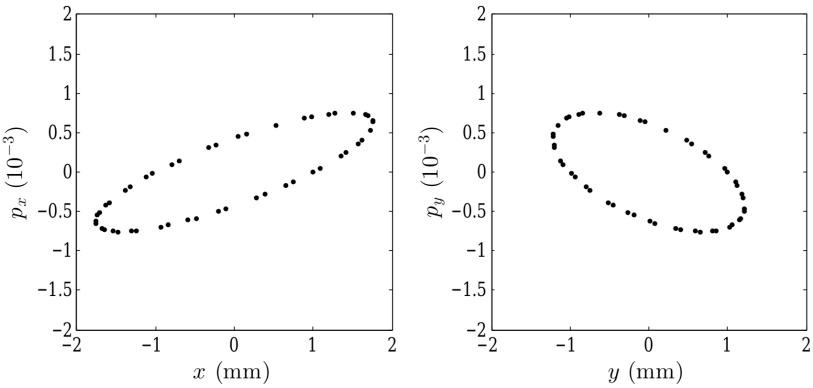

Figure 1.2: (a) "Envelope" representation of a single particle passing through several FODO cells, with each new point taken after passing through an integer number of cells. Image reprinted with publisher permission: *Beam Dynamics in High Energy Particle Accelerators*, Andrzej Wolski, ©2014 Imperial College Press

distributions can also be tracked by their σ values, with the caveat that their shapes will only be modified in linear terms (e.g. rotations and resizing).

To see how this is accomplished, the Twiss parameters are needed (also frequently called the Courant–Snyder parameters). While the derivations to follow will stem from multiparticle transport, we will also expand this to a working example for the single-particle case.

First, we define the *covariance* matrix.

$$\begin{aligned}\Sigma_x &= \frac{1}{N}\sum_i^N \left[\begin{pmatrix} (x_i - \vec{x})^2 & (x_i - \vec{x})(x_i' - \vec{x'}) \\ (x_i - \vec{x})(x_i' - \vec{x'}) & (x_i' - \vec{x'})^2 \end{pmatrix} \right] \\ &= \begin{pmatrix} \sigma_x^2 & \sigma_x\sigma_{x'} \\ \sigma_x\sigma_{x'} & \sigma_{x'}^2 \end{pmatrix} \end{aligned} \tag{1.27}$$

Where the off-diagonal terms are a measure of the coupling between momentum and position along one spatial axis.

Any series of single-element transfer matrices can be concatenated into a single matrix, which makes linear simulation of complicated accelerators with thousands of elements relatively simple to simulate, even for the tens of millions of turns required in operation. This can be represented symbolically as

$$\vec{s}_{final} = M \cdot \vec{s}_0 = M_4 M_3 M_2 M_1 \cdot \vec{s}_0 \tag{1.28}$$

One can then suppose solutions exist for

$$\begin{pmatrix} \sigma_x^2 \\ \sigma_x\sigma_{x'} \\ \sigma_{x'}^2 \end{pmatrix}_{\text{after}} = T \begin{pmatrix} \sigma_x^2 \\ \sigma_x\sigma_{x'} \\ \sigma_{x'}^2 \end{pmatrix}_{\text{before}} \tag{1.29}$$

where the linear symplectic transport matrix M can be represented as

$$M = \begin{pmatrix} M_{11} & M_{12} \\ M_{21} & M_{22} \end{pmatrix} \tag{1.30}$$

It can be shown with straightforward computation that[†]

$$T = \begin{pmatrix} M_{11}^2 & -2M_{11}M_{12} & M_{12}^2 \\ -M_{11}M_{21} & M_{11}M_{22} + M_{12}M_{21} & -M_{12}M_{22} \\ M_{21}^2 & -2M_{12}M_{22} & M_{22}^2 \end{pmatrix} \tag{1.31}$$

This matrix reappears in a more general case, which first requires the general expression for an ellipse centered about an origin[34]

$$\epsilon = \begin{pmatrix} x & , & x' \end{pmatrix} \begin{pmatrix} \gamma_t & \alpha_t \\ \alpha_t & \beta_t \end{pmatrix} \begin{pmatrix} x \\ x' \end{pmatrix} \tag{1.32}$$

This can be assigned a determinant of 1 without losing generality, which then yields

$$\epsilon = \gamma_t x^2 + 2\alpha_t x x' + \beta_t x'^2 \tag{1.33}$$

where our emittance ϵ now has a geometric definition in terms of what are known as the Twiss parameters α_t, γ_t, and β_t (where the subscript t is used to avoid confusion with the relativistic Lorentz parameters). In physical terms, β_t is known as the beta function or betatron function. For a stable beam, it describes the amplitude of a particle's transverse oscillations (the condition of stability has a rule-of-thumb that $|\text{TrM}| < 2$, but Berz' text has a much more thorough analysis on the subject[35]). The beta function and emittance are particularly

[†]There is an underlying assumption here in how M is allowed to combine with the sums defining the covariance matrix, in other words, its terms may be taken inside the sums and this is only valid in the linear case. An alternative, but perhaps more illuminating computation transports sigmas as

$$\begin{aligned} \Sigma_{x_{after}} = M\Sigma_x M^T &= M\frac{1}{N}\sum_i^N \left[\vec{x}_i - \frac{1}{N}\sum_i^N \vec{x}_i\right]\left[\vec{x}_i^T - \frac{1}{N}\sum_i^N \vec{x}_i^T\right] M^T \\ &= \frac{1}{N}\sum_i^N \left[M\vec{x}_i - \frac{1}{N}\sum_i^N M\vec{x}_i\right]\left[\vec{x}_i^T M^T - \frac{1}{N}\sum_i^N \vec{x}_i^T M^T\right] \end{aligned}$$

where $\vec{x}_i = (xx')^T$. This can be seen as the so-called envelope extension of Eq. (1.17), noting $\vec{x}$ and $\vec{x}^T$ terms transform to $M\vec{x}$ and $\vec{x}^T M^T$ respectively.

[34]Berz, *Modern Map Methods in Particle Beam Physics*, p262.

[35]Berz, p250, §7.1.1.

useful in accelerator design and beam monitoring.

It can now be shown with straightforward analysis that[36,37]

$$\begin{pmatrix} \beta_t' \\ \alpha_t' \\ \gamma_t' \end{pmatrix} = T \begin{pmatrix} \beta_t \\ \alpha_t \\ \gamma_t \end{pmatrix} \tag{1.34}$$

Where we have a geometric (envelope) method for tracking along with the multiparticle method. The two concepts can be unified by defining an rms emittance:

$$\epsilon = \sqrt{\langle x^2 \rangle \langle x'^2 \rangle - \langle x x' \rangle^2} \tag{1.35}$$

where angle brackets denote mean values. The derivation of this expression is fairly involved[38] and will not be shown in detail. It is worth noting, though, that this form (mean of squares minus squared mean) is equivalent to the elementary definition of rms deviation for the quantity xx'. Thus, in concrete terms, rms emittance is the rms *covariance* of position and momentum.†

With this definition, some elementary linear algebra leads to the relation

$$\begin{pmatrix} \langle x^2 \rangle & \langle x x' \rangle \\ \langle x x' \rangle & \langle x'^2 \rangle \end{pmatrix} = \begin{pmatrix} \beta_t & -\alpha_t \\ -\alpha_t & \gamma_t \end{pmatrix} \epsilon \tag{1.36}$$

Then, for a periodic lattice, if the geometric definition of emittance Eq. (1.33) (based on machine parameters) agrees with the beam-based rms definition of emittance Eq. (1.36) (based on beam properties) the beam is said to be *matched*. In this case, after a single period $(\beta_t', \alpha_t', \gamma_t') = (\beta_t, \alpha_t, \gamma_t)$. Or, as Wolski puts it in terms of β_t:

> ...since the beta function will be the same for all particles, the size of the beam will vary along the beam line with the same periodicity as the beam line itself.[39]

[36] Lee, *Accelerator Physics*, p51.

[37] Berz, p264.

[38] Wolski, p151-53.

† To the reader unfamiliar with advanced geometry or relativistic dynamics: the term covariance is also used extensively in upcoming chapters, but refers to an entirely different concept pertaining to the differential behavior of vectors and, in the case of Lorentz transformations, their reference-frame invariance.

[39] Ibid., p138.

For a cumulative example, we introduce one remaining concept that is essential in beam physics. This is known as the phase advance, ϕ, and defined as

$$\begin{aligned}\cos(\phi) &= \frac{x}{\sqrt{\epsilon\beta_t}} \\ \sin(\phi) &= -\frac{1}{\sqrt{\epsilon}}\left(x'\sqrt{\beta} + \frac{\alpha x}{\sqrt{\beta}}\right)\end{aligned} \tag{1.37}$$

Where we have again skirted a formal derivation and given a simplistic definition (this time deferring to Wille's proof).[40] Phase advance is, simply put, a point on the phase-space ellipse (for a single particle in a periodic lattice) which matches the current position along the beam line, and which will repeat after one lattice period.† From here, we can develop another form for M, which is compatible with Eq. (1.30) and its ancillary identities:

$$M = \begin{pmatrix} \sqrt{\frac{\beta_t'}{\beta_t}}\left(\cos\phi + \alpha_t \sin\phi\right) & \sqrt{\beta_t'\beta_t}\sin\phi \\ -\frac{1}{\sqrt{\beta_t'\beta_t}}\left[(\alpha_t - \alpha_t') + (1 + \alpha_t\alpha_t')\sin\phi\right] & \sqrt{\frac{\beta_t}{\beta_t'}}\left(\cos\phi - \alpha_t\sin\phi\right) \end{pmatrix} \tag{1.38}$$

where the machine-based M elements, such as those from Eqs. (1.25) or (1.26), which are inherently independent of x and x', can be used to solve for ϕ. For example, with a simple, thin-lens FODO cell (a focusing doublet with drift spaces between quadrupoles)[41]

$$\cos\phi_t = 1 - \frac{\ell^2}{2f^2} \tag{1.39}$$

which lets us solve for the Twiss parameters at the cell entrance

$$\begin{aligned}\alpha_t \sin\phi_t &= -\frac{\ell}{f}\left(1 + \frac{\ell}{2f}\right) \\ \beta_t \sin\phi_t &= \frac{\ell}{f}\left(2f + \ell\right) \\ \gamma_t \sin\phi_t &= \frac{\ell}{f^2}\end{aligned} \tag{1.40}$$

where Eq. (1.34) becomes fully solvable for the Twiss parameters at any point in the cell. In this case we have the means for characterizing a machine element without any explicit knowledge of the beam distribution.

[40] Wille, "The Physics of Particle Accelerators: An Introduction", p88.

† A related concept is the betatron tune: $\nu = \frac{\phi}{2\pi}$. For circular accelerators, monitoring the tune is essential for beam stability: minor steering or focusing errors can resonate strongly if the tune for a single lattice period is an integer value. This is attenuated for half-integer values, and can become negligible for other fractional tunes. Because of this, potential tunes for a machine are typically mapped so an ideal one can be chosen.

[41] Wolski, p144.

As a final remark, we can now clarify the previous mention of reference-momentum shifts. That is, for cases such as an accelerating cavity where energy deviation δ is large, the shifted momentum "breaks" Liouville's theorem and new Twiss parameters are needed:

$$\begin{pmatrix} \beta_t^{'} & -\alpha_t^{'} \\ -\alpha_t^{'} & \gamma_t^{'} \end{pmatrix} \epsilon_t^{\prime} = \begin{pmatrix} 1 & 0 \\ 0 & \frac{p_0}{p_1} \end{pmatrix} \begin{pmatrix} \beta_t & -\alpha_t \\ -\alpha_t & \gamma_t \end{pmatrix} \begin{pmatrix} 1 & 0 \\ 0 & \frac{p_0}{p_1} \end{pmatrix} \epsilon_t \tag{1.41}$$

where p_0 and p_1 are the original and updated reference momenta, respectively. In Chapter 2 we will address whether or not this violation of symplecticity is an unavoidable consequence (with the only candidate for avoiding this issue being a Lorentz-covariant integrator).

We have at this point gathered enough of the essentials of linear tracking to begin discussing its limitations. This optics-like treatment is elegant and was foundational in modern accelerator development, but the reliance on small-angle approximation both along the beam line (thin lens) and perpendicular to it (paraxial) may prove inadequate for improving beam dynamics theory, and, in turn, designing more powerful and precise accelerators. Form here, we will only return to thin-lens linear methods as a reference, first introducing conventional nonlinear tracking (which typically retains the paraxial approximation). Then we turn to the prospect of fully nonlinear, non-approximant Hamiltonians, and the accompanying covariant equations of motion and tracking algorithms.

1.5 Conventional Nonlinear Tracking

The term nonlinear usually calls to mind chaotic or unbounded systems; but we should not overlook the notion that nonlinear algebra may be useful in constructing simpler or more accurate physical models. To first quote Dolotin and Morozov[42] to dispel any ambiguity:

> Linear algebra is the theory of matrices (tensors of rank 2), non-linear algebra is the theory of generic tensors.
>
> There is a widespread feeling that the non-linear world is very different, and it is usually studied as a sophisticated phenomenon of interpolation between different approximately-linear regimes. [...]

[42] Dolotin and Morozov, *Introduction to Non-Linear Algebra*.

> this feeling can be wrong: non-linear world, with all its seeming complexity including "chaotic structures" [...] allows clear and accurate description in terms of ordinary algebraic geometry.

In practical terms, we can test for linearity by checking that the following equation holds:

$$f(\alpha\vec{u} + \vec{v}) = \alpha f(\vec{u}) + f(\vec{v}) \tag{1.42}$$

where both additivity $f(\vec{v} + \vec{u}) = f(\vec{v}) + f(\vec{u})$ and homogeneity $f(\alpha\vec{v}) = \alpha f(\vec{v})$ are necessary conditions.[43] For example, in

$$f(x_i) = \begin{pmatrix} x_1 x_2 \\ x_1^2 \\ x_3 + 1 \\ x_4 \end{pmatrix} \tag{1.43}$$

only the last row is a linear operation (i.e. any additive constants, squared or higher-order polynomial terms, or multiplication of variables means non-linearity). From this perspective, the idea of *linear* physics may seem somewhat absurd to the novice, but breaking down or approximating complex systems into linear constituents (often by first-order series expansion) can shed light onto new physics, particularly in the case of quantum mechanics. Consequently, it has become a common conceit among physicists to routinely add layers of first-order approximations to a system without considering their consequences.

We will do our best to avoid this attitude here and throughout the remainder of the text, proceeding on the assumption that nonlinear terms including basic polynomials, coupled position–momentum, or transverse–longitudinal variables are of equal weight to a system's dynamics as any linear terms.

It is evident from the previous section, Eq. (1.23), that Hamiltonians which are quadratic in $\vec{p}$ and $\vec{x}$ will have transfer matrices which are inherently linear.[†] Explicitly, if an external force on a particle is linear ($F_i = \kappa x_i$), then

$$\begin{aligned} H(\vec{v} = [x_i, p_i]) &= f(x_i^2 | x_i p_i, p_i^2) \\ \partial H = D \cdot \vec{v} \quad ; \quad \frac{d}{dt}\vec{v} &= S \cdot D \cdot \vec{v} \end{aligned} \tag{1.44}$$

[43] Edwards, *Linear Algebra*, p78.

[†] Also keep in mind: potentials or equations of motion involving position and momentum *cofactors* (i.e. $\dot{x_1} = x_1^2 p_1$) are generally nonlinear, but if a potential has a dependence on, e.g., $x_1 p_1$, the dynamics (based on its derivatives) are linear.

where

$$D = D^T \quad ; \quad \vec{v}(t) = M(t) \cdot \vec{v}(0) = \mathcal{M}(\vec{v}_0, t) \quad ; \quad M(t) = e^{tSD} \tag{1.45}$$

and $\mathcal{M}(\vec{v}_0, t)$ is again our transfer matrix.[44,45] To prove[46]

$$\begin{aligned} S \cdot e^{tS\cdot D} &= e^{tS\cdot D} \cdot S \\ \implies M(t)^T S M(t) &= S \end{aligned} \tag{1.46}$$

we manipulate the left-hand side by first Taylor-expanding $e^{tS\cdot J}$ on the left-hand side of the top line, then using $S^2 = -\mathbb{I}$:

$$\begin{aligned} S \cdot e^{tS\cdot D} &= -S\left(1 + SDt + \frac{1}{2}t^2 S\cdot D\cdot S\cdot D \ \ldots\right) S^2 \\ &= -S^2\left(1 + SDt + \frac{1}{2}t^2 D\cdot S\cdot D\cdot S \ \ldots\right)\cdot S \\ &= e^{tD\cdot S}\cdot S \end{aligned} \tag{1.47}$$

Thus

$$\begin{aligned} M(t)^T \cdot S \cdot M(t) &= e^{-tD\cdot S}\cdot S\cdot e^{tS\cdot D} \\ &= e^{-tD\cdot S}\cdot e^{tD\cdot S}\cdot S \\ &= S \end{aligned} \tag{1.48}$$

where we used the identity $S^T = -S$. Here, the concepts of transfer maps and linear forces relating to quadratic Hamiltonians are commonly applied in accelerators, particularly since quadrupole magnets meet this qualification.

Although Eq. (1.48) cannot be assumed to hold for nonlinear transfer matrices, the nonlinear Lie-operator method presented next reduces to this form when Eq. (1.44) is true.

Restricting our notation to Hamiltonians in Euclidian space, we now define the Lie Operator to derive the "miracle" of nonlinear tracking[47]

$$:H:g = \sum_{i=1}^{n}\left(\frac{\partial H}{\partial x_i}\frac{\partial g}{\partial p_i} - \frac{\partial H}{\partial p_i}\frac{\partial g}{\partial x_i}\right) \tag{1.49}$$

[44]Dragt, *Lie Methods for Nonlinear Dynamics with Applications to Accelerator Physics*, p8,592.

[45]Wolski, p76.

[46]Laface, *Accelerator Recipes*.

[47]Forest, *Beam dynamics: A New Attitude and Framework*, p98.

where $g = x_i$ and $g = p_i$ produce the usual Hamiltonian equations of motion[48]

$$\begin{aligned} \dot{x}_i &= :H:x_i = \frac{\partial H}{\partial p_i} \\ \dot{p}_i &= :H:p_i = -\frac{\partial H}{\partial x_i} \end{aligned} \tag{1.50}$$

which generalizes to

$$\frac{d}{dt} f(x_i, p_i) = \frac{\partial f}{\partial x_i}\dot{x}_i + \frac{\partial f}{\partial p_i}\dot{p}_i = -:H:f(x_i, p_i) \tag{1.51}$$

This is the generalized form of Gibbs' extension to Liouville's theorem—see Eqs. (1.20) and (1.21). Then, with the definition

$$(:H:)^2 g =: H: (:H:g) \tag{1.52}$$

we have

$$\ddot{x}_i = \frac{d}{dt}\dot{x}_i = -:H: (-:H:x_i) \tag{1.53}$$

So for a Taylor expansion of a small timestep, the "miracle" tracking algorithm emerges:

$$\begin{aligned} x_i(t) &= \left[x_i + \frac{dx_i}{dt} + \frac{t^2}{2}\frac{d^2 x_i}{dt^2} + \cdots \right]_{t=0} \\ &= \left[x_i - t:H: + \frac{t^2}{2}:H: (:H:x_i) + \cdots \right]_{t=0} \\ &\approx e^{-t:H:} x_i(0) \end{aligned} \tag{1.54}$$

which holds analogously for p_i, such that, in compact form, Eq. (1.14) becomes

$$\vec{v}(t) = e^{-t:H:}\vec{v}(0) \tag{1.55}$$

These properties amount to an extended algebra for the Poisson bracket, where the abstraction of the Lie operator into the exponential form proves useful. For the case of a quadrupole (equivalently, a generic quadratic potential), Eq. (1.55) reduces to Eq. (1.25).

Recalling the symplectic condition, the accuracy of the approximation in Eq. (1.54) can be monitored. For example, in a sextupole magnet:[49]

$$M^T S M = S + \mathcal{O}\left(\kappa^m \ell^{m+1} x_i^{2m-1}\right) \tag{1.56}$$

[48] Laface, *Four Lectures in Particle Dynamics*.
[49] Wolski, p299.

where m is the order of series expansion in the exponential. The order can then be truncated to the condition

$$\kappa^m \ell^{m+1} x_i^{2m-1} \ll 1 \tag{1.57}$$

For long-term simulations, such errors must be truncated carefully (to machine precision if possible) to avoid cumulative error effects.

1.6 Symplectic Integrators

In practice, it is often preferable to use exactly symplectic solutions instead of relying on polynomial truncation. Conventionally, these require Hamiltonians separable in terms of position and momentum

$$H = f(\vec{p}) + g(\vec{x}) \tag{1.58}$$

The basic form for such an integrator begins with the map

$$\vec{v}_1(\vec{x}_1, \vec{p}_1) = \left\{ \prod_{i=1}^{k} \exp(c_i \tau : f[p] :) \exp(d_i \tau : g[x] :) \right\} \vec{v}_0(\vec{x}_0, \vec{p}_0) \tag{1.59}$$

where, the simplest (first-order) solution $k = 1$ is $c_1 = 1$ and $d_1 = 1$; for $k = 2$, one can use $c_1 = c_2 = 1/2$, $d_1 = 1$, and $d_2 = 0$. Fourth-order solutions are also straightforward;[50] higher-order ones can be calculated with the Baker-Campbell–Hausdorff formula.[51] Once discretized to be iterated over a chosen timestep, such solutions belong to the family of numerical simulation techniques known as integrators.

These integrators are typically classified by how values are inherited through the passage of a timestep τ when a system's equations of motion, as in Eq. (1.13), are discretized. For example:

$$\vec{v}_1 = \vec{v}_0 + \tau f(\vec{v}_0) \tag{1.60}$$

is solely dependent on previously solved values, and is referred to as an explicit Euler method. Implicit solvers, though, have a counter-intuitive self-dependence:

$$\vec{v}_1 = \vec{v}_0 + \tau f(\vec{v}_1) \tag{1.61}$$

[50] Forest and Ruth, "Fourth-order symplectic integration".
[51] Yoshida, "Construction of Higher Order Symplectic Integrators".

In this form, a Newton search is needed for machine-precision convergence.[52] However, Yoshida demonstrated that, for seperable Hamiltonians, as in Eq. (1.58), symplectic Taylor-series mappings are time-reversible, making the Poincaré approach viable:

$$\begin{aligned}\vec{x}_1 &= \vec{x}_0 + \tau\left(\frac{\partial H}{\partial \vec{p}}\right)\left[\frac{\vec{x}_0+\vec{x}_1}{2}\,,\ \frac{\vec{p}_0+\vec{p}_1}{2}\,,\ t_0+\frac{\tau}{2}\right]\\ \vec{p}_1 &= \vec{p}_0 - \tau\left(\frac{\partial H}{\partial \vec{x}}\right)\left[\frac{\vec{x}_0+\vec{x}_1}{2}\,,\ \frac{\vec{p}_0+\vec{p}_1}{2}\,,\ t_0+\frac{\tau}{2}\right]\end{aligned} \tag{1.62}$$

which is known as an implicit midpoint technique, and is considered symmetric (i.e. the formula is unchanged for $v_{n+1} \iff v_n$ and $n \iff -n$).

More recent work revived deVogelaere's method,[53] and is known as the symplectic Euler integrator. This requires known equations of motion from a Hamiltonian:

$$\dot{\vec{p}} = -\frac{\partial H}{\partial \vec{x}}(\vec{p},\vec{x}) \quad ; \quad \dot{\vec{x}} = \frac{\partial H}{\partial \vec{p}}(\vec{p},\vec{x}) \tag{1.63}$$

and takes the form

$$\begin{aligned}\vec{p}_{n+1} &= \vec{p}_n - \tau\frac{\partial H}{\partial \vec{x}}(\vec{p}_{n+1},\vec{x}_n) \qquad & \vec{p}_{n+1} &= \vec{p}_n - \tau\frac{\partial H}{\partial \vec{x}}(\vec{p}_n,\vec{x}_{n+1})\\ &\text{or} & &\\ \vec{x}_{n+1} &= \vec{x}_n + \tau\frac{\partial H}{\partial \vec{p}}(\vec{p}_{n+1},\vec{x}_n) \qquad & \vec{x}_{n+1} &= \vec{x}_n + \tau\frac{\partial H}{\partial \vec{p}}(\vec{p}_n,\vec{x}_{n+1})\end{aligned} \tag{1.64}$$

This method is explicit for Hamiltonians with separable position and momentum terms, but implicit in the general Euclidean case. However, it is worth mentioning that in scenarios where[54]

$$\frac{\partial H}{\partial x_i}(\vec{p},\vec{q}) \text{ is independent of } p_j \text{ for } j \geq i \tag{1.65}$$

the vanishing momentum dependence leads to an explicit method, which is true as well for

$$\frac{\partial H}{\partial p_i}(\vec{p},\vec{q}) \text{ is independent of } x_j \text{ for } j \geq i \tag{1.66}$$

In the next chapter, we demonstrate a alternative method for making Eqs. (1.64) fully explicit in terms of Lorentz-covariant potentials.

[52] Forest, p334.

[53] Hairer, Lubich, and Wanner, *Geometric Numerical Integration: Structure-Preserving Algorithms for Ordinary Differential Equations; 2nd ed.* p3.

[54] Hairer, Lubich, and Wanner, p189.

1.7 Classifying Simulation Methods

At this point, the non-expert reader should be familiar enough with the fundamentals of beam physics to follow the upcoming chapters without trouble. To conclude this introductory chapter, we break from technical considerations to take an overview of when linear, nonlinear, and symplectic methods are needed in practice. Forest's ring dynamics dogma serves as a good basis here—it is essentially a hierarchy of simulation methods:[55]

1. Fast, with purely linear transforms
    - Depends on "controlled" limits, (i.e. defined by more accurate benchmarking simulations)
    - Uses small-angle approximations "linear quads and linear bends"
    - Excludes fringe fields
    - Also uses small-angle approximation for misalignments
2. Fairly fast, with explicit symplectic integrators
    - "Laminates" thin-lens slices (i.e. small timesteps) together to actual thicknesses of machine elements
    - Small nonsymplectic effects (e.g. radiation) included
3. Slow, high-order integrators as close as possible to machine precision (for failsafe/reference measurements)

The following chapters may then be seen as an effort to speed up methods from category 3, or to limit the dependence on 3 by bringing the accuracy of explicit symplectic integrators closer to machine precision.

As mentioned earlier, a more general notion to keep in mind when building a simulation is which approximations are used: in the linear case, the paraxial approximation is necessary and the thin-lens approximation is a mainstay; in the non-linear case, the paraxial approximation is still necessary to decouple position and momentum terms in the Hamiltonian (otherwise they will always reside within a square root).

[55] Forest, *Beam dynamics: A New Attitude and Framework*, p330.

References

Arnol'd, V. I., V. V. Kozlov, and A. I. Neishtadt. *Mathematical Aspects of Classical and Celestial Mechanics. Dynamical systems III; 3rd rev.* Encyclopaedia of mathematical sciences. Heidelberg: Springer, 2006. URL: http://cds.cern.ch/record/937549.

Berz, M. *Modern Map Methods in Particle Beam Physics*. 1st ed. Academic Press, 1999. URL: http://bt.pa.msu.edu/pub/papers/AIEP108book/AIEP108book.pdf.

Bryant, P. J. "A brief history and review of accelerators". In: *CAS-CERN Accelerator School: 5th general accelerator physics course, Jyvaskyla, Finland, 7-18 Sep 1992: Proceedings. 2 vol.* 1992, pp. 1–16.

Burshtein, É. L. et al. "Application of the principle of automatic correction of the magnetic field in cyclic superhigh-energy accelerators". In: *The Soviet Journal of Atomic Energy* 12.2 (1962), pp. 122–126. DOI: 10.1007/BF01591425.

Caspi, S. et al. "Canted cosine theta magnet CCT);a concept for high field accelerator magnets". In: *IEEE Transactions on Applied Superconductivity* 24.3 (June 2014), pp. 1–4. DOI: 10.1109/TASC.2013.2284722.

Caspi, S. et al. "Design, fabrication, and test of a superconducting dipole magnet based on tilted solenoids". In: *IEEE Transactions on Applied Superconductivity* 17.2 (2007), pp. 2266–2269. ISSN: 1051-8223. DOI: 10.1109/TASC.2007.899243.

Chambers, J. E. "A hybrid symplectic integrator that permits close encounters between massive bodies". In: *Monthly Notices of the Royal Astronomical Society* 304.4 (1999), pp. 793–799. DOI: 10.1046/j.1365-8711.1999.02379.x.

Dolotin, V and A Morozov. *Introduction to Non-Linear Algebra*. Tech. rep. hep-th/0609022. 2006. URL: http://cds.cern.ch/record/981884.

Dragt, A. J. *Lie Methods for Nonlinear Dynamics with Applications to Accelerator Physics*. College Park, MD, USA: University of Maryland, Forthcoming, 2019. URL: https://www.physics.umd.edu/dsat/dsatliemethods.html.

Edwards, D. A. and L. C. Teng. "Parametrization of linear coupled motion in periodic systems". In: *IEEE Transactions on Nuclear Science* 20.3 (June 1973), pp. 885–888. DOI: 10.1109/TNS.1973.4327279.

Edwards, H. M. *Linear Algebra*. Boston, MA: Birkhäuser Boston, 1995. Chap. Matrices with Polynomial Entries. DOI: 10.1007/978-0-8176-4446-8_8.

Egerton, R. F. et al. *Physical Principles of Electron Microscopy*. Springer, 2005.

Folsom, B. and E. Laface. "Beam dynamics with covariant hamiltonians". In: *Proc. 9th International Particle Accelerator Conference (IPAC'18), Vancouver, BC, Canada, April 29-May 4, 2018*. International Particle Accelerator Conference

9. Geneva, Switzerland: JACoW Publishing, 2018, pp. 3123–3126. DOI: 10.18429/JACoW-IPAC2018-THPAF064.

Forest, E and R. D. Ruth. "Fourth-order symplectic integration". In: *Physica D* 43.LBL-27662 (1989), p. 105. URL: http://cds.cern.ch/record/201901.

Forest, E. *Beam dynamics: A New Attitude and Framework*. Phys. Technol. Part. Phot. Beams. Sidney: Harwood, 1998. URL: http://cds.cern.ch/record/367626.

Gibbs, J. W. *Elementary Principles in Statistical Mechanics*. Dover Books on Physics. Mineola, NY: Dover, 2014. URL: https://cds.cern.ch/record/1987019.

Godeke, A. et al. "Bi-2212 canted-cosine-theta coils for high-field accelerator magnets". English. In: *IEEE Transactions on Applied Superconductivity* 3-2.25 (2015), pp. 1–4. DOI: 10.1109/TASC.2014.2369955.

Hairer, E., C. Lubich, and G. Wanner. *Geometric Numerical Integration: Structure-Preserving Algorithms for Ordinary Differential Equations; 2nd ed.* Dordrecht: Springer, 2006. DOI: 0.4171/OWR/2006/14.

Hecht, E. *Optics*. Vol. 360. London, UK: Pearson Education, Inc., 2002.

Kleiss, R. et al. "On the Feasibility of Tracking with Differential Algebra Maps in Long Term Stability Studies for Large Hadron Colliders". In: (1992). DOI: 10.2172/82307.

Laface, E. *Accelerator recipes*. unpublished. 2018.

— *Four lectures in particle dynamics*. Lecture, Lund University. 2018. URL: http://www.hep.lu.se/courses/fyst17/BDLecture_1.pdf.

Lee, S.-Y. *Accelerator Physics*. World Scientific Publishing Company, 2011. DOI: 10.1142/3977.

Nolte, D. D. "The tangled tale of phase space". In: *Physics Today* 63.4 (2010), 33–38. DOI: 10.1063/1.3397041.

Phillips, J. C. et al. "Scalable molecular dynamics with namd". In: *Journal of computational chemistry* 26.16 (2005), pp. 1781–1802.

Reiser, M. *Theory and Design of Charged Particle Beams*. John Wiley & Sons, 2008.

Rosenzweig, J. *Fundamentals of Beam Physics*. Oxford,UK: University Press, 2003.

Sacherer, F. J. "Rms envelope equations with space charge". In: *IEEE Transactions on Nuclear Science* 18.3 (1971), pp. 1105–1107. DOI: 10.1109/TNS.1971.4326293.

Sagan, D. and D. Rubin. "Linear analysis of coupled lattices". In: *Physical Review Special Topics - Accelerators and Beams* 2.7 (July 1999), p. 074001. DOI: 10.1103/PhysRevSTAB.2.074001.

Sokolov, A. A. and I. M. Ternov. "Synchrotron radiation". In: *Soviet Physics Journal* 10.10 (1967), pp. 39–47. DOI: 10.1007/BF00820300.

Tolman, R. C. *The Principles of Statistical Mechanics*. Dover books on physics. New York, NY: Dover Publ., 1979. URL: http://cds.cern.ch/record/1546394.

Veksler, V. "A new method of relativistic particle acceleration". In: *Dokl. Akad. Nauk SSSR*. Vol. 43. 1944, pp. 346–348.

Wan, W. et al. "Alternating-gradient canted cosine theta superconducting magnets for future compact proton gantries". In: *Physical Review Special Topics - Accelerators and Beams* 18.10 (Oct. 2015), p. 103501. DOI: 10.1103/PhysRevSTAB.18.103501.

Wang, Y., J. Liu, and H. Qin. "Lorentz covariant canonical symplectic algorithms for dynamics of charged particles". In: *Physics of Plasmas* 23.12 (Dec. 2016). arXiv: 1609.07019, p. 122513. DOI: 10.1063/1.4972824.

Wangler, T. P. *RF Linear Accelerators*. John Wiley & Sons, 2008.

Wille, K. "The physics of particle accelerators: an introduction". In: (2000).

Wolski, A. "Alternative approach to general coupled linear optics". In: *Physical Review Special Topics-Accelerators and Beams* 9.2 (2006), p. 024001. DOI: 10.1103/PhysRevSTAB.9.024001.

— *Beam dynamics: In High Energy Particle Accelerators*. London, UK: Imperial College Press, 2014. URL: http://cds.cern.ch/record/1622200.

Yoshida, H. "Construction of higher order symplectic integrators". In: *Physics Letters A* 150.5 (Nov. 1990), pp. 262–268. DOI: 10.1016/0375-9601(90)90092-3.

Chapter 2

An Explicit, Lorentz-Invariant Symplectic Integrator

Appeals to Forest's dogma will be made throughout the remaining text, with the central tenet that simulations are only as good as their foundation upon best-accuracy integrators. To this we add the claim that accuracy and reproducibility improve when minimizing approximations (especially in addressing coupled transverse–longitudinal dynamics). This should ideally be done without sacrificing symplecticity (for long-term stability) and implementing Lorentz covariance (for reproducibility and energy/momentum conservation) where possible.

In fact, Wang's group recently developed a Lorentz-covariant symplectic integrator, which is stable (in terms of energy conservation), comparatively fast (fewer timesteps required versus a Runge–Kutta integrator to simulate an electron acceleration process), and reduces error to machine precision (in a plasma physics context).[1]

This approach amounts to constructing a Hamiltonian from a relativistic Lagrangian, and tracking a particle's proper time $\Delta\tau = \frac{\Delta t}{\gamma}$ in terms of its canonically conjugate four-momentum $\mathcal{P}^\alpha = mV^\alpha + \frac{q}{c}A^\alpha$ where q is charge, V^α is four-velocity, and A^α is the electromagnetic four-potential.

These findings were corroborated in the context of proton tracking through sextupole and octupole magnets by our group at ESS.[2] Here, we also found

[1] Wang, Liu, and Qin, "Lorentz covariant canonical symplectic algorithms for dynamics of charged particles".

[2] Folsom and Laface, "Beam dynamics with covariant hamiltonians".

a significant performance increase versus a nonlinear algorithm based on Lie-operators in truncated series. This benefit is attributable to the covariant algorithm having a fully evaluable solution for any multipole, whereas any Lie-operator result relies on at least a third-order series solution for rivaling accuracy.

Our recommendation for frugal use of approximations is also applicable here, albeit in a subtle way: a time-series approximation was inherent in our definition of symplecticity—as per Eq. (1.12). However, it can be shown that $\det |J| = 1$ exactly by straightforward linear algebra[3] (see also Appendix A.) The Lie-operator method, though, introduces an unavoidable time-series expansion, as in Eq. (1.54).

A veteran computational physicist may yet be dubious at these claims, namely that performance and accuracy gains could go hand-in-hand. To clarify: Wang's method brings performance gains because the timestep is rescaled automatically with changes in γ. Such an integrator still has the weakness of remaining fundamentally semi-implicit (the $\mathcal{P}^{\alpha}_{+1}$ is dependent on itself, thus requiring a costly Newtonian solver at each timestep).

As a counterpoint, Zhang's group has demonstrated a Hamiltonian-splitting scheme which overcomes this issue to produce a fully explicit symplectic integrator, but it is derived at the expense of sacrificing of Lorentz covariance.[4, †]

In the next section, we rectify this, attempting to produce a fully explicit *and* Lorentz covariant symplectic integrator.

This integrator will be used throughout the remaining chapters. In addition to seeking a robust nonlinear benchmark (within realistic computational limits), we introduce it at this point as a prerequisite to addressing issues such as whether space-charge calculation can be done symplectically or whether Liouville's theorem can be applied for envelope (density-based) tracking.

[3] Laface, *Four Lectures in Particle Dynamics*; Rim, "An elementary proof that symplectic matrices have determinant one".

[4] Zhang et al., "Explicit Symplectic Algorithms Based on Generating Functions for Relativistic Charged Particle Dynamics in Time-Dependent Electromagnetic Field".

[†] Their work also demonstrates that implicit and explicit symplectic integrators for charged particles have comparable error (both are greatly improved versus a 6th-order Runge–Kutta method) while showing that an explicit integrator has a approximately 50% reduction in CPU overhead.

2.1 Lorentz Invariant Hamiltonian

We can begin with Jackson's covariant Hamiltonian for a charged particle in an external field[5,6]

$$H = \frac{1}{m}\left(\mathcal{P}_\alpha - \frac{q}{c}A_\alpha\right)\left(\mathcal{P}^\alpha - \frac{q}{c}A^\alpha\right) - c\sqrt{\left(\mathcal{P}_\alpha - \frac{q}{c}A_\alpha\right)\left(\mathcal{P}^\alpha - \frac{q}{c}A^\alpha\right)} \tag{2.1}$$

where the conjugate momentum is

$$\mathcal{P}^\alpha = mV^\alpha + \frac{q}{c}A^\alpha \tag{2.2}$$

and where A^α is a function of the four-position $r_\alpha = (t, -x, -y, -z)$, $\mathcal{P}_\alpha = (\gamma + \Phi, -\vec{\mathcal{P}})$, $A_\alpha = (\Phi, -\vec{A})$,[†] and V^α is constrained by the light-cone condition:

$$V_\alpha V^\alpha = c^2 \tag{2.3}$$

This yields the following equations of motion in terms of proper time ($d\tau = \frac{dt}{\gamma}$)

$$\begin{aligned}\frac{dr^\alpha}{d\tau} &= \frac{\partial H}{\partial \mathcal{P}_\alpha} = \frac{1}{m}\left(\mathcal{P}^\alpha - \frac{q}{c}A^\alpha\right)\\ \frac{d\mathcal{P}^\alpha}{d\tau} &= -\frac{\partial H}{\partial r_\alpha} = \frac{q}{mc}\left(\mathcal{P}_\beta - \frac{q}{c}A_\beta\right)\partial^\alpha A^\beta\end{aligned} \tag{2.4}$$

where m is particle mass, and the ordering of indices α and β merits careful consideration. It may also be helpful to note that the alternative mass-shell Hamiltonian (in natural units)

$$H = \frac{1}{2m}(\mathcal{P}_\alpha - qA_\alpha)(\mathcal{P}^\alpha - qA^\alpha) \tag{2.5}$$

yields the same equations of motion.[7]

2.2 Discretizing and Explicitness

We can immediately test how these equations of motion will discretize, thanks to Heirer's "symplectic Euler" algorithm from Eq. (1.63). Here we use a condensed notation

$$\mathcal{P}^{k+1,\alpha} := \underset{+1}{\mathcal{P}}{}^{\alpha} \quad ; \quad \mathcal{P}^{k,\alpha} := \mathcal{P}^\alpha \tag{2.6}$$

[5] Jackson, *Classical Electrodynamics*, p585.

[6] Barut, *Electrodynamics and Classical Theory of Fields & Particles*, p68 ff.

[†] These are the *covariant* forms, distinguished by the subscripted summation index. The superscripted *contravariant* forms have no relative negative signs. A brief review of the related four-vector algebra identities will be provided shortly.

[7] Goldstein et al., "Classical Mechanics", p352.

and likewise for $r^{k+1,\alpha}$ and r^k. That is,

$$\underset{+1}{\mathcal{P}}{}^{\alpha} = \mathcal{P}^{\alpha} - \Delta\tau \frac{\partial H}{\partial r}\left(\underset{+1}{\mathcal{P}}{}^{\alpha}, r^{\alpha}\right) = \mathcal{P}^{\alpha} + \frac{\Delta\tau q}{mc}\left(\underset{+1}{\mathcal{P}}_{\beta} - \frac{q}{c}A_{\beta}\right)\partial^{\alpha}A^{\beta} \tag{2.7}$$

and for position:

$$\underset{+1}{r}{}^{\alpha} = r^{\alpha} + \Delta\tau \frac{\partial H}{\partial r}\left(\underset{+1}{\mathcal{P}}{}^{\alpha}, r^{\alpha}\right) = r^{\alpha} + \frac{\Delta\tau}{m}\left(\underset{+1}{\mathcal{P}}{}^{\alpha} - \frac{q}{c}A^{\alpha}\right) \tag{2.8}$$

We will soon derive a method for decoupling $\mathcal{P}_\beta$ from the right-hand side terms to make Eq. (2.7) explicit, but we should provide a more thorough comparison with the other related works beforehand. For now, simply note that our momentum expression is *implicit* while our position expression is *explicit*.

Equations (2.7) and (2.8) are the basis for the algorithms used by Wang's, Zhang's, and Zhou's groups.[8] Their works demonstrate—in the context of plasma physics—that symplecticity and Lorentz covariance ensure, respectively, long-term energy stability and frame-invariant tracking; explicitness meanwhile improves performance by avoiding the use of a numerical solver at each timestep.

Such integrators allow for the simulation of, for example, an accelerating electron with a convergent number of timesteps; whereas an implicit, noncovariant scheme needs a monotonically increasing timestep size and can also suffer numerical instabilities for sharp drops in γ.[†] Specifically, covariant tracking inherently includes the zero component of conjugate momentum:

$$\Delta t = \underset{+1}{t} - t = \Delta\tau\left(\underset{+1}{\mathcal{P}}_{0} - \Phi\right) = \Delta\tau\left(\underset{+1}{\gamma} + \underset{+1}{\Phi} - \Phi\right) \tag{2.10}$$

where $\underset{+1}{\Phi} - \Phi$ is typically negligible, so the timestep Δt can be smoothly updated as a function of γ and a constant proper-timestep $\Delta\tau$.

Only Zhou's group reports on a method which fulfills all our criteria (Wang's is symplectic and covariant, but not explicit; Zhang's is symplectic and explicit,

[8] Wang, Liu, and Qin, "Lorentz covariant canonical symplectic algorithms for dynamics of charged particles"; Zhang et al., "Explicit Symplectic Algorithms Based on Generating Functions for Relativistic Charged Particle Dynamics in Time-Dependent Electromagnetic Field"; Zhou et al., "Explicit symplectic methods for solving charged particle trajectories".

[†] This discrepancy related to sharp drops in γ arises since the smallest-scale dynamics is governed (in the plasma-dynamics case) by the electron's gyro-period:

$$T = \frac{2\pi\gamma m}{q|\vec{B}|} \tag{2.9}$$

which can suddenly drop to less than the timestep Δt.

but not covariant). This method requires splitting the Hamiltonian into its components, solving for velocities separately, and mapping them together.[9] We may consider this the ideal method for charged-particle integrators. Its only theoretical weakness is common to such splitting techniques: when calculating the change in velocity of an i-th component, the velocity of the other j spatial components must be treated as constant.[†]

Nevertheless, the resulting error from this approximation can be compensated by taking high-order symplectic mappings, with second-order mappings reaching machine-level precision for sufficiently small timesteps. The performance drawback here is that one must first solve for velocity then find the updated momenta in terms of velocity, then convert the solutions back into position–momentum space.

We can thus attempt to improve on this method by directly solving $\underset{+1}{\mathcal{P}}$ without relying on intermediate solutions for velocity (thus roughly halving the number of calculations needed per timestep).

Throughout this section we will also occasionally check against purely longitudinal potentials, which have the form $A^\alpha = A^z(x, y)$ for multipole magnets. This will also allow us to check against our recent work,[10] where an ideal a magnetic multipole's four-momentum tracks as

$$\begin{aligned} \underset{+1}{\mathcal{P}}{}^z &= \mathcal{P}^z \\ \underset{+1}{\mathcal{P}}{}^x &= \mathcal{P}^x + \frac{\Delta\tau q}{mc}\left(\underset{+1}{\mathcal{P}}{}^z - \frac{q}{c}A^z\right)\frac{\partial A^z}{\partial x} \end{aligned} \tag{2.11}$$

and likewise for $\mathcal{P}^y_{+1}$. This is effectively explicit because $\mathcal{P}^z_{+1} = \mathcal{P}^z$. However, anticipating that space-charge will introduce more complicated potentials,[‡] we will now derive a general solution.

[9] McLachlan and Quispel, "Splitting methods".

[†] The formalism underlying such mappings is straightforward, but lengthy. The reader is strongly encouraged to consult Zhang's work for a concise treatment.

[10] Folsom and Laface, "Beam dynamics with covariant hamiltonians".

[‡] Our more ambitious goal is a fast, symplectic treatment of space charge, which has potentials which are fully dense in terms of $\partial_\alpha A^\beta$.

Here and moving forward we follow Jackson's notation[11]

$$\begin{aligned}
\partial^\alpha &\equiv \frac{\partial}{\partial x_\alpha} = \left(\frac{\partial}{\partial x^0}, -\vec{\nabla}\right) \\
\partial_\alpha &\equiv \frac{\partial}{\partial x^\alpha} = \left(\frac{\partial}{\partial x^0}, \vec{\nabla}\right) \\
A^\alpha &= (A^0, \vec{A}) \quad ; \quad A_\alpha = (A_0, -\vec{A}) \\
\partial^\alpha A_\alpha &= \partial_\alpha A^\alpha = \frac{\partial A^0}{\partial x^0} + \vec{\nabla}\cdot\vec{A} = 0 \text{ (in the Lorenz gauge)} \\
\partial^\alpha A^\alpha &= \partial_\alpha A_\alpha = \frac{\partial A^0}{\partial x^0} - \vec{\nabla}\cdot\vec{A}
\end{aligned} \tag{2.12}$$

along with the Minkowski metric:

$$\begin{aligned}
g_{00} &= 1 \quad ; \quad g_{11} = g_{22} = g_{33} = -1 \\
g^{\alpha\beta} &= g_{\alpha\beta} = g_{\beta\alpha} \quad ; \quad g_{\alpha\gamma}g^{\gamma\beta} = \delta^\beta_\alpha \quad ; \quad \delta^\beta_\alpha \delta^\alpha_\beta = \delta^\alpha_\alpha = 4 \\
x_\alpha &= g_{\alpha\beta}x^\beta \quad ; \quad x^\alpha = g^{\alpha\beta}x_\beta \quad ; \quad x^\alpha = x^\beta \delta^\alpha_\beta
\end{aligned} \tag{2.13}$$

Since the r^α_{+1} expression is explicit as-is, we can focus solely on the momentum, first rearranging the terms in Eq. (2.7) and extracting $g_{\alpha\beta}$'s so that all $\mathcal{P}$ terms are covariant:

$$\begin{aligned}
\underset{+1}{\mathcal{P}}{}^\alpha - \left(\frac{\Delta\tau q}{mc}\right)\underset{+1}{\mathcal{P}}_\beta \partial^\alpha A^\beta &= \mathcal{P}^\alpha - \left(\frac{\Delta\tau q^2}{mc^2}\right) A_\beta\, \partial^\alpha A^\beta \\
g^{\beta\alpha}\underset{+1}{\mathcal{P}}_\beta - \left(\frac{\Delta\tau q}{mc}\right)\underset{+1}{\mathcal{P}}_\beta \partial^\alpha A^\beta &= g^{\beta\alpha}\mathcal{P}_\beta - \left(\frac{\Delta\tau q^2}{mc^2}\right) A_\beta\, \partial^\alpha A^\beta
\end{aligned} \tag{2.14}$$

we then introduce a dummy index λ and left-hand multiply both sides by $g^{\lambda\alpha}/g_{\lambda\alpha}$, which are identical and which can commute past β-only factors. This yields

$$\delta^\beta_\lambda \underset{+1}{\mathcal{P}}_\beta - \left(\frac{\Delta\tau q}{mc}\right)\underset{+1}{\mathcal{P}}_\beta \partial_\lambda A^\beta = \delta^\beta_\lambda \mathcal{P}_\beta - \left(\frac{\Delta\tau q^2}{mc^2}\right) A_\beta\, \partial_\lambda A^\beta \tag{2.15}$$

where δ^β_λ is analogous to the identity matrix here, and thus $\delta^\beta_\lambda \mathcal{P}_\beta = \mathcal{P}_\beta \delta^\beta_\lambda$. We now have

$$\underset{+1}{\mathcal{P}}_\beta \left(\delta^\beta_\lambda - \frac{\Delta\tau q}{mc}\partial_\lambda A^\beta\right) = \mathcal{P}_\beta \delta^\beta_\lambda - \left(\frac{\Delta\tau q^2}{mc^2}\right) A_\beta\, \partial_\lambda A^\beta \tag{2.16}$$

which, for $\lambda = x$ and $A^\beta = A_z(x, y)$ still reduces to Eqn. 2.11. We can then right-hand multiply both sides by $(\delta^\lambda_\beta + \frac{\Delta\tau q}{mc}\partial_\lambda A^\beta)$, leaving

$$\underset{+1}{\mathcal{P}}_\beta \left(4 - \frac{\Delta\tau^2 q^2}{m^2c^2}(\partial^\beta \cdot A^\beta)^2\right) = \left(\mathcal{P}_\beta \delta^\beta_\lambda - \frac{\Delta\tau q^2}{mc^2} A_\beta\, \partial_\lambda A^\beta\right)\left(\delta^\lambda_\beta + \frac{\Delta\tau q}{mc}\partial_\lambda A^\beta\right) \tag{2.17}$$

[11] Jackson, p539 ff.

where we note that $(\partial^\beta \cdot A^\beta)^2$ is a scalar.[†]

It is tempting to check for other solutions here, noting that any cross-terms on the left hand side will contract to the form $\partial_\lambda A^\lambda = \partial^\lambda A_\lambda = 0$. However, the solution shown cancels *component-wise* and is thus the strongest choice unless solving for total momentum.

At this point, we can isolate $\underset{+1}{\mathcal{P}_\beta}$ by division, and expand the right-hand side terms:

$$\underset{+1}{\mathcal{P}_\beta} = \frac{4\mathcal{P}_\beta + \frac{\Delta\tau q}{mc}\mathcal{P}_\beta \delta^\beta_\lambda \partial_\lambda A^\beta - \frac{\Delta\tau q^2}{mc^2} A_\beta\, \partial_\lambda A^\beta \delta^\lambda_\beta - \frac{\Delta\tau^2 q^3}{m^2c^3} A_\beta\, (\partial^\beta \cdot A^\beta)^2}{4 - \frac{\Delta\tau^2 q^2}{m^2c^2}\,(\partial^\beta \cdot A^\beta)^2} \tag{2.18}$$

We can assert here that $(A_\beta \partial_\lambda A^\beta)\delta^\lambda_\beta = \delta^\lambda_\beta x(\partial_\lambda A^\beta A_\beta)$, which can be verified by resolving the Kronecker deltas as $\delta^\lambda_\beta = g^{\lambda\alpha} g_{\alpha\beta}$. Then we right-hand multiply by $\delta^\lambda_\beta g^{\alpha\beta} = g^{\lambda\alpha} g_{\alpha\beta} g^{\alpha\beta}$ to return $\underset{+1}{\mathcal{P}}$ to contraviant form

$$\underset{+1}{\mathcal{P}^\alpha} = \frac{\mathcal{P}^\alpha + \frac{\Delta\tau q}{mc}\left(\mathcal{P}_\beta - \frac{q}{c}A_\beta\right)\partial^\alpha A^\beta - \frac{\Delta\tau^2 q^3}{4m^2c^3} A^\alpha\,(\partial^\beta \cdot A^\beta)^2}{1 - \frac{\Delta\tau^2 q^2}{4m^2c^2}\,(\partial^\beta \cdot A^\beta)^2} \tag{2.19}$$

This is the promised algorithm for Lorentz-covariant, symplectic, and explicit tracking.

In the context of idealized multipole magnets, where $A^\alpha = A^z(x, y)$ and thus $\partial^z A^z = 0$ this solution is identical to Eq. (2.7). Specifically, the x- and z-components of a particle in such a multipole momentum transform as in Eq. (2.11):

$$\underset{+1}{\mathcal{P}^x} = \mathcal{P}^x + \frac{\Delta\tau q}{mc}\left(\mathcal{P}^z - \frac{q}{c}A^z\right)\frac{\partial A^z}{\partial x} \quad ; \quad \underset{+1}{\mathcal{P}^z} = \mathcal{P}^z \tag{2.20}$$

As a side note: the choice of contracting the Kronecker delta in the term $\frac{\Delta\tau q}{mc}\mathcal{P}_\beta \delta^\beta_\lambda \partial_\lambda A^\beta$ from Eq. (2.18) is not arbitrary; had we applied it to the four-gradient instead of the momentum, Eq. (2.20) would become trivial: $\underset{+1}{P^x} = P^x; \underset{+1}{P^z} = P^z$. This exposes the limitation of the using an idealized (i.e. planar)

[†]Explicitly:

$$\begin{aligned}\partial_\lambda A^\beta\, \partial_\lambda A^\beta &= g_{\beta\lambda}\partial^\beta A^\beta g_{\beta\lambda}\partial^\beta A^\beta \\ &= (\partial^\beta \cdot A^\beta)^2 \neq 0\end{aligned}$$

multipole potential–and further justifies avoiding $\partial_\alpha A^\alpha$ terms. In fact, Eq. (2.4) can be reformulated using Eqs. (2.2) and (2.3) to form the identity

$$\frac{4V^\beta V^\alpha}{c^2}\partial_\beta A^\beta = 0 = \partial^\alpha A^\beta \tag{2.21}$$

which is not true for the most commonly used multipole magnet potentials.[†]

This indicates that any potential $A^\alpha = A_z(\tau, x, y, z)$. That is, any transverse-dependent A_z must either have all its components sum to zero or have a nonzero z and τ dependence). We can take this as an incentive for deriving a 3D multipole magnet potential from the typical idealized one (see Appendix C). Fortunately, it can be shown that for accelerator elements, $\partial_z A^z$ is typically negligible with respect to its transverse derivatives. In general, it should be observed that Eq. (2.19) is not unique; the essential process is separating the updated momentum term from the prior-step terms.

2.3 Global Error

Equation (2.19) and the already explicit r^α_{+1} four-position from Eq. (2.7) now fulfill the ideal criteria: long-term stability (symplecticity), frame independence (Lorentz invariance), and efficiency/precision (explicitness). These expressions thus constitute the core algorithm to be examined through the remainder of this work. Figure 2.1 compares the global error $\mathcal{G}$ in position

$$\mathcal{G} = \underset{n}{r^x} - \left[r^x + \Delta\tau\, f\left(r^x, \underset{+1}{\mathcal{P}^x}\right) + \Delta\tau\, f\left(\underset{+1}{r^x}, \underset{+2}{P^x}\right) \ldots \Delta\tau\, f\left(\underset{n}{r^x}, \underset{n+1}{P^x}\right)\right] \tag{2.23}$$

with $\mathcal{P}^x_{+1}$ coming from Eq. (2.20) and from Eq. (1.55) for the explicit and Lie-series cases, respectively. The Lie-series has a tendency to diverge unless choosing impractically small timesteps. This may be due to the fact that it is inherently transverse-only (it requires a Hamiltonian which is *scaled* to p_z and must be periodically updated; whereas the covariant integrator is *dependent on* p_z).

[†]These will be discussed at length in Chapter 4. In cylindrical coordinates, the basic form is

$$A_z = -\frac{NIr^n e^{in\theta}}{cr_0^n} \tag{2.22}$$

where N and I are number of coils and their current, respectively; r_0 is the pole-tip aperture radius; and r and θ are radial and azimuthal coordinates. For now, note simply that $\partial^r A^z + \partial^\theta A^z \neq 0$.

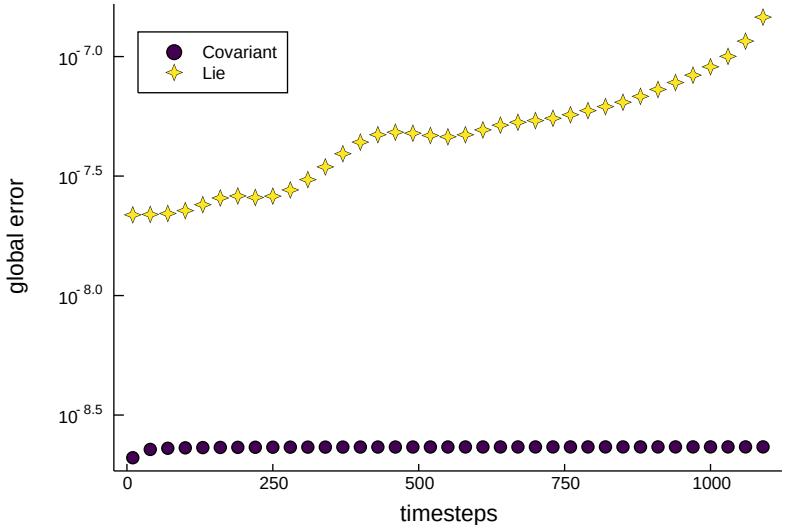

Figure 2.1: Comparison of global error for covariant–explicit and third-order Lie-series integrators. To reach error-precision limits, 1000-proton Gaussian distributions are used with minimal transverse and longitudinal momentum of $0.3\text{keV}\ /\ \text{c}$, step size $\Delta\tau = 0.1$ fs, and average transverse beam size $\sigma_x = \sigma_y = 0.001$ mm passing through an octupole magnet of exaggerated field-on-pole strength $|\beta_0| = 25$ T and pole-tip aperture of 10 mm.

Equation (2.20) can be represented in array form as

$$\begin{pmatrix} \mathcal{P}^x_{+1} \\ \mathcal{P}^y_{+1} \\ \mathcal{P}^z_{+1} \\ r^x_{+1} \\ r^y_{+1} \\ r^z_{+1} \end{pmatrix} = \text{diag} \begin{pmatrix} \left(1 - \frac{\Delta\tau q}{mc}(\mathcal{P}^z - \frac{q}{c}A^z)\frac{\partial A^z}{\partial x}\right) \\ \left(1 - \frac{\Delta\tau q}{mc}(\mathcal{P}^z - \frac{q}{c}A^z)\frac{\partial A^z}{\partial y}\right) \\ 1 \\ 1 + \frac{\Delta\tau}{m}\mathcal{P}^x_{+1} \\ 1 + \frac{\Delta\tau}{m}\mathcal{P}^y_{+1} \\ 1 + \frac{\Delta\tau}{m}(\mathcal{P}^z_{+1} - \frac{q}{c}A^z) \end{pmatrix} \begin{pmatrix} \mathcal{P}^x \\ \mathcal{P}^y \\ \mathcal{P}^z \\ r^x \\ r^y \\ r^z \end{pmatrix} \tag{2.24}$$

which implies a compatibility with tracking via concatenated transfer matrices using truncated power-series algebra (TPSA).[12] In the general case of Eq. (2.19), where A^α has a t or z dependence, the transfer matrix takes a 4×4 shape, with numerator and denominator terms that must be truncated independently. It should also be noted that truncation is not necessary: so long as A^α has differentiable components, this array represents an exact analytical solution.

[12] Berz, "The Method of Power Series Tracking for the Mathematical Description of Beam Dynamics".

2.4 Envelope Solution

For a fastest-possible envelop method, which transports a bunch in terms of its phase-space density instead of individual particle trajectories, Eq. (2.4) can be applied to the Liouville equation:

$$\frac{d\rho}{dt} = \frac{\partial\rho}{\partial t} + \sum_{i=1}^{n}\left(\frac{\partial\rho}{\partial r_i}\dot{r}_i + \frac{\partial\rho}{\partial\mathcal{P}_i}\dot{\mathcal{P}}_i\right) = 0 \tag{2.25}$$

For example, if we use a time-independent bi-Gaussian

$$\rho(r^\alpha, \mathcal{P}^\alpha) = e^{-(r^\alpha)^2-(\mathcal{P}^\alpha)^2} \tag{2.26}$$

then we have

$$r^\alpha\dot{r}^\alpha = \mathcal{P}^\alpha\dot{\mathcal{P}}^\alpha \tag{2.27}$$

where the ρ factors have canceled. Thus, by Eqs. (2.4)

$$\begin{aligned} r^\alpha &= \mathcal{P}^\alpha\frac{q}{m^2c^3}\left(\mathcal{P}_\beta - \frac{q}{c}A_\beta\right)\partial^\alpha A^\beta\left(\mathcal{P}^\alpha - \frac{q}{c}A^\alpha\right) \\ &= \mathcal{P}^\alpha\frac{q}{c^3}V_\beta V^\alpha\partial^\alpha A^\beta = \mathcal{P}^\alpha\frac{4q}{c}\partial_\alpha A_\beta \end{aligned} \tag{2.28}$$

where to arrive at the first line we have used the constraint

$$\left(\mathcal{P}^\alpha_{+1} - \frac{q}{c}A^\alpha\right)\left(\mathcal{P}_\alpha - \frac{q}{c}A_\alpha\right) = m^2c^2 \tag{2.29}$$

and for the second line, we have allowed V^α to commute, then used an alternative form of Eq. (2.21).

This value for r^α can be transcribed as r_β then substituted in to Eq. (2.19), to yield

$$\mathcal{P}^{\ \alpha}_{+1} = \frac{\mathcal{P}^\alpha + \frac{\Delta\tau}{4m}r_\beta - \frac{\Delta\tau q^2}{mc^2}A_\beta\partial^\alpha A^\beta - \frac{\Delta\tau^2q^3}{4m^2c^2}A^\alpha\left(\partial^\alpha\cdot A^\alpha\right)^2}{1 - \frac{\Delta\tau^2q^2}{4m^2c^2}(\partial^\alpha\cdot A^\alpha)^2} \tag{2.30}$$

which may not seem like a drastic simplification. However, in eliminating $\mathcal{P}^\alpha\frac{q}{c}\partial^\alpha A^\beta$, there are no longer any vector products to be calculated at each step—recalling that $(\partial^\alpha\cdot A^\alpha)^2$ is a scalar while $A_\beta\partial^\alpha A^\beta$ does not typically need to be updated stepwise.[†]

[†]Meanwhile, the form for r^α_{+1} is unchanged from Eq. (2.8):

$$r^{\ \alpha}_{+1} = r^\alpha + \frac{\Delta\tau}{m}\left(\mathcal{P}^{\ \alpha}_{+1} - \frac{q}{c}A^\alpha\right) \tag{2.31}$$

For cases of non-Gaussian distributions, the unaltered form of Eq. (2.19) suffices. The explicit canonical momenta $\mathcal{P}^{\alpha}_{+1}$ can be obtained either way, and the updated expressions can be inserted into the distribution. That is

$$\rho(r^{\alpha}, \mathcal{P}^{\alpha}) \xrightarrow{\Delta\tau} \rho\left(\underset{+1}{r}{}^{\alpha}, \underset{+1}{\mathcal{P}}{}^{\alpha}\right) \tag{2.32}$$

where a new phase-space density can either be taken from the deviation values (Gaussian); or the exponential in ρ can be populated with nonlinear (polynomial) terms and thus requires TPSA (non-Gaussian).

For distributions with a non-exponential shape on any axis, $\frac{\partial\rho}{\partial r_i}$ and $\frac{\partial\rho}{\partial\mathcal{P}_i}$ are no longer of the form $f(r_i)\rho_i$ and $f(\mathcal{P}_i)\rho_i$, and finding explicit solutions becomes case-dependent.

Such density-based solutions are included here mainly as a pedagogical companion to those commonly used in linear tracking—their practical value beyond Eq. (2.30) or similar simplifications is likely to be limited. For example, in terms of analysis, any component of ρ will typically be dependent on several other components. That is, in general

$$\underset{+1}{r_x} = r_x + f(r_0, r_x, r_y, r_z, P_0, P_x, P_y, P_z) \tag{2.33}$$

which makes ρ quantities more difficult to visualize than explicit plots of individual trajectory values. In other words, the notion of 2D phase-space density becomes ambiguous since any coordinate has an intrinsic 8D dependency.

Fortunately, when using a covariant integrator there is less demand to begin with for envelope tracking. That is, since the degree and number of polynomials for any r^{α}_{+1} or P^{α}_{+1} do not change at each timestep (because the old value is additive with the new expression), only the *coefficients* are updated. This is a strong contrast to the case of TPSA Lie-series tracking, where every timestep yields a lengthier polynomial expression than the previous one (because the old value is used as an input in a recursive Poisson-bracket expression), requiring truncation and an occasional "reset" of global error by numerical evaluation.

Thus, in the covariant case, a concatenation of several thin-film element slices for a single machine element is mapped by an updating set of coefficients (which *will* become more a more lengthy polynomial for changing potentials, but not stepwise). Since this can be considered a fully analytical solution, it precludes the more performance-driven need for envelope tracking. In other words, covariant envelope tracking is only likely to be beneficial for simplifications such as Eq. (2.30) on the grounds of computational performance.

References

Barut, A. O. *Electrodynamics and Classical Theory of Fields & Particles*. Mineola, NY, USA: Dover, 2010; reprint, New York: MacMillan, 1964.

Berz, M. "The method of power series tracking for the mathematical description of beam dynamics". In: *Nuclear Instruments and Methods in Physics Research Section A: Accelerators, Spectrometers, Detectors and Associated Equipment* 258.3 (Aug. 1987), pp. 431–436. DOI: 10.1016/0168-9002(87)90927-2.

Folsom, B. and E. Laface. "Beam dynamics with covariant hamiltonians". In: *Proc. 9th International Particle Accelerator Conference (IPAC'18), Vancouver, BC, Canada, April 29-May 4, 2018*. International Particle Accelerator Conference 9. Geneva, Switzerland: JACoW Publishing, 2018, pp. 3123–3126. DOI: 10.18429/JACoW-IPAC2018-THPAF064.

Goldstein, H. et al. "Classical mechanics". In: *American Journal of Physics* 70 (2002).

Jackson, J. D. *Classical Electrodynamics*. New York, NY, USA: John Wiley & Sons Inc., 1999, pp. 579–585,661–663.

Laface, E. *Four lectures in particle dynamics*. Lecture, Lund University. 2018. URL: http://www.hep.lu.se/courses/fyst17/BDLecture_1.pdf.

McLachlan, R. I. and G. R. W. Quispel. "Splitting methods". In: *Acta Numerica* 11 (2002), 341–434. DOI: 10.1017/S0962492902000053.

Rim, D. "An elementary proof that symplectic matrices have determinant one". In: *Advances in Dynamical Systems and Applications (ADSA)* 12.1 (2017), pp. 15–20. URL: https://www.ripublication.com/adsa17/adsav12n1_03.pdf.

Wang, Y., J. Liu, and H. Qin. "Lorentz covariant canonical symplectic algorithms for dynamics of charged particles". In: *Physics of Plasmas* 23.12 (Dec. 2016). arXiv: 1609.07019, p. 122513. DOI: 10.1063/1.4972824.

Zhang, R. et al. "Explicit symplectic algorithms based on generating functions for relativistic charged particle dynamics in time-dependent electromagnetic field". In: *Physics of Plasmas* 25.2 (Feb. 2018), p. 022117. ISSN: 1070-664X. DOI: 10.1063/1.5012767.

Zhou, Z. et al. "Explicit symplectic methods for solving charged particle trajectories". In: *Physics of Plasmas* 24.5 (2017), p. 052507. DOI: 10.1063/1.4982743.

Chapter 3

Space Charge and Radiation

Space charge refers to the collective interparticle effects in a distribution of charged particles. The discussion of space charge has been deliberately avoided up to this point because of its incongruence with conventional beam dynamics theory (i.e. it is inherently non-linear and seemingly non-symplectic). Its calculation also requires a pairwise summation of distances from all particles in a distributions—a prohibitively costly operation in essentially all practical cases.

In contrast with plasma physics, where space charge can be difficult to predict and requires nuanced modeling, accelerator physics is primarily concerned with individual species of charged particles,[†,1] allowing for a variety of approximation methods.

For example, one can overlay space-charge calculations onto the more straightforward (and much less costly) calculations from external forces. This approach, in the context of storage rings, is well-summarized by Wolski:[2]

> Without including radiation effects in our analysis, we cannot completely determine the equilibrium distribution; however, we can calculate the shape of an invariant distribution, that is, a distribution of particles in phase space that remains unchanged as the particles move around the storage ring. The equilibrium distribution will be an invariant distribution covering a certain area of phase space. We

[†] At least until the point of collision, or in exotic cases such as electron lensing.

[1] Burov et al., "Landau damping by electron lenses"; Mirarchi et al., "Hollow electron-lens assisted collimation and plans for the LHC"; Stancari et al., "Collimation with Hollow Electron Beams".

[2] Wolski, *Beam dynamics: In High Energy Particle Accelerators*, p431.

> can estimate the area from considering synchrotron radiation effects separately. In other words, we determine the shape of the equilibrium distribution from space-charge effects, and the size of the distribution from synchrotron radiation effects. Taking this approach avoids the need to solve equations that include simultaneously space-charge and synchrotron radiation effects[...]

In simplest terms, space charge is a fundamental limit in the confinement regime of beam physics: the notion of tightly focusing and steering bunches might immediately call to mind to a novice that the repulsive Coulomb force must at some point be indomitable by even the strongest available superconducting magnets. While this is essentially true, space-charge effects are often negligible for high-energy accelerators except in the injection stage, especially for smaller β_t amplitudes.[3, †]

Nevertheless, to study higher-brightness beams and higher-precision machines, a more fundamental picture of space charge is necessary. Although the theory on space-charge-limited beams is robust,[4] especially for injectors, its effects are often seen as puzzling or fundamentally chaotic. The most precise space-charge simulations—which are particularly important in the the nascent discipline of plasma-wakefield acceleration—generally use Poisson solvers (requiring boundary conditions and numerical approximations of fields). These typically use a particle-in-cell (PIC) method to interpolate field values at rectilinear meshpoints onto particle trajectories; and often exploit symmetric beam distributions (i.e. Gaussian) to simplify calculation.[5]

[3] Wolski, p416.

[†] Tune-shift is a one of the most pervasive side-effects of space charge. This is linearly proportional to the *perveance* $K = 2I_r/(\beta_t^3\gamma^3 r)$ where r is the beam radius and I_r is the ratio of total current to a characteristic maximal current. For electrons, this characteristic current is the Alfvén current of $\sim$15.045 kA. It is clear that this dependence on K is minimized for increasing β and γ in a high-energy beam. It should also be stressed that this estimation technique requires small space-charge forces, treats β_t as a constant, and assumes a continuous (not bunched) beam.

[4] Tiefenback and Keefe, "Measurements of Stability Limits for a Space-Charge-Dominated Ion Beam in a Long A. G. Transport Channel"; Bazarov, Dunham, and Sinclair, "Maximum Achievable Beam Brightness from Photoinjectors"; Sigmond, "Simple Approximate Treatment of Unipolar Space-charge-dominated Coronas"; Lagniel, "Chaotic Behaviour and Halo Formation from 2D Space-Charge Dominated Beams"; Gadjev et al., "High-gain FEL in the space-charge dominated Raman limit".

[5] Keinigs and Jones, "Two-dimensional Dynamics of the Plasma Wakefield Accelerator"; Tarkeshian et al., "Transverse Space-Charge Field-Induced Plasma Dynamics for Ultraintense Electron-Beam Characterization"; Lu et al., "Nonlinear Theory for Relativistic Plasma Wakefields in the Blowout Regime"; Blue et al., "Plasma-Wakefield Acceleration of an Intense Positron Beam"; Pukhov and Farmer, "Stable Particle Acceleration in Co-Axial Plasma Chan-

3.1 The Liénard–Wiechert Potentials and Two-Particle Systems

In terms of *ab initio* methods, recent simulations using Lorentz-boosted frames have also been shown to reduce numerical instability and provide 4–6 order of magnitude speedups,[6] along with high parellelizability.[7] Similar techniques have also shown promise with accelerator elements such as undulators[8] or electron guns[9] when using the Liénard–Weichert (LW) potentials.[10]

These can be seen as the Lorentz-covariant extension of the Coulomb potentials (they actually comprise a single electromagnetic four-potential). They are, in effect, the best-known method for simulating charged-particle interactions; and are essentially just a retarded-time extension of the Coulomb potential. An LW-based integrator is thus an ideal candidate for fulfilling Forest's dogma of having a failsafe or baseline simulation to compare against linear or other heavily approximate methods.

The LW potentials are, in Gaussian units[†],[11]

$$\Phi = \left[\frac{q}{\left(1-\vec{\beta}_{s(t)}\cdot\hat{n}\right)R}\right]_{t=t_r} \quad ; \quad \vec{A} = \left[\frac{q\,\vec{\beta}_{s(t)}}{\left(1-\vec{\beta}_{s(t)}\cdot\hat{n}\right)R}\right]_{t=t_r} \tag{3.1}$$

where it is necessary to define position four-vectors s^α and r^α for the source and test particles, respectively, and where the light-cone constraint implies

$$R \equiv |\vec{r}-\vec{s}(t_r)| = r_0 - s_0(t_r) = c(t-t_r) \tag{3.2}$$

---

nels"; Birdsall, "Particle-in-cell charged-particle simulations, plus Monte Carlo collisions with neutral atoms, PIC-MCC"; Malka et al., "Principles and Applications of Compact Laser–plasma Accelerators".

[6] Vay et al., "Numerical methods for instability mitigation in the modeling of laser wakefield accelerators in a Lorentz-boosted frame".

[7] Debus et al., "Simulating radiation from laser-wakefield accelerators".

[8] Ryne, "Finding Matched Rms Envelopes in Rf Linacs".

[9] Salah, "Analysis of Space Charge Fields Using the Lienard-Wiechert Potential and the Method of Images During the Photoemission of the Electron Beam from the Cathode".

[10] Kosyakov, "Classical Yang-Mills Field Generated by Two Colored Point Charges"; Feynman, Leighton, and Sands, *The Feynman Lectures on Physics, Vol. 2: Mainly Electromagnetism and Matter*; Jackson, *Classical Electrodynamics*.

[†] The reader is encouraged to familiarize themselves with these units: it is easier to do unit checks throughout upcoming calculations (especially so terms in a Hamiltonian remain energy-like). We use these units as a default throughout, with exceptions primarily for reporting SI values for magnet field strength and standard constants such as dipole moments.

[11] Talman, *M.K.S / Gaussian Unit Conversion*; Napolitano, *SI and CGS Units in Electromagnetism*; Littlejohn, *Gaussian, SI and Other Systems of Units in Electromagnetic Theory*.

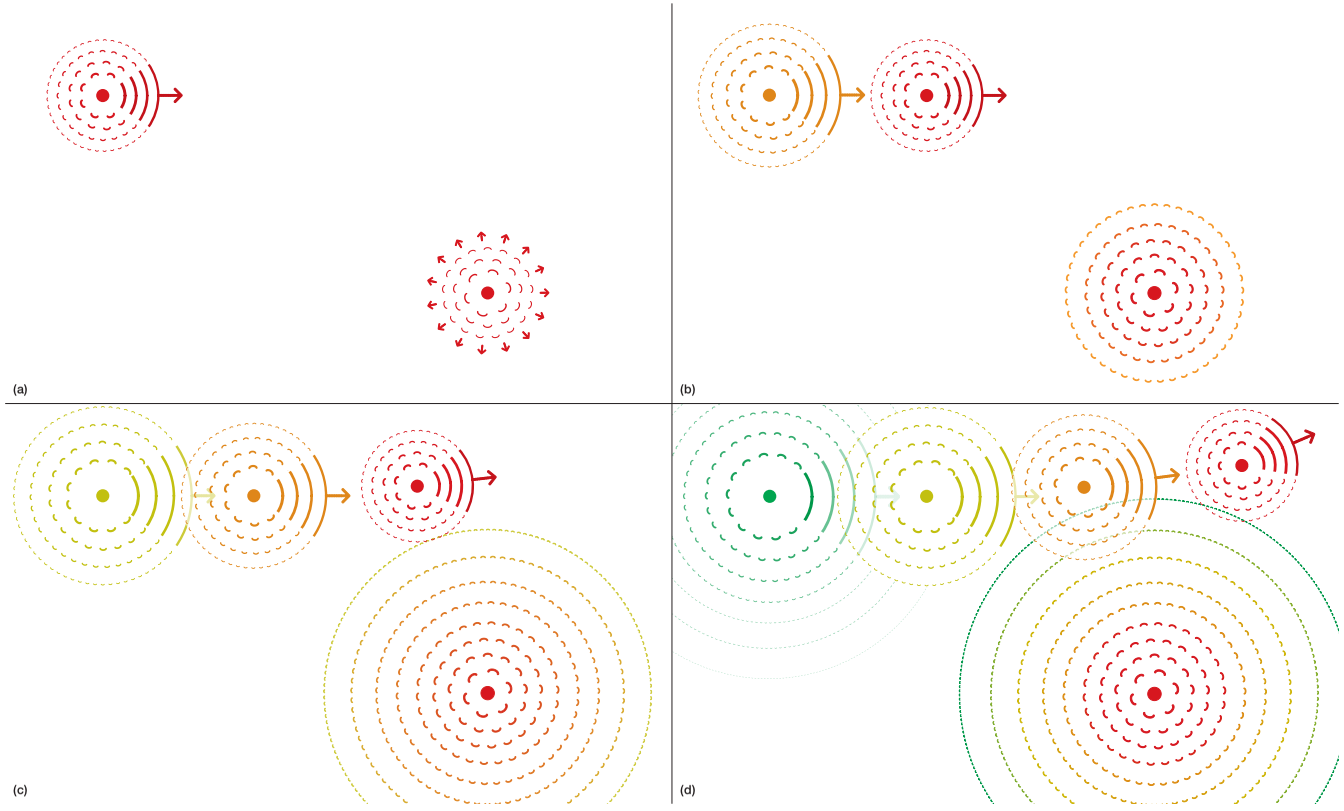

Figure 3.1: A sketch of protons interacting as per the Liénard–Weichert potentials. Color-coded red→orange→yellow→green with red as the latest and green as the oldest timestep. Dashed wedges and solid arrows indicate scalar and vector potentials, respectively. The spacing between potential lines is arbitrary; these should not be interpreted as time-dependent wavefronts: at this scale, the Liénard–Wiechert potentials propagate at c continuously.

Here, t_r the retarded time, is always in reference to the trajectory of the source particle, and $\hat{n}$ is the unit vector separating the particles pointing *from the source to the test point*:

$$\hat{n} = \frac{\vec{r} - \vec{s}}{|R|} \tag{3.3}$$

Figure 3.1 sketches an elementary case of space-charge: repulsion between two like-charged particles (protons in this case) with one at rest. Note that the incoming proton's *scalar* magnitude is roughly double that of the rest proton (here the incoming β is 0.5). As long as the two particles are assumed to comprise a completely isolated system, the distance scale here is essentially arbitrary in the upper limit; however, it is crucial to note that here and going forward we do not consider any effects on the femtometer scale unless explicitly noted.

A subtle, but non-trivial effect to note in terms of velocity dependence is that the test particle does not witness any potential from the source—as in Fig. 3.1(d)—until the source particle has already begun to deflect from its original trajectory. Such effects are worth considering when implementing the LW potentials in simulation, where a cache of several timesteps is necessary for the pairwise calculations.

The interaction between vector-potential components is more complicated: if we were to shift to the center-of-mass frame for the two protons, all longitudinal vector components cancel, leaving two perfectly collimated repulsive potential-fronts, see Fig.3.2(a–c). If we were switch one particle to an electron, then all transverse components cancel, as in Fig.3.2(d–f), leaving two perfectly collimated attractive fronts.

Before proceeding, we offer a disclaimer: although pursuing a first-principles electrodynamics formalism, we will ignore self-fields and will not presume to broach quantum spin or any other quantum effects unless explicitly stated. Instead, we will only operate under the assumption that, on a pico- or nanometer scale, charged relativistic point particles may freely rotate and propagate in accordance with their field interactions. Still, there are a number of cases where the LW potentials are relevant to quantum phenomenon, which will be cited where appropriate.

For now, we stress that the LW potentials are the basis for classical soft bremsstrahlung theory,[12] whereas the quantum-field theory picture has an en-

[12]Itzykson and Zuber, *Quantum Field Theory*, p36–39.

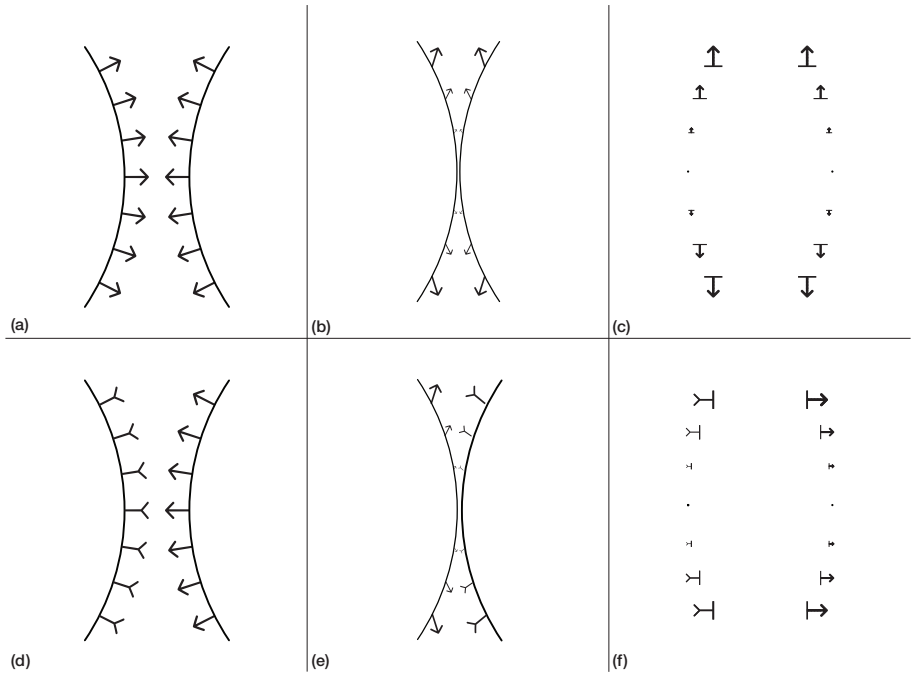

Figure 3.2: A sketch of velocity-dependent vector potentials emitted from two charged particles approaching head-on along the horizontal axis, as per the Liénard–Wiechert potentials, with timesteps proceeding left to right. The respective particle velocities are relativistic, but appreciably less than the speed of light, such that the potentials interact well in advance of collision. (a–c) Shows a like-charge interaction where all horizontal components cancel. In the opposite-charge interaction (d–f) all vertical components cancel (the tail-first arrows in the latter case indicate negative charge). Scalar potentials are not shown.

tirely analogous formulation.[13] Thus, one can view the LW potentials as a relativistic precursor to quantum radiative interactions, operating in the regime where the two interacting particles' trajectories remain distinguishable.

Continuing in classical terms, for a high enough deflection angle between two protons, a photon is emitted. In general (not only with like-sign particles), this constitutes classical radiation.[15]

Figure 3.3 then illustrates (externally stimulated) electron–proton interactions in the rest frame of the proton, with Fig. 3.3a demonstrating a deflection in which bremsstrahlung radiation is emitted. In Fig. 3.3b, the deflection is strong enough that the electron cannot escape the proton's orbit, and the emitted light is termed "recombination radiation".[16]

[13]Peskin and Schroeder, *An Introduction to Quantum Field Theory*, p179–83.

[15]James et al., "General Description of Electromagnetic Radiation Processes Based on Instantaneous Charge Acceleration in 'endpoints'".

[16]Yousif et al., "Experimental Observation of Laser-Stimulated Radiative Recombination"; Schramm et al., "Observation of Laser-Induced Recombination in Merged Electron and Proton

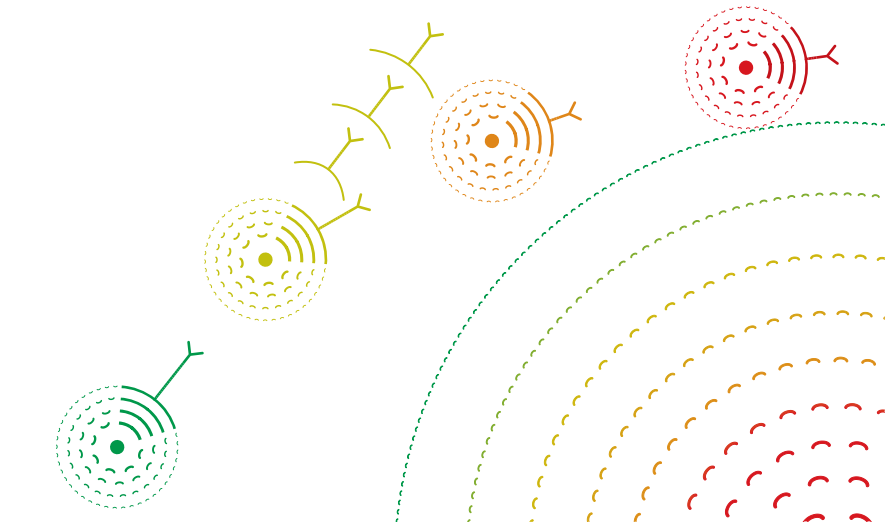

(a)

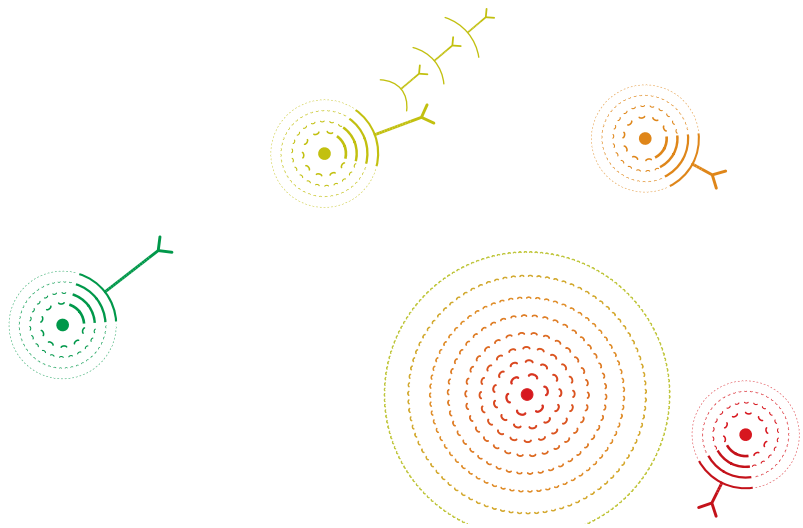

(b)

Figure 3.3: Electron–proton interactions as modeled by the Liénard–Wiechert potentials, seen from the proton's rest frame. As in the previous figure, dashed wedges indicate scalar potentials and solid curves and arrows indicate velocity-dependent ones. The electron's negatively charged potentials have convex wedges and inverse arrow tips. (a) An electron passes near enough to a proton to change direction significantly and emit bremsstrahlung radiation.[14] (b) An electron falls into a stable orbit and emits recombination radiation.

Although such effects are not typically relevant in beam physics simulation, we will examine the proton–electron system a bit further. We do this on the grounds

Beams"; Lang, *NASA's Cosmos*.

that a first-principles framework for space charge is fundamentally incomplete if only considering the predominantly repulsive potentials between like-charged species. Such analysis may also have bearing on plasma-wakefield accelerator simulations[17] and loss phenomenon such as interparticle stripping of H− ions.[18]

For example, in some cases we cannot neglect the emitted retarded potentials dependent on magnetic dipole moments.† These are:[19]

$$\vec{A} = \frac{\vec{\mu} \times \hat{n}}{(1 - \vec{\beta}_s \cdot \hat{n})R^2} + \frac{d}{dt}\left(\frac{\vec{\mu} \times \hat{n}}{(1 - \vec{\beta}_s \cdot \hat{n})Rc}\right) \tag{3.4}$$

where $\vec{\mu}$ is the source particle's magnetic dipole moment, and all terms are evaluated at the retarded time.

We then note that any $\vec{\mu}$ tends to align with a dominant external magnetic field, and that the kinetic potential resulting from such an interaction is $U = \vec{\mu} \cdot \vec{B}_{ext}$ (keep in mind this is *not* an emitted potential). Then, under the assumption that the dominant fields are varying smoothly, we can treat $\vec{\mu} \times \hat{n}$ as constant.‡ Thus, for a constant source velocity $\vec{\beta}_s$, we find

$$\begin{aligned} \vec{A} &= \frac{\vec{\mu} \times \hat{n}}{(1 - \vec{\beta}_s \cdot \hat{n})R^2} - \frac{(\vec{\mu} \times \hat{n})(\vec{\beta}_s \cdot \hat{n})}{(1 - \vec{\beta}_s \cdot \hat{n})R^2} \\ &= \frac{\vec{\mu} \times \hat{n}}{R^2} \end{aligned} \tag{3.5}$$

where $\frac{d}{dt}(Rc)^{-1}$ yields a $\vec{\beta}$ component solely in the source–objective direction.

The full retarded-potential expressions for a electron with a constant $\vec{\beta}$ falling into orbit a proton are thus fairly straightforward. Both dipole moments will align with the dominant field contribution $\nabla \times \vec{A} \propto \beta_o \hat{z}$, , where $\hat{z}$ is perpendicular to both the separation $\hat{n}$ and the orbital $\hat{o}$ directions (since only $\partial/\partial r$ yields nonzero terms). For simplicity, we can also assume $\beta_o \gg \beta_z$ (while also noting that μ_e is intrinsically negative). Considering a reference frame where the proton

[17] McGuffey et al., "Ionization Induced Trapping in a Laser Wakefield Accelerator"; Clayton et al., "Self-Guided Laser Wakefield Acceleration beyond 1 GeV Using Ionization-Induced Injection".

[18] Shishlo et al., "First observation of intrabeam stripping of negative hydrogen in a superconducting linear accelerator".

† We neglect the electric dipole moment, since these are a matter of hypothesis for the species under consideration, and certainly negligible in this context.

[19] Monaghan, "The Heaviside-Feynman expression for the fields of an accelerated dipole".

‡ This trait and several other characteristics of beam physics in terms of magnetic dipoles will be addressed in detail in Chapter 5.

and electron "share" an equal orbital β_o, but only the electron taking on a β_n, this yields:

$$A_p^\alpha = \frac{q}{R} \quad , \quad -\left(\frac{q\beta_o}{R} + \frac{|\mu_p|\hat{o}}{R^2}\right)\hat{o}$$
$$A_e^\alpha = -\frac{q}{R(1-\beta_n)} \quad , \quad \frac{1}{(1-\beta_n)}\left(\frac{q\beta_o}{R} - \frac{|\mu_e|}{R^2}\right)\hat{o} - \frac{q\beta_n\hat{n}}{(1-\beta_n)R} \tag{3.6}$$

where μ_p and μ_e are the respective proton and electron magnetic dipole moments.

We can now examine a stable electron–proton orbit wherein the dipole-based potentials and the velocity-dependent LW terms cancel attractive scalar potential.

To start, this allows us to solve for R in terms of $\vec{\beta}$. For example, for the case where $\vec{\beta}\cdot\hat{n} = 0$ (or equivalently, the total source velocity $\vec{\beta} = \beta_o$ in the tangential, orbital direction), we can take the total LW-based Lorentz force and dipole-based forces where they reach an equilibrium in the $\hat{n}$ direction.[†] That is, for a stationary proton and neglecting the proton dipole moment in favor of the electron's stronger one:

$$0 = \vec{F}_e\hat{n} + \vec{F}_p\hat{n} = -\frac{2q^2}{\gamma^2R^2} + \frac{\beta_o|q||\mu_e|}{R^3} \tag{3.8}$$

which yields

$$R = \frac{|\mu_e|\gamma^2\beta_o}{2|q|} \tag{3.9}$$

where μ_e is the electron magnetic dipole moment. Thus, for an electron passing tangentially to a proton with $\gamma \approx 100$, the attractive electrostatic force cancels at a separation distance of 1 nm. This relation is attenuated by a nonzero $\vec{\beta}\cdot\hat{n}$, namely

$$R = \frac{\gamma^2|\mu_e\beta_o|(1-\vec{\beta}\cdot\hat{n})}{2|q|} \tag{3.10}$$

When accounting for the forces in all directions, along with the time-dependent radiative effects arising from the rightmost term of Eq. (3.4) and the LW potentials, we can assert that some periodic motion about such a stable radius is likely to occur. What is important to recognize is that *only* the magnetic dipole

[†]Using the $\vec{B}$ form of Eq. (3.4) is helpful here (ignoring the radiative terms)

$$\vec{B} = \frac{3(\vec{\mu}\cdot\hat{n})\hat{n} - \vec{\mu}}{R^3} \tag{3.7}$$

where it is important to carefully track the *source* factors here distinctly from the *self* factors q and $\vec{v}$ appearing in the Lorentz force equation. The $\vec{E}$ and $\vec{B}$ field forms of the electric LW potentials are also useful here. These are given in Eq. (3.17).

moments and a sufficient tangential velocity can provide a countervailing force to the electrostatic attraction in the $\hat{n}$ direction.

For this scenario, we can balance the particles' potentials at a midpoint while assigning the orbital velocity to the proton so that the electron's velocity components are all due to gyration. (We will use classical orbital velocity here $\beta_o = \alpha_{EM} \approx \frac{1}{137}$). Taking the square of the potentials allows us to account for potential contributions from components of the gyration perpendicular to $\hat{n}$. This squaring reduces the magnitude of the dipole-component terms to $\vec{\mu}^2/R^4$, so that they can be neglected (while keeping in mind that we have treated them as the driving factor in establishing the gyration). This leaves the condition

$$(\Phi_p)^2 - (\alpha_{EM})^2 = (\Phi_e)^2 - \left(\vec{A}_e\right)^2$$

$$1 - \alpha_{EM}^2 = \left(\frac{1}{1 - \vec{\beta}_s \cdot \hat{n}}\right)^2 - \left(\frac{\vec{\beta}_s}{1 - \vec{\beta}_s \cdot \hat{n}}\right)^2 \equiv \Phi_e^* - \vec{\mathcal{A}}_e^* \qquad (3.11)$$

where $\hat{n}$ is constant and we define the stripped potentials for convenience further on. We are now able to solve for average gyration velocity $|\beta_s|$ by taking potential values along discrete points of the electron's spin-radius and breaking $\vec{\mathcal{A}}_e^*$ into its components' unit vectors: $\hat{o}$, $\hat{n}$, and $\hat{z}$, which lie in the orbital, source–particle, and z directions respectively.

Specifically, we can examine the emission from $i \to m$ points along the gyration ($\vec{\beta}_s \to \sum_{i=1}^{m} \vec{\beta}_i/m$). Although these emitted potentials cannot interfere, as they propagate at c from the electron along its gyration trajectory. However, we can take the approximation that the proton witnesses several gyrations from an approximately stationary point in the orbital path (assuming $|\beta_s| \gg \alpha_{EM}$); which allows us to balance the proton's potential with an summed potential over a single gyration for the electron. This scenario can be modeled as

$$1 - \alpha_{EM}^2 = \left(\frac{1}{m}\sum_{i=1}^{m} \Phi_e^*\right)^2 - \left(\sum_{i=1}^{m} \mathcal{A}_{i-\hat{o}}^*\right)^2 - \left(\sum_{i=1}^{m} \mathcal{A}_{i-\hat{n}}^*\right)^2 - \left(\sum_{i=1}^{m} \mathcal{A}_{i-\hat{z}}^*\right)^2 \qquad (3.12)$$

where only the scalar components are weighted by m.[†]

There is a subtlety here: we assume that the emitted potentials from the m segments of $\vec{\mathcal{A}}_e^*$ will interfere coherently, and thus these are added before squaring.

[†]This is due to scalar potentials diverging for increasing m; whereas the vector-potential components will converge as further subdivisions in the gyration orbit are taken with increasing m because of opposite-phase segments canceling.

As an alternative, one might consider a model where the scalar components are summed

For example, with a simple (non-oblique) gyration about the orbital axis and only sampling the minimum, maximum, and transverse points ($m = 4$) with respect to $\vec{\beta}_s \cdot \hat{n} \equiv \beta_n$, we have

$$\begin{aligned} \vec{\mathcal{A}}_e^* &= \frac{\beta_n}{1-\beta_n} - \frac{\beta_n}{1+\beta_n} \\ &= 2\gamma^2\beta_n^2 \end{aligned} \tag{3.14}$$

This method produces the spin contours shown in Fig. 3.4 for $m = 4$ sample points in the gyration. Here, θ_0 and α_s are the respective starting gyration angles projected to $\hat{n}$ and $\hat{z}$ in the orbital plane. (Explicitly: $\cos^{-1}\left(\frac{\beta_z}{|\vec{\beta}_s|}\right) \equiv \alpha_s$ and likewise for θ_0.)

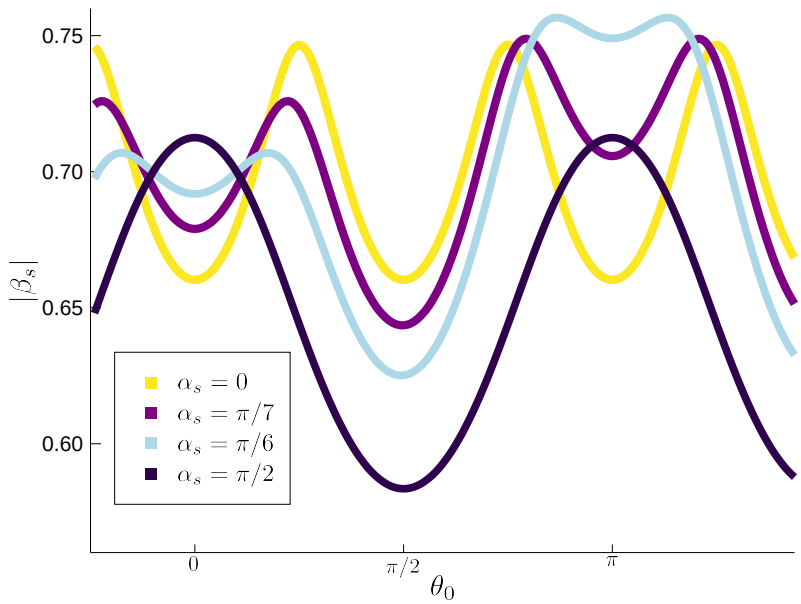

(a)

Figure 3.4: Electron gyration angular velocity as a function of starting angle θ_0 relative to $\hat{n}$ in the orbital plane about a proton. Orbital velocity $\beta_o = \alpha_{EM}$. All curves shown are for a moderate off-orbital-plane translational motion, approximated by $\Delta\beta_z \sim \frac{3}{10}\beta_z$. The angle α_s indicates the initial angle of gyration electron perpendicular to the orbital plane.

---

after squaring and the vector potentials *are* averaged

$$1 - \alpha_{EM}^2 = \sum_{i=1}^{m}\left(\frac{1}{m}\Phi_e^*\right)^2 - \left(\frac{1}{m}\sum_{i=1}^{m}\mathcal{A}_{i-\hat{o}}^*\right)^2 - \left(\frac{1}{m}\sum_{i=1}^{m}\mathcal{A}_{i-\hat{n}}^*\right)^2 - \left(\frac{1}{m}\sum_{i=1}^{m}\mathcal{A}_{i-\hat{z}}^*\right)^2 \tag{3.13}$$

This effectively treats all components coming from as m distinct electrons, and is better suited for modeling high β_o cases.

Here we have high-$\vec{\beta}_s$ solutions for a periodic β_z, where $|\beta_s|$ approaches a maximum for $\alpha_s \to \pm\frac{\pi}{6}$. Moreover, off-plane translational motion is approximated by assuming an offset in β_z for opposite points in the spin orbit $\Delta\beta_z \approx |\beta_z^{m_1}| - |\beta_z^{m_3}|$. This gives rise to potentials with a moderate $\Delta\beta_z \geq \frac{\beta_z}{10}$ having intersecting contours in $|\vec{\beta}_s|$. The $|\beta_s|$ then attenuates toward a unity as $\Delta\beta_z \to 0$ and $\alpha_s \to \pm\frac{\pi}{2}$ (i.e. high obliquity). Electrons with incoming β_s of approximately α_{EM}, on the other hand, tend to remain in low-energy wells or inaccessible bands (not shown).

Figure 3.5 then sketches the case of a high-$\vec{\beta}_s$ electron effecting a slight velocity shift to the proton ($\beta_{e\to p}$), which is reflected back to the electron at a later time ($\beta_{p\to e}$). For a low-energy electron ($\vec{\beta}_s \approx \alpha_{EM}$), this generates an echoed potential with an offset $\beta_{p\to e} \cdot \hat{n}_2 = |\beta_{p\to e}| \cos(\pi - 2\alpha_{EM})$.

The effect here is that the segment of the electron's gyration path pointed most directly at the proton (which grows exponentially in magnitude proportionally with $|\beta_{\hat{n}_1}|$) contributes significantly to the outgoing potential. The reflected potential is approximately planar when returning to the electron, but oriented in the original $\hat{n}_1$ direction. To check the magnitude of this effect, one can use Jackson's conjugate-momentum formalism introduced in the last chapter[20] and assuming the proton's initial velocity to be zero (and, again, ignoring its dipole moment). This gives a velocity kick of the form

$$\begin{aligned}\beta_{\hat{n}_1-p}c &= -\frac{q_p}{m_p c}A_{e\to p} = -\frac{q_p}{m_p c}\left(\frac{q_e\beta_{\hat{n}_1-e}}{|R|(1-|\beta_{\hat{n}_1-e}|)}\right) \\ &= \frac{q_p^2\beta_{\hat{n}_1-e}}{m_p c|R|(1-|\beta_{\hat{n}_1-e}|)} \end{aligned} \tag{3.15}$$

where Gaussian units are used. Then, as $\beta_{\hat{n}_1-e} \to 0.9999$ ($\gamma > 70$), the velocity shift of the proton becomes substantial. Equation 3.15 can be used again for the echoed potential's resulting velocity shift, which has an upper limit of roughly one part in 10^6; it is nevertheless a possible source for perturbations preventing a perfectly planar orbit (with both static and vector components). For high-velocity orbits, as the angle between $\hat{n}_1$ and $\hat{n}_2$ approaches the upper limit of two radians, the reflected potential is nearly perpendicular to the orbital trajectory.

To summarize, we have outlined a pseudoclassical means for predicting that a pointlike electron will not follow a planar orbit as it falls in toward the proton. Instead, for low incoming $\vec{\beta}$, any initial non-negligible tangential velocity components relative to the proton will lead to its inscribing an irregular spherical path.

[20] Jackson, *Classical Electrodynamics*, p579 ff.

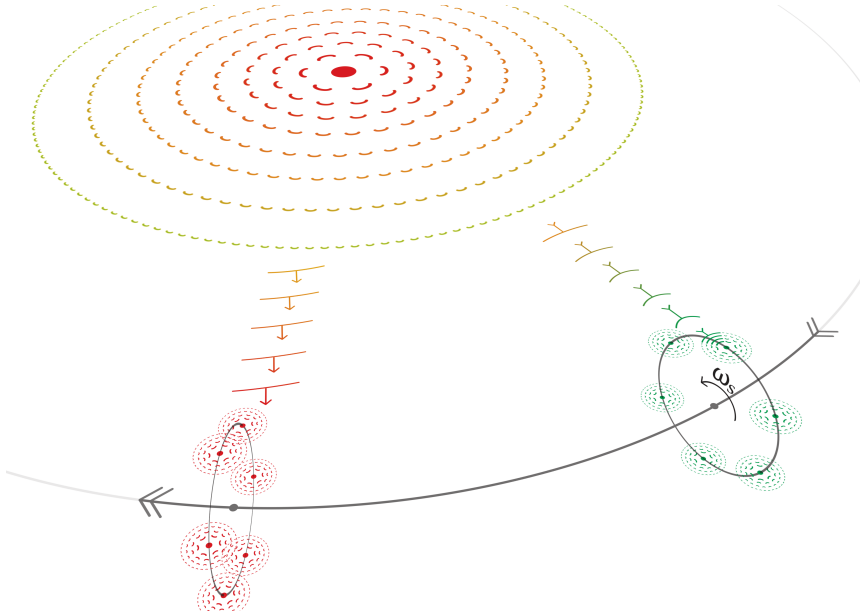

Figure 3.5: Indirect self-interaction of the orbiting electron given a fast, oblique gyration ($\gamma_s \gtrsim 75$, $\alpha_s = \pi/2$), which kicks the proton slightly. This, in turn, generates a velocity-dependent potential emitted from the proton which is parallel to the original separation vector $\hat{n}_1$ but oblique to the new one $\hat{n}_2$. (As before, red-orange-yellow-green coloring indicates timesteps from present to past.)

For a more practical example, Figure 3.6 sketches how the LW potentials for magnetic dipole moments can be expected to affect electron and proton interactions. It is worth noting how bunches with polarization schemes like those here may be of use in multi-beam acceleration or in certain wakefield acceleration applications.

Dipole-moment polarization may also merit further study in terms of colliding particles — although the $\vec{\mu} \times \hat{n}$ dependence of the emitted potentials inherently has no effect along the separation vector, it may be exploited to affect the collision dynamics (e.g. colliding protons with both dipole moments aligned along their separation vector will be more likely to interact).[†]

A more thorough study would incorporate the electron and proton magnetic

[†]We should note that the displacement of the electron is governed by

$$\frac{1}{m_e}\left(\mathcal{P}^\alpha + \frac{q_e}{c}A^\alpha\right) \tag{3.16}$$

which is more volatile than the proton's dynamics, owing to its low mass. One should also keep in mind that the electron's dipole moment is considerably greater in magnitude than the proton's.

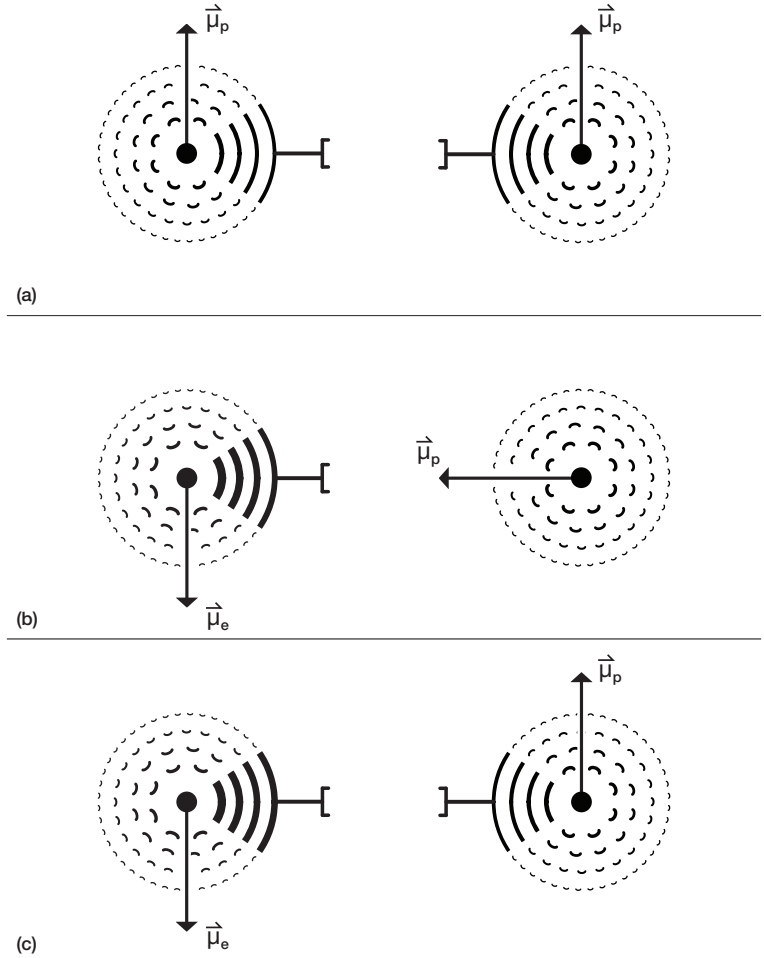

Figure 3.6: Lorentz-force interactions of protons (convex dashes) and electrons (concave) in the $\hat{n}$ direction due to emitted magnetic-dipole-moment fields as per the LW potentials. Bracketed lines indicate the effective force imparted on the opposite particle. The interactions are at a point of nearest approach, with velocities antiparallel: the left-hand particles travel out of the page and the right-hand ones go into the page.

moments into the equations of motion, as per Anandan.[21] We will address this topic in terms of neutron beam dynamics in Chapter 5.

One can also extend the Liénard–Wiechert potentials to study quantum effects. For example, they were shown to be compatible with quantum radiation theory by Childers,[22] where Grassman variables are necessary to quantize to the relativistic Dirac particle[23] (a similar form of Jackson's conjugate-momentum formalism

[21] Anandan, "Classical and Quantum Interaction of the Dipole".

[22] Childers, "Long-distance Lienard-Wiechert potentials and qq^- spin dependence".

[23] Gromes, "Relativistic corrections to the long-range quark antiquark potential electric flux

is used as in covariant symplectic tracking). Radiation increase proportional to spin is derived explicitly by Arakelyan and Grigoryan,[24] where a relativistic point-particle LW treatment coincides with classical radiation theory and QED.

Although such a fine-scale application of the LW potentials may seem unnecessary for beam dynamics, they have been included here in the spirit of Forest's failsafe dogma. Still, predicting an electron's orbital dynamics in this pseudoclassical regime overlooks critical effects such as Thomas precession.

However, such a framework could prove useful in predicting recombination radiation energies associated with electron cloud interactions or other beam-loss mechanisms. Other applications on few-particle systems could include simulating spontaneous fermion spin flipping;[25] or any scenario where mixed particle species are known to interact. It should also not be overlooked that with such an approach the formation of radiative photons is modeled inherently: as a particle changes trajectory, any residual coherent radiated fields can be tracked independently.

3.2 Collision Considerations

While the precision of an LW-based space charge code should provide more accuracy than solely Coulomb-based codes, LW calculations carry a greater risk of having numerical blow-ups; this is especially true for particles with predominant head-on trajectories, due to the $([1 - \vec{\beta} \cdot \hat{n}]|R|)^{-1}$ dependence.

A simple method for avoiding such blow-ups could involve adding random perturbations or oscillations to a particle's trajectory (transverse to $\hat{n}$) proportional to its de Broglie wavelength whenever a highly aligned collision is imminent. Imposing a such shifts on a particle's previously smooth trajectory would eliminate the probability of a perfect head-on collision; the longitudinal velocity fields would inevitably lose a large fraction of their momentum transversely if $|R|$ is proportional to the imposed de Broglie oscillation.

tubes, and area law".

[24] Arakelyan, Grigoryan, and Grigoryan, "Lienard-Wiechert Potential and Synchrotron Radiation of a Relativistic Spinning Particle in the Pseudoclassical Theory"; Grigoryan and Grigoryan, "Synchrotron Radiation from a Longitudinally Polarized Relativistic Spinning Particle in Pseudoclassical Theory".

[25] Jackson, "On understanding spin-flip synchrotron radiation and the transverse polarization of electrons in storage rings".

3.3 Lorentz Force and Multiparticle Effects

When passing through any machine element, the local transverse dynamics of a bunch may be chaotic, with outlying space-charge dependent velocity shifts (both longitudinal and transverse) greatly exceeding the average transverse velocity. Although space charge simulation is a facet of beam dynamics software,[26] it is typically simplified to a static Coulomb potential $\frac{q}{|R|}$, which is the nonrelativistic limit for the LW potentials.

To examine the Coulomb and LW-dependent forms of space charge, we can re-express the LW potentials in terms of their fields:

$$\vec{E} = q\left[\frac{\hat{n}-\vec{\beta}}{\gamma^2(1-\vec{\beta}\cdot\hat{n})^3R^2}\right]_{t=t_r} + \frac{q}{c}\left[\frac{\hat{n}\times\left\{(\hat{n}-\vec{\beta})\times\dot{\vec{\beta}}\right\}}{(1-\vec{\beta}\cdot\hat{n})^3R}\right]_{t=t_r}$$
$$\vec{B} = [\hat{n}\times\vec{E}] \tag{3.17}$$

where the $\frac{1}{R^2}$ terms are "velocity fields". These are often ignored; the $\dot{\vec{\beta}}$ terms are what drives radiation and typically of greater interest.

Specifically, the total radiated power of a particle is a often critical quantity (e.g. in electron synchotron storage rings). In its nonrelativstic limit, Eq. (3.17) can be reduced to the familiar Larmor equation

$$\mathbb{P} = \frac{2}{3}\frac{q_e^2}{c^2}|\dot{\vec{v}}|^2 \tag{3.18}$$

by using $\vec{E}_{LW} = -\partial_\alpha A^\alpha$ from Eq. (3.1) and retaining only the $\dot{\vec{\beta}}$ dependent terms by assuming a $\vec{\beta} \ll 1$ reference frame.

However, if all terms in Eqs.(3.17) are accounted for, the corrected form of Larmor's equation is[27]

$$\mathbb{P} = \frac{2}{3}\frac{q_e^2}{c}\gamma^6\left[\dot{\vec{\beta}}^2 - (\vec{\beta}\times\dot{\vec{\beta}})^2\right] \tag{3.19}$$

which for the case of $\beta\times\dot{\vec{\beta}}$ transverse and parallel to an observation point reduces

[26] Uriot and Pichoff, *TraceWin*; Zhukov, "Open XAL status report 2017"; Qiang et al., "High resolution simulation of beam dynamics in electron linacs for x-ray free electron lasers".

[27] Jackson, *Classical Electrodynamics*, p666.

to

$$\mathbb{P}_{\|} = \frac{2}{3}\frac{q_e^2}{c}\gamma^6 \dot{\vec{\beta}}^2$$
$$\mathbb{P}_{\perp} = \frac{2}{3}\frac{q_e^2}{c}\gamma^4 \dot{\vec{\beta}}^2 \tag{3.20}$$

A toy example is worth considering here: two bunches are being transversely focused in high-frequency pulses to a practical density limit, rapidly compressing and decompressing such that $\sum \dot{\beta}_{\|}^{\ 2}$ is non-negligible but $\beta_{\|} \approx 0$, relative to test point in the center of either bunch. One bunch, prior to focusing, has acquired a spin in the transverse plane[28] such that $|\beta_{\perp}| >> 0$ and thus $\gamma >> 1$.

In this case, the radiation power witnessed at the test point is proportional to γ^4 for the spinning bunch and 1 for the other bunch. For a test point outside the spinning bunch in the transverse plane, the observed radiated power is then proportional to $\gamma^4/2 + \gamma^6/2$. The potential for such power to be radiated toward the center of the spinning bunch leads to the conjecture that high-energy interactions may be expected to occur therein. A similar phenomenon of transverse–longitudinal recirculation will be discussed in the next chapter.

Although radiation fields from Eqs. (3.17) are often of greater interest, it is worthwhile to consider the velocity fields as they diverge from the Coulomb-like form in the nonrelativistic limit.

For example, if we examine the Lorentz force attributable to the velocity fields, we find the $\hat{n}$ components to be[†]

$$F_{\vec{B}} = \frac{-q^2\beta^2(1-\beta^2)(1-cos^2(\theta))}{(1-\beta cos(\theta))^3 R}\hat{n}$$
$$F_{\vec{E}} = \frac{q^2(1-\beta^2)}{(1-\beta cos(\theta))^2 R}\hat{n} \tag{3.21}$$

which are mapped in Fig. 3.7 for a relativistic charged particle overtaking a like-signed particle at $|\beta_z|$ (i.e. in the lab frame, the "self" particle travels at β_z and the "source" particle passes with $2\beta_z$).

Here, the attractive dip in the force map for off-center trajectories is due to $F_{\vec{B}}$ while the considerable repulsive peak is due to $F_{\vec{E}}$. Such forces may be worth

[28] Zioutas, "Particle acceleration by resonant absorption of radiation"; Chabert, Luong, and Promé, "Beam Dynamics in Separate Sector Cyclotrons".

[†] Here we have used $\hat{n} \times (\hat{n} - \beta_z) = \cancel{\hat{n} \times \hat{n}} - \hat{n} \times \beta_z$ along with the identity $\beta_z \times (-\hat{n} \times \beta_z) = -[(\beta_z \cdot \beta_z)\hat{n} - (\beta_z \cdot \hat{n})\beta_z]$

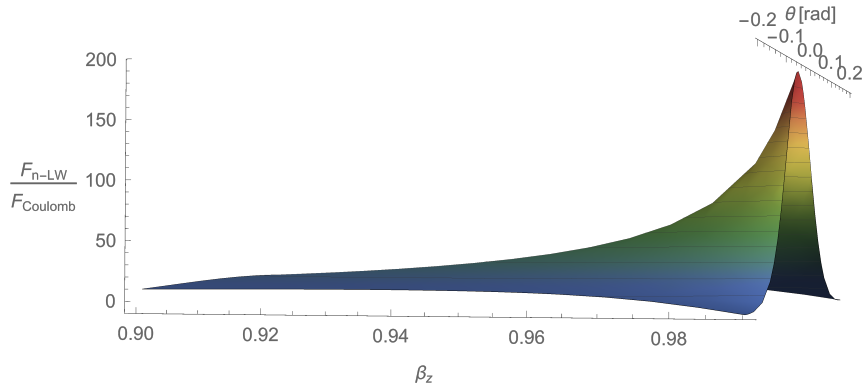

(a)

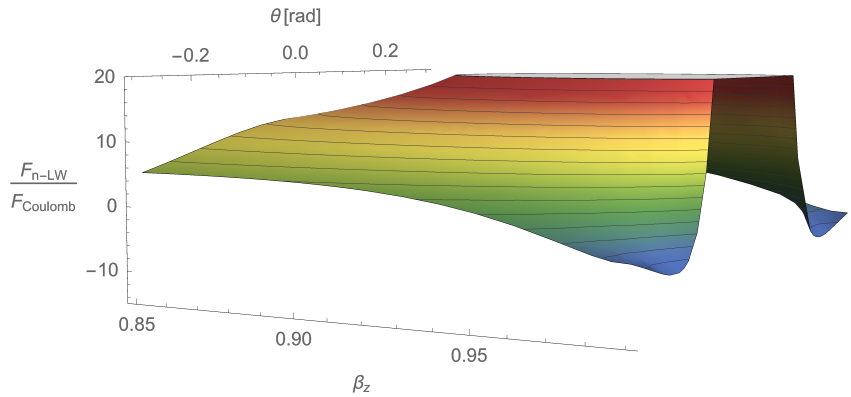

(b)

Figure 3.7: Ratio of Lorentz-force contributions from the summed Liénard–Weichert $\vec{E}$ and $\vec{B}$ velocity fields to the Coulomb force of two like-sign particles, a "self" particle, traveling at a speed β_z and a "source" particle overtaking it at βz where $\hat{z}$ is the direction of propagation. The angle θ is the projection of the self–source separation $\hat{n}$ and their colinear velocity direction $\hat{z}$. Positive values represent repulsive forces. In (a), the $\vec{E}$ contribution falls to 1 for low β_z and has a substantial peak for the ultrarelativstic case. The detail in (b) highlights the attractive contribution at high β due to $\vec{B}$.

considering when simulating, e.g., inter-beam scattering, or highly compressed bunch centers as discussed above. In terms of bunch crossings, this attractive dip may be a worthwhile phenomenon for stabilizing bunches without large spatial deflections (assuming a particulary narrow transverse σ).

For the case where two like-charge particles are approaching one another (*anti-parallel* β_z) the Lorentz forces remain repulsive, but do drop sharply toward zero for velocities exceeding $|\beta_z| \approx 0.9$ and $|\theta| \gtrsim 0.5$ rad, thus negating the Coulomb force.

Figure 3.8 sketches how the space charge behavior can be expected to differ for

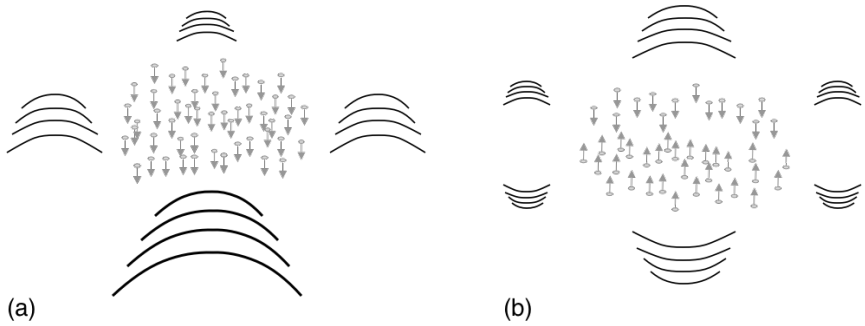

Figure 3.8: Accelerations (arrows) and corresponding emitted potentials (curves) for an electron bunch entering (a) dipole and (b) quadrupole magnets centered on the horizontal axis. Concave and convex potentials are negative and positively charged, respectively.

a bunch entering a bending (dipole) and focusing (quadrupole) magnet. For the dipole, the resulting radiation (not shown) is emitted in the forward longitudinal direction, resulting in the familiar synchotron radiation. For the quadrupole, a strong braking occurs near the middle of the bunch, dampening the emitted potentials. However, the accompanying sharp deflections for low $|R|$ values within the bunch may lead to substantial $(\hat{n} - \vec{\beta})/|R|^2$ terms. This indicates that velocity fields may dominate the focusing limits for a bunch.

The distribution of particles within a bunch is also critical in calculating radiative effects and space charge. While the scalar potentials outside equivalently populated but differently shaped bunches are roughly identical, the $\vec{A}$ terms are distinct, as illustrated in Fig. 3.9.

The dependence here on

$$\frac{\vec{\beta}}{1 - \vec{\beta} \cdot \hat{n}} \tag{3.22}$$

cannot be overstated: $\vec{A}$ falls to an attractive limit of $-1/2$ of the Coulomb potential for $\beta \to -1$, while for $\beta \to 1$ the for repulsive potentials appears divergent.[†]

Thus, while static potentials may be expected to dominate low-to-medium β transverse beam dynamics, the δ-like $\vec{A}$ potential for the hollowed distribution in Fig 3.9 indicates that it is a lowest-energy state. A comparable result was reported by Wangler,[29] with high-intensity beams evolving to have a central core and a small halo. A similar result was also reported recently with respect to

[†]Note, however, that in terms of *forces* Fig. 3.7 indicates a limit of a roughly 200-to-1 ratio versus the Coulomb potential.

[29]Wangler et al., "Relation Between Field Energy and Rms Emittance in Intense Particle Beams".

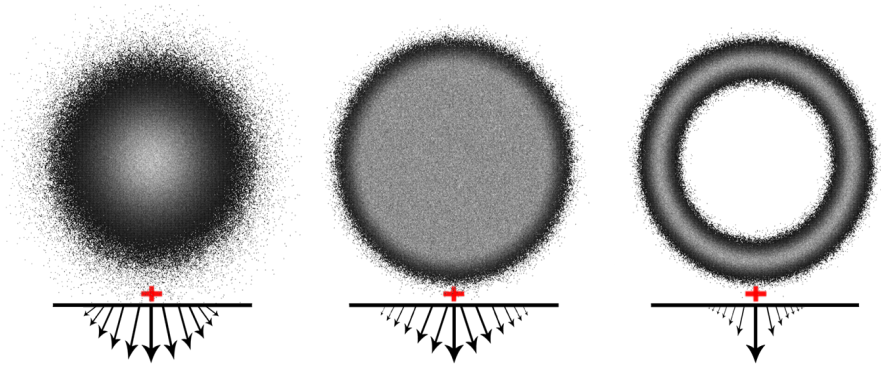

Figure 3.9: Sketch of net space-charge contributions following Eq. (3.1) for test particles on the edges (points marked in red) of isotropic distributions: Gaussian (left), uniform with exponential fall-off (center), and hollowed (right). All three assume a $\langle\vec{\beta}\rangle$ biased center–outward. The arrows' horizontal components cancel when summing bins, leaving the rightmost distribution as the most δ-like distribution.

longitudinal hollowing,[30] and may be particularly relevant for ongoing studies of hollow-beam collimation,[31] plasma lensing[32] and halo asymmetry.[33]

3.4 Improved Particle-in-Cell Tracking

Equipped now with a means for robust charged-particle tracking, the major obstacle in space-charge dynamics remains to be addressed: pairwise distance calculation. That is, in Eq. (3.1), the variables $|R|$ and $\hat{n}$ are unique for each particle pair, and the full LW potential acting on a particle within a bunch must be summed over all its neighbors. This leads to a computationally prohibitive $\mathcal{O}(N^2)$ dependence for bunches (which typically contain upwards of $N = 10^{10}$ particles).

The most obvious improvement here is avoiding redundant calculations (i.e. only calculating $|R|_{ij} = |R|_{ji}$ once); this is routinely done to reduce calculation time by a factor of two. However, further optimization typically requires introducing a number of mesh points M, interpolating a source density at each mesh point, then using a Poisson solver to find potentials for particle positions. Such a scheme has $\mathcal{O}(N + M \log M)$ performance and is known as particle-in-cell (PIC) tracking.[34] Directly computing short-range interactions can then improve accuracy, while

[30] Oeftiger et al., "Flat Bunches with a Hollow Distribution for Space Charge Mitigation".
[31] Stancari et al., "Collimation with Hollow Electron Beams".
[32] Neuner et al., "Shaping of Intense Ion Beams into Hollow Cylindrical Form".
[33] Franchetti et al., "Space Charge Effects on the Third Order Coupled Resonance".
[34] Greengard and Rokhlin, "A Fast Algorithm for Particle Simulations".

gridless calculation (relegating all long-range interactions to a center-of-mass approximation) has an estimated performance of $\mathcal{O}(N \log N)$.[35]

In practice, mesh algorithms are often needed, wherein each particle N is treated as a macroparticle, which represents enough particles to eliminate the need for $\mathcal{O}(10^{10})$ calculations. Then, within each macroparticle, forces are either averaged or neglected.[36] As mentioned earlier, interactions between macroparticles are typically treated as Coulombic (no velocity fields or radiation). The expected spatial expansion of (and particle flow between) the macroparticles themselves is typically ignored, treating them instead as immutable in shape and population.

The LW-based method outlined in the previous section may offer insight into intra-bunch phenomena, but this bears an obvious cost of significantly increased computational complexity (i.e. evaluating $\sim 10^{10}$ Coulomb-potential pairs versus as many iterations of Eq.[2.20]).

To counter this, we propose an optimized method for pairwise distance calculations. Any improvement seems impossible at first, as the 3D Euclidean distance formula appears to be essentially irreducible:

$$d = \sqrt{(x_1 - x_0)^2 + (y_1 - y_0)^2 + (z_1 - z_0)^2} \tag{3.23}$$

However, by abandoning the rectilinear mesh, an alternative can be found that—using lookup tables—presents a significant speedup.

To do so, we begin with spherical coordinates

$$\begin{aligned} x &= r \sin(\theta) \cos(\phi) \\ y &= r \sin(\theta) \sin(\phi) \\ z &= r \cos(\theta) \end{aligned} \tag{3.24}$$

where r is radius, θ is inclination, and ϕ is azimuth. At this point, the distance formula is no simpler:

$$d = \sqrt{r_1^2 + r_0^2 - 2 r_1 r_0 \left[\sin(\theta_1) \sin(\theta_0) \cos(\phi_1 - \phi_0) + \cos(\theta_1) \cos(\theta_0)\right]} \tag{3.25}$$

The angle-dependent terms are entirely periodic, however; so while r, θ, and ϕ may continue to infinity, the bracketed trigonometric expression falls to predictable values for procedurally generated θ's and ϕ's. To further simplify matters, one can extrude an Archimedean spiral

$$r = \pm b \theta^{\frac{1}{n}} \tag{3.26}$$

[35] Appel, "An Efficient Program for Many-Body Simulation".

[36] Machida, "Space-Charge Effects in Low-Energy Proton Synchrotrons"; Lapostolle et al., *A Modified Space Charge Routine for High Intensity Bunched Beams*.

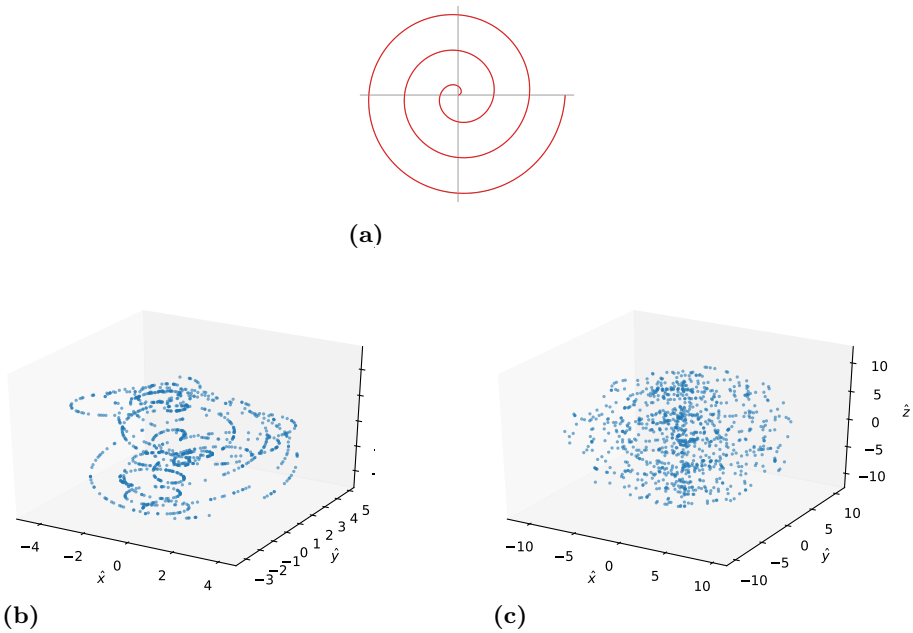

Figure 3.10: (a) A normal Archimedean spiral ($r = \pm\theta$) where each successive revolution has a uniformly spaced distance from the origin. (b) Scatter plots of a normal Archimedean spiral extruded into 3D for $-4\pi \leq \theta \leq 4\pi$ and (c) for $-400\pi \leq \theta \leq 400\pi$.

into 3D space,[37] such that, for $n = 1$ and $b = 1$:

$$\begin{aligned} x &= \theta \sin(\theta) \cos(\phi) \\ y &= \theta \sin(\theta) \sin(\phi) \\ z &= \theta \cos(\theta) \end{aligned} \tag{3.27}$$

By then defining $\phi = \theta\epsilon$, where ϵ is irrational, one can populate 3D space pseudorandomnly, with a single parameter θ (see Fig. 3.10).

The generation of θ-dependent gridpoint values in this case should be anti–center-weighted to create a uniform distribution since, as can be seen in Fig. 3.10(c), low x and y values are overpopulated. (For a Fermat spiral, with $n = 2$, z values do become uniform.) The single-variable 3D distance formula for $n = 1$ is then

$$d = \sqrt{\theta_1^2 + \theta_0^2 - 2\theta_1\theta_0 \left[\sin(\theta_1)\sin(\theta_0)\cos(\epsilon\{\theta_1 - \theta_0\}) + \cos(\theta_1)\cos(\theta_0)\right]} \tag{3.28}$$

Here, one can also see the bracketed term as a result of the cosine law $d^2 =$

[37] Parker, "Dynamics of the interplanetary gas and magnetic fields."

$r_1^2 + r_2^2 - 2r_2 r_1 \cos(\gamma)$, with

$$\cos(\gamma) = \frac{\vec{v}_1(x_1, y_1, z_1) \cdot \vec{v}_2(x_0, y_0, z_0)}{|v_1||v_2|} \tag{3.29}$$

where the $\vec{v}$ vectors are taken from Eq. (3.27). Then, presuming the bracketed term can be implemented via a lookup table (denoted LUT), wherein $\theta \to \theta \% 2\pi$, we can use the shorthand

$$d = \sqrt{\theta_1^2 + \theta_2^2 - \theta_1 \theta_2 \left[2\cos(\gamma)_{LUT}\right]} \tag{3.30}$$

Then we have a distance formula requiring 8 operations, considering that the factor of 2 can be absorbed into the lookup-table operation. This seems a modest gain against the Euclidean formula, which required 9 operations.[†]

However, if we consider parallelization, there is an advantage to the spiral coordinates. That is, if we track operations by interdependency, we have for the Euclidean case:

$$\sqrt{\underbrace{(x_1 - x_0)^2}_{=A} + \underbrace{(y_1 - y_0)^2}_{=B} + \underbrace{(z_1 - z_0)^2}_{=C}} \qquad \text{3 parallel subtractions}$$

$$\sqrt{\underset{=D}{A^2} + \underset{=E}{B^2} + \underset{=F}{C^2}} \qquad \text{3 parallel powerings}$$

$$\sqrt{\underbrace{D + E}_{=G} + F} \qquad \text{1 serial addition}$$

$$\sqrt{\underbrace{G + F}_{=H}} \qquad \text{1 serial addition}$$

$$\sqrt{H} \qquad \text{1 square root} \tag{3.31}$$

[†]Though, for the ideal case of calculating space-charge for a full, realistic bunch, this does still translate to $\sim 10^{10}$ fewer calculations per timestep.

Whereas for the spiral case we have

$$\sqrt{\underset{=A}{\theta_1^2} + \underset{=B}{\theta_0^2} - \underbrace{\theta_1\theta_0}_{=C}\underbrace{[2cos(\gamma)]}_{=D}} \qquad \text{4 parallel (2 powering, 1 mult., 1 lookup)}$$

$$\sqrt{\underbrace{A+B}_{=E} - \underbrace{C\cdot D}_{=F}} \qquad \text{2 parallel (1 addition, 1 mult.)}$$

$$\sqrt{\underbrace{E-F}_{=G}} \qquad \text{1 serial addition}$$

$$\sqrt{G} \qquad \text{1 square root} \tag{3.32}$$

This also provides ample intermediate steps for the lookup table value of an upcoming distance pair to be pre-calculated. Meanwhile, the Euclidean case is unavoidably bottlenecked by the three consecutive serial operations; and the performance advantage of indexing over a 1D list (vs. a 3×1 array of 3D Cartesian points) may also prove substantial. As a preliminary result, Fig. 3.11 reports a substantial speedup (roughly a factor of 1.6) for the spiral case using the Distances.jl and BenchmarkTools.jl in the Julia language.[38]

With spiral coordinates, the macroparticle formalism remains viable, with the advantage that there are no intersecting gridpoints and that the number of macroparticles along θ is not the only throttle for *spatial resolution*, since b in Eq. (3.26) can be adjusted to an ideal spacing between revolutions.

Also, with the covariant LW potentials at our disposal, the cycle of discrete calculations (densities and fields fields) $\Longleftrightarrow$ mesh-free calculations (forces and trajectories)[39] becomes superfluous, since we calculate trajectories directly from potentials.

However, the use of densities need not be dismissed entirely. For example, consider a speed-priority code in which gridpoints represent a density of macroparticles which are allowed to migrate as per Eq. (2.25). In this case (and ignoring β dependence in potentials for the moment), an expansion tendency would occur: highly populated position and momentum bins will migrate outward isotropically

[38] Carlsson and Lin, "A Julia package for evaluating distances(metrics) between vectors.: JuliaStats/Distances.jl"; Revels, *BenchmarkToools.jl: A benchmarking framework for the Julia language.*

[39] Westermann, "Numerical Modelling of the Stationary Maxwell–Lorentz System in Technical Devices".

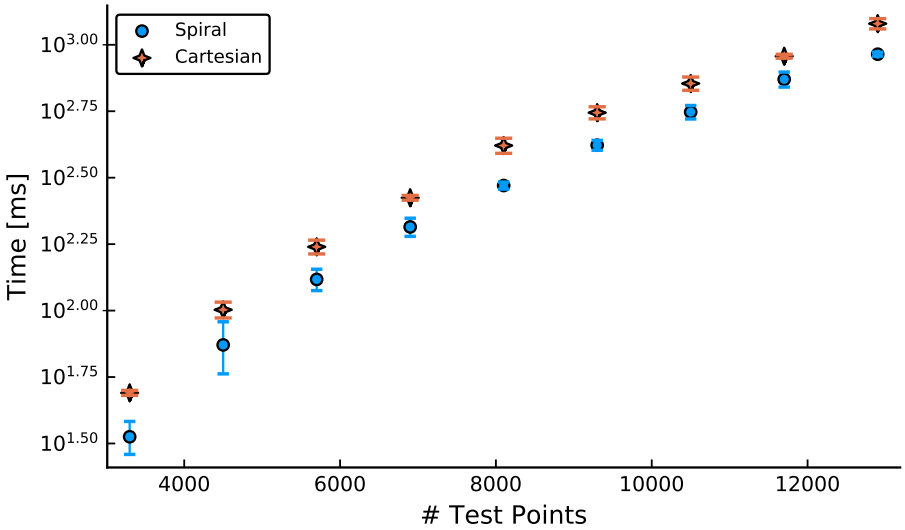

Figure 3.11: Log plot benchmarking identical test-point distributions evaluated with pairwise 3D Cartesian and spiral distance formulas. Error bars are standard deviations for 30 trials.

due to space charge. If we then account for velocity fields, the bins can still be expected to flatten smoothly, but not isotropically. Such a scheme could then incorporate external potentials via Eq. (2.31) which would stand as a fastest-possible first-principles simulation method for Gaussian distributions of charged particles.

One further speedup technique bears mentioning. This involves a cross-dependence of particle positions on θ_1 and θ_0:

$$\begin{aligned} r_1 &= \sqrt{\theta_1 + \theta_0} & r_0 &= \sqrt{\theta_0 + \theta_1} \\ x_1 &= r_1 \sin(\theta_1)\cos(\theta_0) & x_0 &= r_0 \sin(\theta_0)\cos(\theta_1) \\ y_1 &= r_1 \sin(\theta_1)\sin(\theta_0) & y_0 &= r_0 \sin(\theta_0)\sin(\theta_1) \\ z_1 &= r_1 \cos(\theta_1) & z_0 &= r_0 \cos(\theta_0) \end{aligned} \tag{3.33}$$

which imposes the constraints $r_1 = r_0$, $x_1 = x_0 \frac{\tan(\theta_1)}{\tan(\theta_0)}$, and $y_1 = y_0$. This is likely only useful for cherry-picking qualifying values as a preconditioning step. The quantity of such values are doubled for evenly spaced θ_1 and θ_0 which proceed from the origin with opposite signs (versus both θ's proceeding with the same sign). This type of spiral system has a dramatically simplified distance equation:

$$d = \sqrt{(\theta_1 + \theta_0)\left[(\cos(\theta_1) - \cos(\theta_0))^2 + \sin^2(\theta_1 - \theta_0)\right]} \tag{3.34}$$

where the bracketed term is again viable as a lookup-table operation, for a total of 4 operations (addition and lookup in parallel→multiplication→square-root).

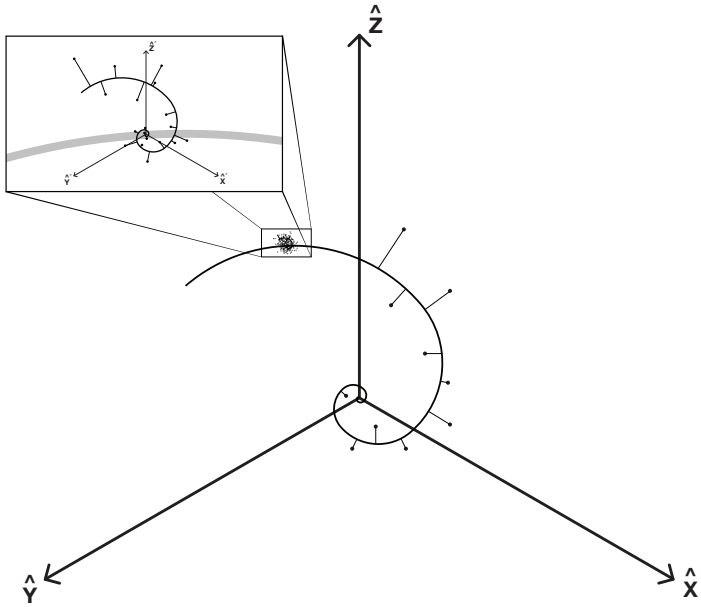

Figure 3.12: A sketch of recursive spiral systems, where selected macroparticles are embedded with subsystems of individual particles or smaller macroparticles. For clarity, only a starting portion ($\theta \sim \pi/4$) is shown.

Despite its simplistic distance formula, this method should be treated carefully, as θ loses its intuitive physical interpretation.

For a slower, but more robust method, we can consider recursive spiral coordinate systems, such that an individual macroparticle (e.g. in an especially high-velocity or high-density region) is treated as a subsystem, as illustrated in Fig. 3.12. This is an approach commonly used in astrophysics and computational physics to reach $\mathcal{O}(NlogN)$ performance,[40] and even pushing toward $\mathcal{O}(N)$ performance when combined with the fast-multipole method.[41]

In this case, the embedded coordinate system need not be rotated, so long as the spacing parameter $b \ll b'$ and the origin is shifted appropriately. This allows for recycling of lookup tables and simplifies the appending of primed coordinates to

[40] Barnes and Hut, "A hierarchical O(N log N) force-calculation algorithm".
[41] Roberts, "Hierarchical N-body calculations".

the base coordinates. It is also illustrated here that, as with the rectilinear case, macroparticles and actual particles need not fall precisely along the $r = \theta$ line, but can simply take LW potential values at the nearest gridpoint (or, for greater accuracy, averaging nearest-neighbor gridpoints from an inner and outer r value to ensure that potentials are acting on both hemispheres of the macroparticle are accounted for).

For completeness, a reminder is in order that $\hat{n}$ in Eq. (3.1) is dependent on the *direction* between particles and not solely distance. This entails an additional calculation for each pair which is quite costly compared to the Coulomb potential (in which $\beta_s \cdot \hat{n}$ is treated as zero).

Fortunately, the calculation of $\hat{n}$ involves a repeated subtraction in spiral coordinates:

$$\hat{n} = \frac{1}{d}\left[(\theta_1 - \theta_0)\hat{\theta} + \epsilon(\theta_1 - \theta_0)\hat{\phi} + (\theta_1 - \theta_0)\hat{r}\right] \tag{3.35}$$

which is also a drastic improvement over its Euclidean counterpart.

This spiral-coordinates approach and LW methods can be used independently; they are presented here as complementary, with the former allowing scalable precision, and the latter offering first-principles accuracy. Neither method is strictly suited to beam dynamics, so we conclude this chapter with an informal note on their broader applicability.

3.5 Applications

Spiral coordinates may prove viable in any simulation of interacting particles with a large enough population to push computational limits. Other groups have tested similar systems in terms of astrophysics, magnetohydrodynamics, signal processing, and computational physics,[42] with one group reporting order-of-magnitude speedup improvements.[43] In general, defining a grid with no intersecting points may help alleviate smoothing and noise concerns known to arise in typical rectilinear-grid methods.[44]

Liénard–Wiechert potentials have already been applied to nuclear and heavy-ion

[42] Wiengarten et al., "MHD simulation of the inner-heliospheric magnetic field"; Rabiner, Schafer, and Rader, "The chirp z-transform algorithm".

[43] Lee and Greengard, "The type 3 nonuniform FFT and its applications".

[44] Birdsall, "Particle-in-cell charged-particle simulations, plus Monte Carlo collisions with neutral atoms, PIC-MCC".

physics simulations.[45] They have also been used as a flat-spacetime complement to gravitational dynamics studies,[46] which is discussed in Appendix B. In general, these potentials are an uncontested baseline for charged-particle interaction and radiation, but the full expressions for the potentials are not typical used directly for dynamics calculation. This is understandable, especially historically in terms of computing capability; but to probe intensity limits and pico–nano scale wakefield dynamics, it is unlikely that it will suffice to continue treating even low transverse $\langle\beta\rangle$ bunches classically.

References

Anandan, J. S. "Classical and quantum interaction of the dipole". In: *Physical Review Letters* 85.7 (Aug. 2000). arXiv: hep-th/9910018, pp. 1354–1357. DOI: 10.1103/PhysRevLett.85.1354.

Appel, A. "An efficient program for many-body simulation". In: *SIAM Journal on Scientific and Statistical Computing* 6.1 (Jan. 1985), pp. 85–103. ISSN: 0196-5204. DOI: 10.1137/0906008.

Arakelyan, S. A., G. V. Grigoryan, and R. P. Grigoryan. "Lienard-Wiechert potential and synchrotron radiation of a relativistic spinning particle in the pseudoclassical theory". In: *Physics of Atomic Nuclei* 63.12 (Dec. 2000). arXiv: hep-th/9902159, pp. 2115–2122. DOI: 10.1134/1.1333882.

Barnes, J. and P. Hut. "A hierarchical O(N log N) force-calculation algorithm". In: *Nature* 324 (Dec. 1986), 446 EP. DOI: 10.1038/324446a0.

Bazarov, I. V., B. M. Dunham, and C. K. Sinclair. "Maximum achievable beam brightness from photoinjectors". In: *Physical Review Letters* 102.10 (Mar. 2009), p. 104801. DOI: 10.1103/PhysRevLett.102.104801.

Berg, R. A. and C. N. Lindner. "Electron-proton bremsstrahlung". In: *Nuclear Physics* 26.2 (Aug. 1961), pp. 259–279. DOI: 10.1016/0029-5582(61)90138-9.

Birdsall, C. K. "Particle-in-cell charged-particle simulations, plus monte carlo collisions with neutral atoms, pic-mcc". In: *IEEE Transactions on Plasma Science* 19.2 (1991), pp. 65–85. DOI: 10.1109/27.106800.

Bjorken, J. D. and E. A. Paschos. "Inelastic electron-proton and γ-proton scattering and the structure of the nucleon". In: *Physical Review* 185.5 (Sept. 1969), pp. 1975–1982. DOI: 10.1103/PhysRev.185.1975.

[45] Kosyakov, "Classical Yang-Mills Field Generated by Two Colored Point Charges"; Kosyakov, Popov, and Vronskiĭ, "The bag and the string: Are they opposed?"

[46] Hilborn, "Gravitational waves from orbiting binaries without general relativity".

Blue, B. E. et al. “Plasma-wakefield acceleration of an intense positron beam”. In: *Phys. Rev. Lett.* 90 (21 2003), p. 214801. DOI: 10.1103/PhysRevLett.90.214801.

Burov, A. et al. “Landau damping by electron lenses”. In: *Proc. 9th International Particle Accelerator Conference (IPAC'18), Vancouver, BC, Canada, April 29-May 4, 2018*. (Vancouver, BC, Canada). International Particle Accelerator Conference 9. Geneva, Switzerland: JACoW Publishing, 2018, pp. 2921–2924. DOI: 10.18429/JACoW-IPAC2018-THYGBD4.

Carlsson Kristoffer, I. D. and D. Lin. “A Julia package for evaluating distances(metrics) between vectors.: JuliaStats/Distances.jl”. In: (2018). URL: https://github.com/JuliaStats/Distances.jl.

Chabert, A., T. T. Luong, and M. Promé. “Beam dynamics in separate sector cyclotrons”. In: *Seventh International Conference on Cyclotrons and their Applications: Zürich, Switzerland, 19–22 August 1975*. Ed. by W. Joho. Basel: Birkhäuser Basel, 1975, pp. 245–248. DOI: 10.1007/978-3-0348-5520-4_49.

Childers, R. W. “Long-distance lienard-wiechert potentials and qq^- spin dependence”. In: *Physical Review D* 36.12 (Dec. 1987), pp. 3813–3816. DOI: 10.1103/PhysRevD.36.3813.

Clayton, C. E. et al. “Self-guided laser wakefield acceleration beyond 1 GeV using ionization-induced injection”. In: *Phys. Rev. Lett.* 105 (10 2010), p. 105003. DOI: 10.1103/PhysRevLett.105.105003.

Debus, A. et al. “Simulating radiation from laser-wakefield accelerators”. en. In: *Proceedings of ICAP12*. Rostock-Warnemü nde, Germany, 2012, p. 28. URL: http://accelconf.web.cern.ch/accelconf/icap2012/talks/tusbc1_talk.pdf.

Feynman, R. P., R. B. Leighton, and M. Sands. *The Feynman Lectures on Physics, Vol. 2: Mainly Electromagnetism and Matter*. Reading, MA, USA: Addison–Wesley, 1979, pp. 14–4,25–5.

Franchetti, G. et al. “Space charge effects on the third order coupled resonance”. In: *Physical Review Accelerators and Beams* 20.8 (Aug. 2017), p. 081006. DOI: 10.1103/PhysRevAccelBeams.20.081006.

Gadjev, I. et al. “High-gain FEL in the space-charge dominated Raman limit”. In: *Proceedings, 37th International Free Electron Laser Conference (FEL 2015): Daejeon, Korea, August 23-28, 2015*. 2015, TUP008. DOI: 10.18429/JACoW-FEL2015-TUP008.

Greengard, L and V Rokhlin. “A fast algorithm for particle simulations”. In: *Journal of Computational Physics* 73.2 (Dec. 1987), pp. 325–348. DOI: 10.1016/0021-9991(87)90140-9.

Grigoryan, G. V. and R. P. Grigoryan. “Synchrotron radiation from a longitudinally polarized relativistic spinning particle in pseudoclassical the-

ory". en. In: *Physics of Atomic Nuclei* 64.5 (May 2001), pp. 937–940. DOI: 10.1134/1.1378885.

Gromes, D. "Relativistic corrections to the long-range quark antiquark potential electric flux tubes, and area law". In: *Zeitschrift für Physik C Particles and Fields* 22.3 (1984), pp. 265–270. DOI: 10.1007/BF01575791.

Hilborn, R. C. "Gravitational waves from orbiting binaries without general relativity". In: *American Journal of Physics* 86.3 (Feb. 2018), pp. 186–197. ISSN: 0002-9505. DOI: 10.1119/1.5020984.

Hirose, A. *Radiation by moving charges*. 2012. URL: http://physics.usask.ca/~hirose/p812/p812fp.htm.

Itzykson, C. and J.-B. Zuber. *Quantum Field Theory*. International series in pure and applied physics. Also a reprint ed.: Mineola, Dover, 2005. New York, NY: McGraw-Hill, 1980. URL: http://cds.cern.ch/record/100772.

Jackson, J. D. "On understanding spin-flip synchrotron radiation and the transverse polarization of electrons in storage rings". In: *Rev. Mod. Phys.* 48 (3 1976), pp. 417–433. DOI: 10.1103/RevModPhys.48.417.

Jackson, J. D. *Classical Electrodynamics*. New York, NY, USA: John Wiley & Sons Inc., 1999, pp. 579–585,661–663.

James, C. W. et al. "General description of electromagnetic radiation processes based on instantaneous charge acceleration in 'endpoints'". In: *Physical Review E* 84.5 (Nov. 2011), p. 056602. DOI: 10.1103/PhysRevE.84.056602.

Keinigs, R. and M. E. Jones. "Two-dimensional dynamics of the plasma wakefield accelerator". In: *The Physics of Fluids* 30.1 (Jan. 1987), pp. 252–263. DOI: 10.1063/1.866183.

Kosyakov, B. P. "Classical Yang-Mills field generated by two colored point charges". In: *Physics Letters B* 312.4 (Aug. 1993), pp. 471–476. ISSN: 0370-2693. DOI: 10.1016/0370-2693(93)90984-P.

Kosyakov, B. P., E. Yu. Popov, and M. A. Vronskiĭ. "The bag and the string: Are they opposed?" In: *Phys. Lett.* B744 (2015), pp. 28–33. DOI: 10.1016/j.physletb.2015.02.044.

Lagniel, J.-M. "Chaotic behaviour and halo formation from 2d space-charge dominated beams". In: *Nuclear Instruments and Methods in Physics Research Section A: Accelerators, Spectrometers, Detectors and Associated Equipment* 345.3 (July 1994), pp. 405–410. DOI: 10.1016/0168-9002(94)90490-1.

Lang, K. *NASA's Cosmos*. 2010. URL: http://ase.tufts.edu/cosmos/view_picture.asp?id=1418.

Lapostolle, P. et al. *A Modified Space Charge Routine for High Intensity Bunched Beams*. English. Tech. rep. CEA-DSM-GECA-GT–96-01. Laboratoire National Saturne, 1996. URL: http://inis.iaea.org/Search/search.aspx?orig_q=RN:29005993.

Lee, J.-Y. and L. Greengard. "The type 3 nonuniform fft and its applications". In: *Journal of Computational Physics* 206.1 (2005), pp. 1 –5. ISSN: 0021-9991. DOI: 10.1016/j.jcp.2004.12.004. URL: http://www.sciencedirect.com/science/article/pii/S002199910400511X.

Littlejohn, R. *Gaussian, SI and other systems of units in electromagnetic theory.* 2018. URL: http://bohr.physics.berkeley.edu/classes/221/1112/notes/emunits.pdf.

Lu, W. et al. "Nonlinear theory for relativistic plasma wakefields in the blowout regime". In: *Physical Review Letters* 96.16 (Apr. 2006), p. 165002. DOI: 10.1103/PhysRevLett.96.165002. URL: https://link.aps.org/doi/10.1103/PhysRevLett.96.165002.

Machida, S. "Space-charge effects in low-energy proton synchrotrons". In: *Nuclear Instruments and Methods in Physics Research Section A: Accelerators, Spectrometers, Detectors and Associated Equipment* 309.1–2 (Nov. 1991), pp. 43–59. DOI: 10.1016/0168-9002(91)90091-4.

Malka, V. et al. "Principles and applications of compact laser–plasma accelerators". en. In: *Nature Physics* 4.6 (June 2008), pp. 447–453. ISSN: 1745-2481. DOI: 10.1038/nphys966. (Visited on 06/27/2018).

McGuffey, C. et al. "Ionization induced trapping in a laser wakefield accelerator". In: *Phys. Rev. Lett.* 104 (2 2010), p. 025004. DOI: 10.1103/PhysRevLett.104.025004.

Mirarchi, D. et al. "Hollow electron-lens assisted collimation and plans for the LHC". In: *61st ICFA Advanced Beam Dynamics Workshop on High-Intensity and High-Brightness Hadron Beams (HB2018) Daejeon, Korea, June 17-22, 2018*. 2018. URL: http://lss.fnal.gov/archive/2018/conf/fermilab-conf-18-311-ad-apc.pdf.

Mo, L. W. and Y. S. Tsai. "Radiative corrections to elastic and inelastic ep and up scattering". In: *Reviews of Modern Physics* 41.1 (Jan. 1969), pp. 205–235. DOI: 10.1103/RevModPhys.41.205.

Monaghan, J. J. "The Heaviside-Feynman expression for the fields of an accelerated dipole". In: *Journal of Physics A: General Physics* 1.1 (1968), pp. 112–117. DOI: 10.1088/0305-4470/1/1/315.

Napolitano, J. *SI and CGS units in electromagnetism.* 2018. URL: http://www.rpi.edu/dept/phys/Courses/PHYS4210/S10/NotesOnUnits.pdf.

Neuner, U. et al. "Shaping of intense ion beams into hollow cylindrical form". In: *Physical Review Letters* 85.21 (Nov. 2000), pp. 4518–4521. DOI: 10.1103/PhysRevLett.85.4518.

Oeftiger, A. et al. "Flat bunches with a hollow distribution for space charge mitigation". In: *arXiv:1605.01616 [physics]* (May 2016). arXiv: 1605.01616. URL: http://arxiv.org/abs/1605.01616.

Parker, E. N. “Dynamics of the interplanetary gas and magnetic fields.” In: *The Astrophysical Journal* 128 (1958), p. 664.

Peskin, M. E. and D. V. Schroeder. *An Introduction to Quantum Field Theory*. Reading, USA: Addison-Wesley, 1995. URL: http://www.slac.stanford.edu/~mpeskin/QFT.html.

Pukhov, A. and J. P. Farmer. “Stable particle acceleration in co-axial plasma channels”. In: *arXiv:1806.02123 [physics]* (June 2018). URL: http://arxiv.org/abs/1806.02123.

Qiang, J. et al. “High resolution simulation of beam dynamics in electron linacs for x-ray free electron lasers”. In: *Phys. Rev. ST Accel. Beams* 12 (10 2009), p. 100702. DOI: 10.1103/PhysRevSTAB.12.100702.

Rabiner, L., R. Schafer, and C. Rader. “The chirp z-transform algorithm”. In: *IEEE Transactions on Audio and Electroacoustics* 17.2 (1969), pp. 86–92. DOI: 10.1109/TAU.1969.1162034.

Revels, J. *Benchmarktoools.jl: a benchmarking framework for the Julia language*. 2018. URL: https://github.com/JuliaCI/BenchmarkTools.jl.

Roberts, S. “Hierarchical n-body calculations”. In: *Theoretical and Numerical Aspects of Geometric Variational Problems*. Canberra AUS: Centre for Mathematics and its Applications, Mathematical Sciences Institute, The Australian National University, 1991, pp. 211–224. URL: https://projecteuclid.org/euclid.pcma/1416323564.

Ryne, R. D. “Finding matched rms envelopes in rf linacs: a hamiltonian approach”. In: *arXiv:acc-phys/9502001* (Feb. 1995). URL: http://arxiv.org/abs/acc-phys/9502001.

Salah, W. “Analysis of space charge fields using the Lienard-Wiechert potential and the method of images during the photoemission of the electron beam from the cathode”. en. In: *The European Physical Journal Plus* 132.1 (Jan. 2017), p. 18. DOI: 10.1140/epjp/i2017-11300-9.

Schramm, U. et al. “Observation of laser-induced recombination in merged electron and proton beams”. In: *Physical Review Letters* 67.1 (July 1991), pp. 22–25. DOI: 10.1103/PhysRevLett.67.22.

Shishlo, A. et al. “First observation of intrabeam stripping of negative hydrogen in a superconducting linear accelerator”. In: *Phys. Rev. Lett.* 108 (11 2012), p. 114801. DOI: 10.1103/PhysRevLett.108.114801.

Sigmond, R. S. “Simple approximate treatment of unipolar space-charge-dominated coronas: The Warburg law and the saturation current”. In: *Journal of Applied Physics* 53.2 (Feb. 1982), pp. 891–898. DOI: 10.1063/1.330557. (Visited on 06/27/2018).

Stancari, G. et al. “Collimation with hollow electron beams”. In: *Phys. Rev. Lett.* 107 (8 2011), p. 084802. DOI: 10.1103/PhysRevLett.107.084802.

Talman, R. *M.K.S / Gaussian unit conversion*. 2018. URL: http://uspas.fnal.gov/materials/02Yale/Units.pdf.

Tarkeshian, R. et al. "Transverse space-charge field-induced plasma dynamics for ultraintense electron-beam characterization". In: *Physical Review X* 8.2 (May 2018), p. 021039. DOI: 10.1103/PhysRevX.8.021039.

Tiefenback, M. G. and D. Keefe. "Measurements of stability limits for a space-charge-dominated ion beam in a long A. G. transport channel". In: *IEEE Transactions on Nuclear Science* 32.5 (Oct. 1985), pp. 2483–2485. DOI: 10.1109/TNS.1985.4333954.

Uriot, D and N Pichoff. *TraceWin*. Saclay, France: CEA Saclay, 2014, p. 150.

Vay, J.-L. et al. "Numerical methods for instability mitigation in the modeling of laser wakefield accelerators in a lorentz-boosted frame". In: *Journal of Computational Physics* 230.15 (2011), pp. 5908 –5929. DOI: 10.1016/j.jcp.2011.04.003.

Wangler, T. P. et al. "Relation between field energy and rms emittance in intense particle beams". In: *IEEE Trans.Nucl.Sci.* 32 (1985), p. 2196. DOI: 10.1109/TNS.1985.4333859.

Westermann, T. "Numerical modelling of the stationary Maxwell–Lorentz system in technical devices". en. In: *International Journal of Numerical Modelling: Electronic Networks, Devices and Fields* 7.1 (Jan. 1994), pp. 43–67. DOI: 10.1002/jnm.1660070106.

Wiengarten, T. et al. "MHD simulation of the inner-heliospheric magnetic field". In: *Journal of Geophysical Research: Space Physics* 118.1 (2013), pp. 29–44. DOI: 10.1029/2012JA018089.

Wolski, A. *Beam dynamics: In High Energy Particle Accelerators*. London, UK: Imperial College Press, 2014. URL: http://cds.cern.ch/record/1622200.

Yousif, F. B. et al. "Experimental observation of laser-stimulated radiative recombination". In: *Physical Review Letters* 67.1 (July 1991), pp. 26–29. DOI: 10.1103/PhysRevLett.67.26.

Zhukov, A. et al. "Open XAL status report 2017". In: *Proceedings, 8th International Particle Accelerator Conference (IPAC 2017): Copenhagen, Denmark, May 14–19*. 2017, THPVA093. DOI: 10.18429/JACoW-IPAC2017-THPVA093.

Zioutas, K. "Particle acceleration by resonant absorption of radiation". In: *Physics Letters A* 189.6 (1994), pp. 460 –469. ISSN: 0375-9601. DOI: 10.1016/0375-9601(94)91210-6. URL: http://www.sciencedirect.com/science/article/pii/0375960194912106.

Chapter 4

Multipole Magnets

Here and in the final chapter, we present technical cases well-suited to the nonlinear tracking. Space charge will no longer be discussed in depth, although we will continue to draw upon the LW potentials and the covariant formalism used thus far. In this chapter, we consider magnets with more than two sets of dipoles (i.e. higher order than quadrupoles), which we informally refer to as multipoles.

4.1 Field Gradients and Potentials

For symplectic, covariant tracking of bunches passing through bending (dipole), focusing (quadrupole) and higher-order magnets, any relevant external potentials must be derived, then trajectories can be calculated with a Hamiltonian. This is in contrast with the Poisson-solver approach, where external fields can be approximated numerically, and the dynamics are then determined by the resulting Lorentz forces (although the covariant Hamiltionian Eq. [2.1] is also derived from the Lorentz force equation).

The potentials for these magnets fortunately only have a longitudinal component in their idealized form ($A^\alpha = A^z$). This form ignores alignment fringe effects, but is well-suited for introducing the subject.

Equation (2.20) shows such a potential, but still lacks a clear definition for A^z itself. To remedy this, Wolski and Wille's contour integral approach is

particularly cogent.[1][2]

Here, the B field for a single pole of a multipole magnet is treated as only having nonzero components in the radial direction and having a solenoid-like strength:

$$\begin{aligned} B_r &= C_n r^{n-1} \\ \int_{-z}^{z}\int_{0}^{r_0} B_r dr dz &= \frac{NI}{c} \end{aligned} \tag{4.1}$$

where the integral can be solved to find C_n. Here n denotes number of dipoles, such that $n = 2$ is a quadrupole, $n = 3$ is a sextupole, and so on. Evaluating over all poles (i.e. introducing a dependence on θ, which spans the transverse plane) and converting to the customary Cartesian system yields

$$B_\theta + iB_r = \frac{4\pi NInr^{n-1}e^{in\theta}e^{i\phi}}{cr_0^n} \tag{4.2}$$

$$\begin{aligned} B_y + iB_x &= \frac{4\pi NInr^{n-1}e^{i(n-1)\theta}e^{i\phi}}{cr_0^n} \\ &= \frac{4\pi NIn(x+iy)^{n-1}e^{i\phi}}{cr_0^n} \end{aligned} \tag{4.3}$$

where N is number of turns per magnet coil, r_0 is the pole-tip aperture radius, and ϕ is alignment of the Gaussian cylinder used to define B_r such that $\phi = 0$ and $\phi = \pi$ produce "normal" multipoles and $\phi = \pm\pi/2$ produces "skew" ones (see Fig. 1.1). This leads directly (via Maxwell's Equations) to

$$\begin{aligned} A_z &= -\frac{4\pi NIr^n e^{i\phi}}{cr_0^n} \\ &= -\frac{4\pi NI(x+iy)^n e^{i\phi}}{cr_0^n} \end{aligned} \tag{4.4}$$

where the non-canceling units are current per c, which is consistent with energy in Gaussian units.[‡]

[1] Wolski, *Beam dynamics: In High Energy Particle Accelerators*, pp20, 25–26.

[2] Wille, "The Physics of Particle Accelerators: An Introduction", p57.

[‡] If a reference strength is needed, the quantity $B_0 = \mu_0 NIn/r_0$, with I in amps and r_0 in meters gives the field strength at the magnetic pole tip in Teslas. We also note that units of amu·mm·ns are particularly useful in a beam physics context: despite the inconvenience of making the initial conversions, the proton mass is approximately one, the proton charge is roughly 10^{-5}, and c is approximately 299.8; keeping these essential constants near unity is more readable and helps avoid computational overflows when testing high energies.

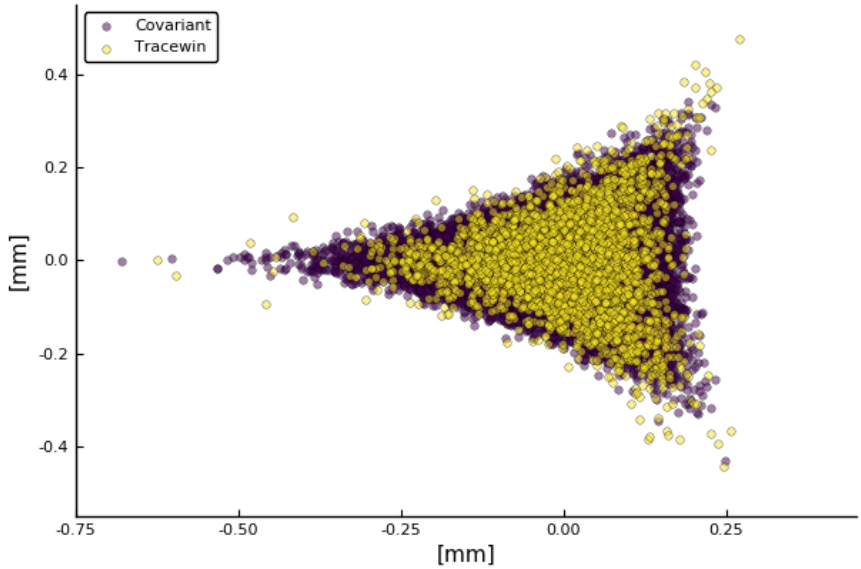

Figure 4.1: Comparison between Tracwin and a covariant integrator (see Eqs. [2.20] and [4.4]) for a 1 TeV bunch through a 1100 mm sextupole (n=3), $I = 20\,\mathrm{A}$, $r_0 = 1\,\mathrm{mm}$, $B_0 = 8\,\mathrm{T}$. Undersized pole-tip aperture and exagerrated field strength are used to emphasize transverse-space reshaping.

Figure 4.1 shows a benchmark comparison using this potential versus the commercial software package TraceWin[3] for a bunch passing through a sextupole magnet ($n = 3$). A highly relativistic bunch along with unrealistically high field strength and narrow aperture are used here to emphasize transverse shaping. Good matching is also observed for nonrelativistic bunches and more realistic machine parameters.

A noteworthy phenomenon arises for such z-only potentials: cursory examination of Eq. (2.1)[†] shows that a covariant Hamiltonian has terms proportional to A_z^2. Recalling the definition

$$\mathcal{P}^\alpha = p^\alpha + \frac{qA^\alpha}{c} \tag{4.6}$$

with an additional identity from Jackson:[4]

[3] Uriot and Pichoff, *TraceWin*.

[†] Reprinted here for convenience:

$$H = \frac{1}{m}\left(\mathcal{P}_\alpha - \frac{q}{c}A_\alpha\right)\left(\mathcal{P}^\alpha - \frac{q}{c}A^\alpha\right) - c\sqrt{\left(\mathcal{P}_\alpha - \frac{q}{c}A_\alpha\right)\left(\mathcal{P}^\alpha - \frac{q}{c}A^\alpha\right)} \tag{4.5}$$

[4] Jackson, *Classical Electrodynamics*, p585.

$$c\sqrt{\left(\mathcal{P}_\alpha - \frac{q}{c}A_\alpha\right)\left(\mathcal{P}^\alpha - \frac{q}{c}A^\alpha\right)} = mc^2 \tag{4.7}$$

we can then test the condition

$$\mathcal{A}^z = D\frac{qp^z}{c} \tag{4.8}$$

where D is an arbitrary scalar value, and we define a simple, non-rotating P^α as

$$\begin{aligned}\mathcal{P}^\alpha &= (\mathcal{P}_0, \mathcal{P}_r, \mathcal{P}_z) = (p_0, p_r, p_z + \frac{qA_z}{c}) \\ &= (\gamma mc, \gamma m\beta_r c, \gamma m\beta_z c + \frac{qA_z}{c})\end{aligned} \tag{4.9}$$

where r is a the radially transverse axis, and z is longitudinal. Then, for example, with $D = 1/2$ we have

$$P^z = -\frac{q}{c}A^z \tag{4.10}$$

this results in an $(A^z)^2$ dependent Hamiltonian, which can be converted to show explicit velocity dependence as follows:

$$\begin{aligned}H &= \frac{1}{m}\left(\mathcal{P}_0^2 - \vec{\mathcal{P}}^2 + \frac{2qA_z\vec{\mathcal{P}}}{c} - \frac{q^2A_z^2}{c^2}\right) - mc^2 \\ &= mc^2(\gamma - 1) - \frac{p_r^2}{m} - \frac{4q^2}{mc^2}A_z^2 \\ &= mc^2\gamma^2\left(1 - \frac{1}{\gamma^2} - \beta_r^2 - \beta_z^2\right)\end{aligned} \tag{4.11}$$

One can also note that, in general, the A_z^2 term is always attractive toward the origin for ultra-cold bunches (i.e. where $\beta_r \to 0$).

The case for $D = 1/20$ is illustrated in Fig. 4.2 for realistic beam conditions ($\beta_z \gg \beta_r$), where high β_z and β_r values lead to negative H values.

The more substantial consequence of this condition, in terms of multipole magnets, is illustrated by setting Eqs. (4.8) and (4.4) equal, which yeilds:

$$r = \left(\frac{\beta_z\gamma mc^2 n}{DqIN}\right)^{\frac{1}{n}} r_0 \tag{4.12}$$

which is illustrated in Fig. 4.3 for $D = 1/20$. For higher-order multipoles, this critical radius value approaches r_0 at lower β_z. However, the opposite is true for $D > 1$.

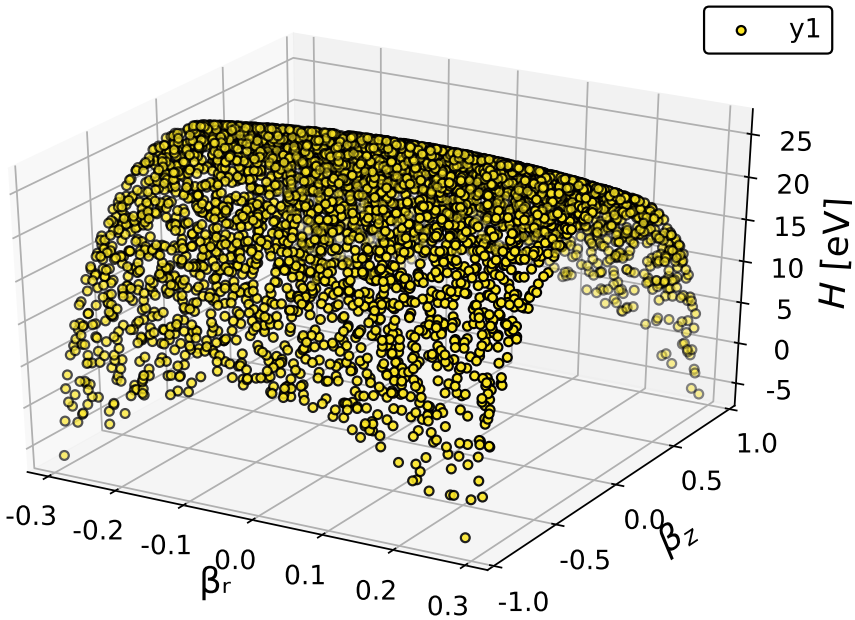

Figure 4.2: Hamiltonian magnitude for A_z^2 dominance condistions, with $D = 1/20$ and β_z and β_r spanning values for realistic beams.

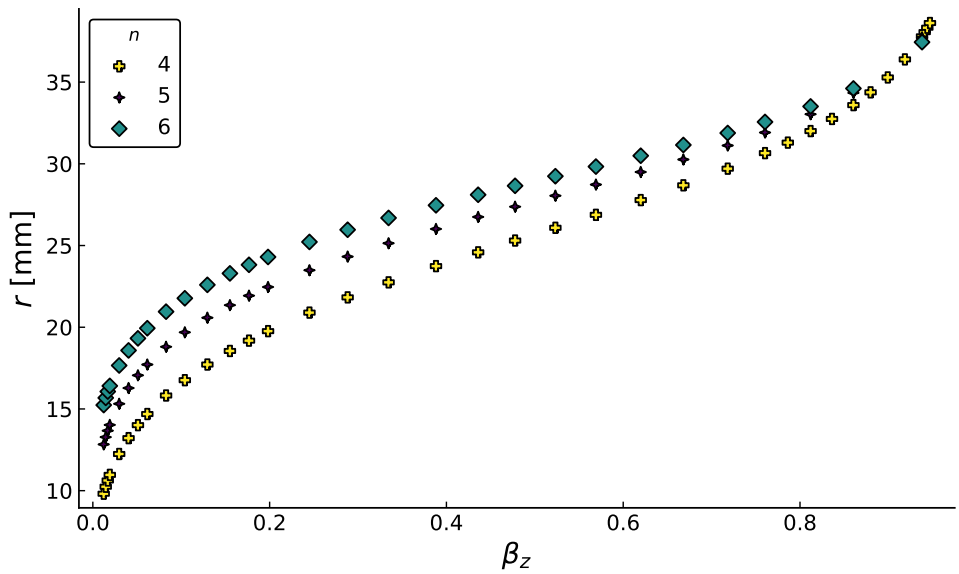

Figure 4.3: Critical radius for an octupole, decapole and dodecapole magnet $n = 4$,5, and 6, respectively, where the A_z^2 term is dominant. Here $D = 1/20$, current $I = 20$[A], number of coils $N = 2200$, and pole-tip radius $r_0 = 30$ [mm].

In practical terms, as magnet current or number of coils is increased or as β_z is decreased, the critical radius is reduced. For cases where the critical radius becomes less than the physical magnet radius r_0, this may present an effectively passive method for beam confinement.

On a related note: a peculiar trait arises for multipole magnets in cases where p_z is distributed about zero, as with two bunches upon collision or within a bunch's reference frame. In these cases, the transverse beam shaping behaves as with an equivalent $2n$ magnet—that is, passing through a quadrupole potential in this low p_z frame will shape a bunch as if it is passing through an octupole.

More generally, Jackson's covariant Hamiltonian is strikingly both nonlinear and deterministic. We have seen here how its nonlinear dependence is non-negligible on practical scales. The notion of nonlinearity as a fundamental trait of electrodynamics contrasts with its typical role as an element of chaos, randomness, or pseudorandomness; especially since we have operated under the Lorenz gauge, the Minkowski metric, and Maxwell's equations without any modification. In particular, the manifestation of universally attractive or respulsive $(A^\alpha)^2$ terms may be of interest beyond the realm of accelerator physics.

However, Jackson considers this Hamiltonian to be problematic for being a Lorentz scalar that is not energylike and identically equal to zero, thanks to Eqs. (4.6) and (4.7) and the identity $p_\alpha p^\alpha = mc^2$. To complicate the matter, Goldstein's similar Hamiltonian[5] reduces to $H = \frac{mc^2}{2}$ while Barut demonstrates that the two definitions are identical in terms of dynamics.[6] With Jackson's criticisms in mind, such covariant Hamiltonians should not be implemented without careful benchmarking.

4.2 Octupoles and 4N Symmetry

For charged-particle or ion bunches, an octupole displaces the outermost particles, reshaping a Gaussian transverse profile to a flattened or concave one.[7] Inherent to this flattening property is a four-fold rotational symmetry octupoles impart on transverse beam distributions (specifically, symmetry along each x–y diagonal).

Because of this, it is standard practice to introduce octupoles in pairs with

[5] Goldstein et al., "Classical Mechanics", p352.

[6] Barut, *Electrodynamics and Classical Theory of Fields & Particles*, p72.

[7] Tsoupas et al., "Uniform Particle Beam Distributions Produced by Octupole Focusing"; Yuri, "Beam uniformization system using multipole magnets at the JAEA AVF Cyclotron"; Folsom and Laface, "Beam dynamics with covariant hamiltonians".

respective quadrupoles so that their effects are only appreciable along one axis. This counteracts the defocusing of off-center particles near the diagonals. Such an approach is desirable when correcting high-order errors in beam-focusing or beam-steering optics.[8]

With this single-axis flattening, however, a number of transverse and longitudinal shaping phenomena are disregarded. This section reports on simulations of such effects. We show in the following sections that x–y decoupled, alternating-gradient, and dual-pulse multipoles can act on transversely symmetric 2D bunches to induce a variety of shaping effects such as low-loss flattening, isotropic focusing, transverse trapping, and longitudinal momentum biasing.

For a normal octupole, the potential term is

$$K_4\mathbb{R}(x+iy)^4 = K_4(x^4 - 6x^2y^2 + y^4) \tag{4.13}$$

What is noteworthy here is that the leading-order terms are both positive, resulting in the observed four-fold rotational symmetry. This carries for higher-order 4n-pole magnets (since $\mathrm{i}^{4n} = 1$), where the sign parity of like-order terms ensures identical distributions along the x and y axes. For example, the potential term for the hexadecapole is

$$K_8(x^8 - 28x^6y^2 + 70x^4y^4 - 28x^2y^6 + y^8) \tag{4.14}$$

To generalize, any $4n$ pole magnet could be considered "octupole like", with all other $2n$ pole magnets as "quadrupole like". In the latter case, x and y profiles may have symmetry about their own axes, but their profile shapes are always dissimilar. For both types, as the number of poles is increased, the shaping effect converges toward a circular 2D profile, with particles along the circumference driven between narrowing cusps.

Before moving on to other effects, one general trait is worth considering: due to the $(r/r_0)^n$ dependence, magnets with increasing n require much higher currents to achieve strengths comparable to dipoles or quadrupoles (except near the poles). Conversely, this ratio dictates that the field-strength curve becomes sharper for high-n magnets (Fig. 4.4). Because of this, higher-order $4n$ magnets can be expected to have a virtual aperture effect, potentially acting as non-mechanical beam scrapers.

[8] Meigo et al., "Beam flattening system based on non-linear optics for high power spallation neutron target at J-PARC"; Ho et al., *Octupole Correction of Geometric Aberrations for High-Current Heavy-Ion Beams*; Brinkmann and Raimondi, "Halo reduction by means of non linear optical elements in the NLC final focus system".

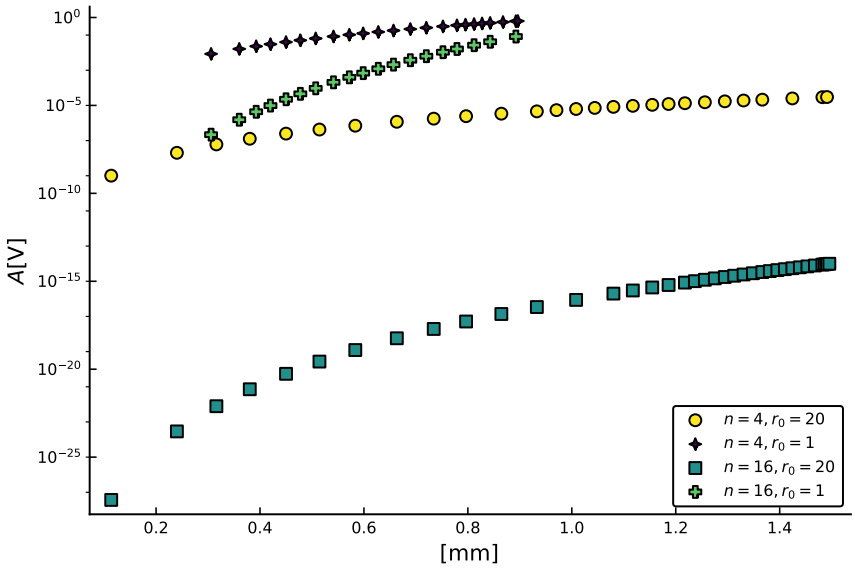

Figure 4.4: Semilog plot of $(r/r_0)^n$ behavior as per Eq. (4.4). With magnets of current $I = 20[\mathrm{A}]$, and number of coils $N = 300$.

4.3 Horizontal–Vertical Decoupling

Recent works have demonstrated how octupoles can be virtually decoupled in a periodic lattice by using quadrupole and dipole inserts on either side of an octupole.[9] That is,

$$H_4 \propto K_4(x^4 - \cancel{6x^2y^2} + y^4) \tag{4.15}$$

Figure 4.5 illustrates how a magnet with this idealized potential would improve beam flattening. Since decoupled multipoles are not implemented into standard beam-tracking software, these simulations were carried out solely with an in-house Lie-algebra code, using rudimentary space-charge kicks on either side of the magnet:

$$p = p_0 + \frac{C}{2}\,\mathrm{erf}\left(\frac{x}{\sigma_x}\right) \tag{4.16}$$

with

$$C = \frac{I\tau}{6\pi} \tag{4.17}$$

where I is beam current, τ is timestep, and the factor of $1/2$ in Eq. (4.16) reflects a halving of the magnet length and "erf" is the error function (this is

[9] Antipov, Nagaitsev, and Valishev, "Single Particle Dynamics in a Quasi-Integrable Nonlinear Accelerator Lattice"; Nagaitsev, Valishev, and Danilov, "Nonlinear optics as a path to high-intensity circular machines".

an approximation which assumes a linear space-charge force with a sigmoidal shape). This equation was verified to match Tracewin for Gaussian distributions in drift spaces with wide enough apertures to avoid image effects.

A key trait of the decoupled octupole is its virtually lossless flattening: a coupled magnet of the same field strength can only produce a similarly flattened profile by ejecting a significant percentage of its outermost particles. For example, the coupled octupole in Fig. 4.5a loses 1% of its particles to beyond $6\sigma_x$, whereas the decoupled octupole's losses are $\lesssim$0.1%.

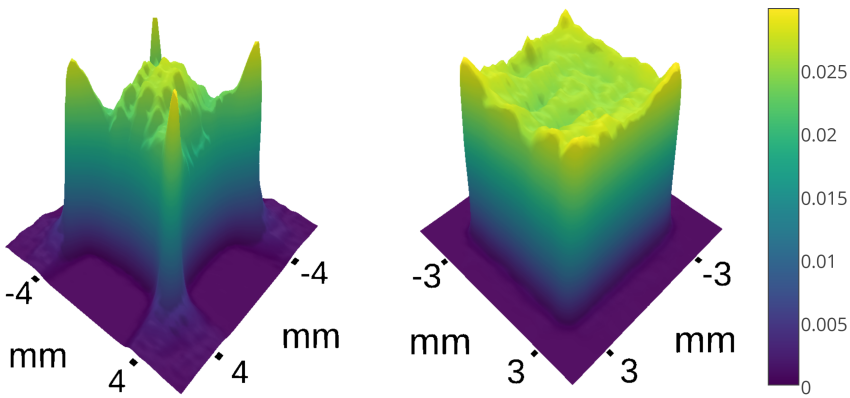

(a) (b)

Figure 4.5: Surface plot of Gaussian distributions (100k protons) passing through (a) coupled and (b) uncoupled octupoles, normalized to maximum bin occupancy. Beam and magnet parameters are otherwise identical: $a_0 = 25$ [mm], $\epsilon_\perp = 0.5$ [$\pi \cdot$ mm $\cdot$ mrad], $\beta_\perp = 1$ [mm/($\pi \cdot$ mrad)], $B_0 = 3$ T, $K_E = 4$ MeV, I = 30 mA, and magnet length $L = 500$ mm.

As field strength is increased, focusing can also be observed in decoupled magnets with a reduced loss rate (i.e. a reduction of σ_x by 50% with ~7% ejecta for decoupled magnets and $\gtrsim$30% ejecta for coupled magnets).

However, the use of Eq. (4.15) in obtaining these results must be considered an idealization, since in practice, the inserts required for virtual decoupling are calibrated via the thin-lens approximation.

4.4 Alternating-gradient Octupole Arrays

While we have established that better flattening can be achieved with decoupled octupoles than with unmodified ones such as in Fig. 4.5a; in either case, doing so typically requires a significant dilation of the transverse dimensions.

This can be improved if we consider a hypothetical multipole magnet lattice with successive kicks of $-9, -6, -3, 0, 3, 6, 9$ T as one half-period (with a symmetrically descending second half). It is important here to make the distinction that this is an *effective* RF multipole, in that the bunch witnesses a vitually oscillating field; but it is not an actual RF system, as the fields remain fixed in the lab frame to avoid induced electric fields.

The results to follow consider such stepped-gradient $4n$ pole lattices with effective periods between 1 MHz and 1 THz, and with simulations carried out in TraceWin.[†]

For lower magnet strengths (or stronger emittances), this effectively creates a virtual aperture: Initially, a shell of the outermost particles is lost in the first few cycles (which can be kept negligible by gradually ramping to the maximum amplitude over, say, a dozen cycles). After a few hundred cycles ($\sim$100 mm), the beam distribution tends toward a conical shape and the loss rate drops effectively to zero. This phenomenon holds for Gaussian distributions, but is more easily observed with waterbag or KV distributions.

When accounting for space charge, the shaping effects are similar, with losses occurring at a constant rate that increases with beam current. At higher field strengths, losses can be eliminated altogether—transverse positions are effectively frozen after an initial dilation. Tests performed for high beam currents (exceeding 1 A) show a similar, stable transverse fixation effect.

Figure 4.6 shows the longitudinal effects of trapping a 50 MeV electron beam. With an initial $\sigma_{z'}$ of 0.002 mrad, the longitudinal momentum quickly dilates symmetrically, as in Fig. 4.6a. Particles with high transverse momenta then begin to recirculate with a bias in the positive z' direction—Fig. 4.6b. A RF-dependent rotation of the momentum distribution about the z'-axis also occurs. Such recirculation and rotation effects may have a considerable bearing on the velocity-depending LW potentials (both Coulombic and magnetic-dipole-moment based).

Here, an extremely small pole-tip aperture is used to exaggerate the effect — with more realistic parameters, an increase in momentum of a factor of 10 can be observed, with a similar forward-weighting of the electron population toward positive z'.

[†]Although constructing such a lattice at lower frequencies may be feasible, 1 THz effective frequency upper limit is not a realistic parameter, but we consider it on the premise that such high-frequency multipole magnets may be of interest in micro-scale acceleration studies. The 10 T magnet strength limit is also exaggerated to make the shaping effects more apparent.

The cost effecting this z' bias comes as emittance gains (proportional to beam current). Here, the longitudinal emittance increases steadily, but transverse emittance levels off quickly as the particles become trapped. We note that these simulations were carried out solely in TraceWin; thus covariant space-charge effects developed in the prior chapters are not accounted for.

At higher frequencies, hollowing can be observed, with the bunch collapsing centrally as the magnet length is increased (see Fig. 4.7). Similar effects were reported by Neuner, Stancari and Blaugrund.[10] In this case, hollowing can be seen as an extension of beam flattening—a beam becomes approximately flat before it begins to populate the halo. Moreover, at comparable frequencies but increased field strengths, focusing can be achieved with zero ejecta (which forgoes hollowing and rapidly condenses the central region).

4.5 Double-Pulse Shaping

The aforementioned traits of alternating-gradient multipoles may be worth investigating further, but the fabrication of such devices is likely to require prohibitive stress tolerances or materials costs (though possibly realizable with emerging technologies such as superconducting canted cosine-theta magnets).[11]

For a simpler design, an initial octupole can provide a brief high-strength pulse so that a passing bunch arrives at the second octupole with a compacted momentum distribution but before its position distribution has been significantly altered. The second magnet then gives a longer, weaker pulse which effectively traps the perturbed central trajectories. This results in a sharper beam flattening than can be achieved with individual magnets, with an improvement comparable to that shown in Fig. 4.5. In preliminary tests, this scheme induces negligible losses when shaping to a bunch perimeter of $\sim 3\sigma_x$. By increasing the initial pulse strength, a width reduction to $\sim 2\sigma_x$ can be achieved with $\sim 1\%$ losses.

[10] Neuner et al., "Shaping of Intense Ion Beams into Hollow Cylindrical Form"; Stancari et al., "Collimation with hollow electron beams"; Blaugrund and Cooperstein, "Intense focusing of relativistic electrons by collapsing hollow beams".

[11] Wan et al., "Alternating-gradient canted cosine theta superconducting magnets for future compact proton gantries"; Fajardo et al., "Designs and prospects of Bi-2212 canted-cosine-theta magnets to increase the magnetic field of accelerator dipoles beyond 15 T".

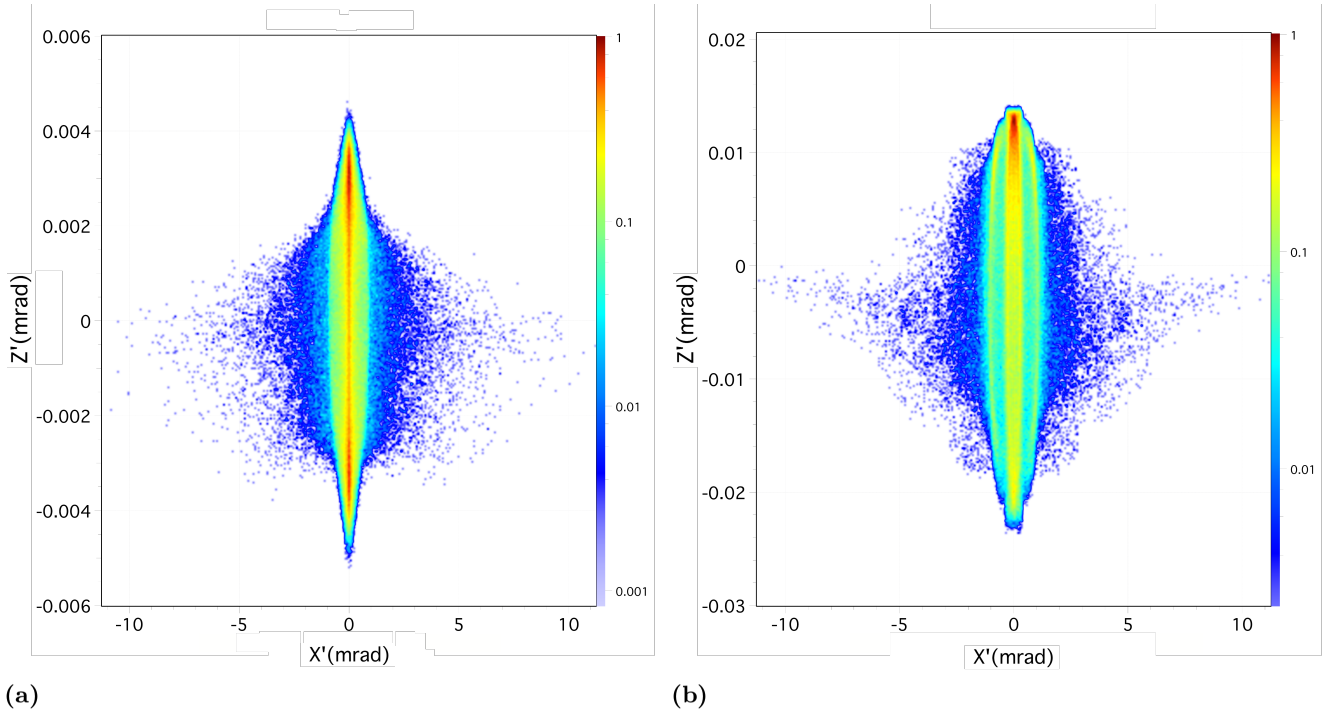

Figure 4.6: Transverse–Longitudinal momentum-density mapping for 500k electrons in a 30 GHz RF octupole at (a) 40 mm and (b) 400 mm; $a_0 = 1$ [mm], $\epsilon_\perp = 0.25$ [$\pi \cdot$ mm $\cdot$ mrad], $\epsilon_\parallel = 0.35$ [$\pi \cdot$ mm $\cdot$ mrad], $\beta_\perp = 4$ [mm/($\pi \cdot$ mrad)], $\beta_\parallel = 5$ [mm/($\pi \cdot$ mrad)], $B_0 = 10$ T, $K_E = 25$ MeV, I $= 50$ mA. The yellow-red bands diverge in the timesteps between (a) and (b) into a recirculation pathway wih a front-heavy chirp signature. Calculated and plotted with TraceWin.[a]

[a] Uriot and Pichoff, *TraceWin*.

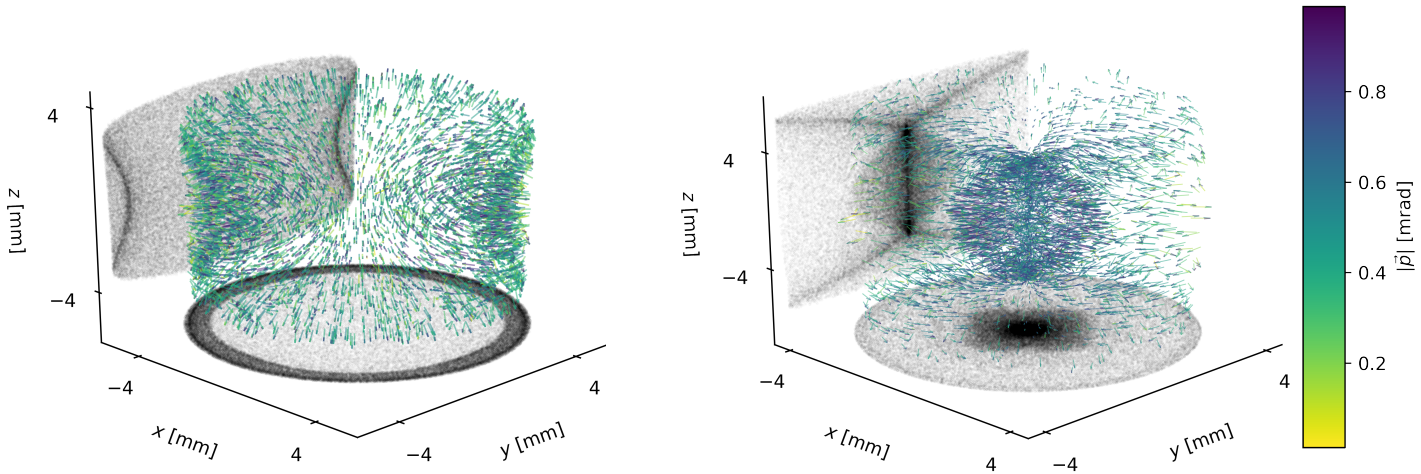

(a) **(b)**

Figure 4.7: Beam hollowing and subsequent collapse of electrons (100k, Gaussian) in a 1 THz, $B_{max} = 9$ T, RF octupole. Pole-tip radius $r_0 = 20$ [mm], $\epsilon_\perp = 0.25$ [$\pi \cdot$ mm $\cdot$ mrad], $\beta_\perp = 4$ [mm/($\pi \cdot$ mrad)], $K_E = 0.75$ MeV, I $= 62$ mA. Magnets lengths are 0.375 and 0.778 m and momenta are scaled to maxima of 20.9 and 24.5 mrad for (a) and (b) respectively. Calculated with TraceWin.[a]

[a]Uriot and Pichoff, *TraceWin*.

4.6 Remarks

We have only taken a preliminary look into the beam-shaping capabilities of high-order magnets. A more complete effort would simulate such devices in realistic lattices using an LW-based space-charge code and a covariant integrator. We have simply intended to highlight traits of multipoles which may merit further inquiry (and which require a sound nonlinear framework for accurate characterization).

An additional technique for fast simulation of multipoles by decoupling position and momentum terms is provided in Appendix D.

References

Antipov, S. A., S. Nagaitsev, and A. Valishev. "Single particle dynamics in a quasi-integrable nonlinear accelerator lattice". In: *arXiv preprint arXiv:1604.08565* (2016).

Barut, A. O. *Electrodynamics and Classical Theory of Fields & Particles*. Mineola, NY, USA: Dover, 2010; reprint, New York: MacMillan, 1964.

Blaugrund, A. E. and G. Cooperstein. "Intense focusing of relativistic electrons by collapsing hollow beams". In: *Physical Review Letters* 34.8 (Feb. 1975), pp. 461–464. DOI: 10.1103/PhysRevLett.34.461.

Brinkmann, R. and P. Raimondi. "Halo reduction by means of non linear optical elements in the NLC final focus system". In: *PACS2001. Proceedings of the 2001 Particle Accelerator Conference (Cat. No.01CH37268)*. Vol. 5. 2001, pp. 3828–3830. DOI: 10.1109/PAC.2001.988267.

Fajardo, L. G. et al. "Designs and prospects of Bi-2212 canted-cosine-theta magnets to increase the magnetic field of accelerator dipoles beyond 15 T". In: *IEEE Transactions on Applied Superconductivity* 28.4 (2018), pp. 1–5. DOI: 10.1109/TASC.2018.2818278.

Folsom, B. and E. Laface. "Beam dynamics with covariant hamiltonians". In: *Proc. 9th International Particle Accelerator Conference (IPAC'18), Vancouver, BC, Canada, April 29-May 4, 2018*. International Particle Accelerator Conference 9. Geneva, Switzerland: JACoW Publishing, 2018, pp. 3123–3126. DOI: 10.18429/JACoW-IPAC2018-THPAF064.

Goldstein, H. et al. "Classical mechanics". In: *American Journal of Physics* 70 (2002).

Ho, D. D. M. et al. *Octupole correction of geometric aberrations for high-current heavy-ion beams*. 1991. URL: http://cds.cern.ch/record/1054399.

Jackson, J. D. *Classical Electrodynamics*. New York, NY, USA: John Wiley & Sons Inc., 1999, pp. 579–585,661–663.

Meigo, S.-i. et al. "Beam flattening system based on non-linear optics for high power spallation neutron target at J-PARC". In: *Proceedings, 5th International Particle Accelerator Conference (IPAC 2014): Dresden, Germany, June 15-20, 2014*. 2014, MOPRI116. URL: http://jacow.org/IPAC2014/papers/mopri116.pdf.

Nagaitsev, S., A Valishev, and V Danilov. "Nonlinear optics as a path to high-intensity circular machines". In: *arXiv preprint arXiv:1207.5529* (2012).

Neuner, U. et al. "Shaping of intense ion beams into hollow cylindrical form". In: *Physical Review Letters* 85.21 (Nov. 2000), pp. 4518–4521. DOI: 10.1103/PhysRevLett.85.4518.

Stancari, G. et al. "Collimation with hollow electron beams". In: *Physical Review Letters* 107.8 (Aug. 2011), p. 084802. DOI: 10.1103/PhysRevLett.107.084802.

Tsoupas, N. et al. "Uniform particle beam distributions produced by octupole focusing". In: *Nuclear Science and Engineering* 126.1 (May 1997), pp. 71–79. URL: http://epubs.ans.org/?a=24458.

Uriot, D and N Pichoff. *TraceWin*. Saclay, France: CEA Saclay, 2014, p. 150.

Wan, W. et al. "Alternating-gradient canted cosine theta superconducting magnets for future compact proton gantries". In: *Phys. Rev. ST Accel. Beams* 18 (10 2015), p. 103501. DOI: 10.1103/PhysRevSTAB.18.103501.

Wille, K. "The physics of particle accelerators: an introduction". In: (2000).

Wolski, A. *Beam dynamics: In High Energy Particle Accelerators*. London, UK: Imperial College Press, 2014. URL: http://cds.cern.ch/record/1622200.

Yuri, Y. et al. "Beam uniformization system using multipole magnets at the JAEA AVF Cyclotron". In: *Conf. Proc.* C0806233 (2008), THPC045.

Chapter 5

Neutron Steering by Magnetic Moment

5.1 Introduction

Neutrons, while uncharged, are susceptible to external magnetic fields thanks to their magnetic dipole moment. In this case, the dominant potential is

$$U = -\vec{\mu}_n \cdot \vec{B} \tag{5.1}$$

where $\vec{\mu}_n$ is the neutron dipole moment (-6.02×10^{-8} eV/T $= -6.02 \times 10^{-12}$ eV/G) and $\vec{B}$ is an external magnetic field.[†] This is analogous to the term $\vec{v} \cdot \vec{A}$ arising in the relativistic Lagrangian for charged particles in external EM fields. In practice, the dipole moment aligns either parallel or antiparallel to the external field unless $\vec{B}$ is very small or rapidly changing.[1] This is often referred to as the adiabatic condition, which simplifies Eq. (5.1) to

$$U = \mp \mu_n |\vec{B}| \tag{5.2}$$

The adiabatic condition here can be stated in terms of the Larmour frequency ω_L as

$$\omega_L = -\frac{2\mu_n \vec{B}}{\hbar} \gg \frac{|\dot{\vec{B}}|}{\vec{B}} = \omega_B \tag{5.3}$$

[†]This applies to any neutral particle/antiparticle, atom, or molecule.

[1]Vladimirskii, "Magnetc mirrors, channels and bottles for cold neutrons"; Kügler et al., "Nestor — A magnetic storage ring for slow neutrons"; Opat, Wark, and Cimmino, "Electric and magnetic mirrors and gratings for slowly moving neutral atoms and molecules".

where it should be noted that ω_B is the change in $\vec{B}$ witnessed by the neutron. This may be defined alternatively as

$$\frac{\nabla|\vec{B}|\cdot\vec{v}}{|\vec{B}|^2} \ll \gamma_n \tag{5.4}$$

where $\vec{v}$ is the neutron's velocity and $\gamma_n = 1.83\times10^8\ \mathrm{s^{-1}T^{-1}} = 1.83\times10^4\ \mathrm{s^{-1}G^{-1}}$ is known as its gyromagnetic ratio.[2]

When adiabicity is not ensured, spontaneous spin-flipping can occur. A simple means of avoiding this is to construct a beamline with no drift spaces (e.g. a dipole field running longitudinally throughout).

In fact, storage rings have been constructed using this approach to measure the neutron lifetime.[3] These largely rely on sextupoles whose coils are aligned coaxially with the beam pipe, and their fields become circular near the transverse-plane origin.[†] The need for this realignment can be understood in terms of our covariant formalism by noting that the dipole-based potential is dependent on $\vec{B}$ instead of $\vec{B} = \nabla\times\vec{A}$.

Thus, for neutrons, this translates to dipole-like bunch shaping from a coaxial quadrupole, sextupole-like shaping from a coaxial octupole, and so on. For covariant tracking, we then have

$$\begin{aligned}
\underset{+1}{\mathcal{P}_z} &= \mathcal{P}_z \\
\underset{+1}{\mathcal{P}_y} &= \mathcal{P}_y + \frac{\tau\mu_n}{mc}\left(\mathcal{P}_z - \frac{\mu_n}{c}|B_z|\right)\frac{\partial|B_z|}{\partial r_y} \\
\underset{+1}{\mathcal{P}_x} &= \mathcal{P}_x + \frac{\tau\mu_n}{mc}\left(\mathcal{P}_z - \frac{\mu_n}{c}|B_z|\right)\frac{\partial|B_z|}{\partial r_x} \\
\underset{+1}{r_x} &= \nabla_x \\
\underset{+1}{r_y} &= \nabla_y \\
\underset{+1}{r_z} &= \nabla_z + \frac{\tau}{m}\left(\mathcal{P}_z - \frac{\mu_n}{c}|B_z|\right)
\end{aligned} \tag{5.5}$$

[2] Lee, *Final report - accelerator physics research at Indiana University in 2012–2016*.

[3] Kügler, Paul, and Trinks, "A magnetic storage ring for neutrons"; Kügler et al., "Nestor — A magnetic storage ring for slow neutrons"; Paul et al., "Measurement of the neutron lifetime in a magnetic storage ring".

[†] Such magnets are often referred to as "linear" which we will not use here to avoid with the definition of multipole magnets themselves as nonlinear. For clarity, we could suggest referring to conventional multipole magnets as radially coiled/aligned and these lengthwise ones as longitudinally coiled/aligned. For now, we will use the terms coaxial and radial for brevity.

Where we have (seemingly haphazardly) substituted $\mu_n|B_z|$ for qA_z. However, these quantities do have equivalent units; and the elemental definition here is the conjugate momentum:

$$\mathcal{P}^\alpha = p^\alpha + \frac{\mu_n}{c}|\vec{B}| \tag{5.6}$$

where, barring magnetic monopoles, a scalar B_0 is undefined.[†]

5.2 Confinement Considerations

Many notable traits of neutron storage rings relying on such coaxial-multipole steering were derived by McChesney.[4] We highlight a few of them here:

- For a normal-conducting ring (E $\approx$ 1 μeV), the required radius of curvature is only $\rho \approx 1$ m
- Intra-beam effects can be ignored (to an extremely high-density limit)
- Gravitational effects are minor, but non-negligible (needing a correcting magnetic gradient of ≈ 1.7 T / m, which is about a tenth that needed for the normal-conducting ring parameters listed above). Appropriate compensation to the vertical-axis dipoles must be made.
- So long as a scalar B_0 is applied, a time-dependent $B_z(t)$ can theoretically be used to accelerate or decelerate neutrons (that is, by alternating the current in the coaxial magnets except for a "base" dipole). This makes a standing-wave effect; similar systems emulating traveling-wave type acceleration as with RF cavities may also allow for sophisticated phase-space manipulation.[5]

[†]Alternatively, we can recast $\vec{\mu}\cdot\vec{B}$ using the Liebniz Integral Rule (also known as Feynman's Technique), where

$$\begin{aligned}\vec{\mu}\cdot\vec{B} &= \vec{\mu}\cdot(\nabla\times\vec{A}) \\ &= \nabla(\vec{A}\times\vec{\mu}) + \vec{A}\cdot(\cancel{\nabla\times\mu})\end{aligned} \tag{5.7}$$

which we can thus implement into a covariant integrator without defining $\vec{B}$. For example, if $A^\alpha = A^z$ and $\vec{\mu} = \mu^x$ in a Cartesian system, we have

$$\nabla\cdot(A^z\times\mu^x) = -\frac{\partial}{\partial y}A^z\mu^x \tag{5.8}$$

[4]McChesney, "Neutron accelerator physics".

[5]Summhammer, Niel, and Rauch, "Focusing of pulsed neutrons by traveling magnetic potentials".

We will assume that most neutron storage applications would avoiding spin-flips. However, it should be mentioned that the energy shifts involved in spin-flipping can be leveraged for focusing of ultracold neutrons.[6] They can also be used for acceleration and flattening,[7] where "nonabiatic" spin-flip devices in multiple stages can ensure that the dipole moment remains aligned with the external field and the resulting energy shift at each stage is "comparable to to the relative energy change of charged particles within a single accelerator cavity".[8]

An alternative means for focusing ultracold neutrons presents itself when testing Eqs. (5.5). Although the coaxial multipole-shaping effects are otherwise equivalent to those of $n+1$ radial multipoles, for magnet apertures approaching the limit of the bunch's transverse diameter, a superimposition appears of the expected profile and its skew counterpart (Fig. 5.1). This effect is due to the dependence on the absolute value of $\vec{B}$. The preferential populating of the overlapping areas then creates the focusing effect. Although the fabrication of such strong narrow-aperture magnets is prohibitive, the required field strengths do become more practicable for slower neutrons.

Once such a distribution is formed, a continued narrowing of the multipole aperture can focus the beam further with negligible losses. Higher order multipoles can also be used with a tradeoff of reduced losses for a less dramatic focusing effect.

For such focusing, the average transverse velocity can be seen to increase, especially in outlying particles. However, if the bunch was passed preemptively through a weak *radial* multipole magnet, the dipole moments of the neutrons furthest from the origin could be intentionally misaligned with the longitudinal axis. This would have the effect of skewing all the neutrons' dipole moments toward or away from the beam axis. In this way, particles furthest from the beam axis would receive weaker kicks from the subsequent coaxial magnets than those nearest the center, allowing for a smoother focusing. The downside here is that dealing with non-aligned dipole moments means sacrificing the simplicity of $U = \mp\mu_n|\vec{B}|$ and reverting to $U = \vec{\mu}_n \cdot \vec{B}$.

A basic application of such concepts could be the use of neutron storage rings as a backup supply in spallation sources to improve reliability. In the case of accelerator-driven nuclear transmutation or energy production[9] no matter how

[6] Arimoto et al., "Demonstration of focusing by a neutron accelerator".

[7] Alefeld, Badurek, and Rauch, "Observation of the neutron magnetic resonance energy shift".

[8] Weinfurter et al., "Inelastic action of a gradient radio-frequency neutron spin flipper".

[9] Bowman et al., "Nuclear energy generation and waste transmutation using an accelerator-driven intense thermal neutron source".

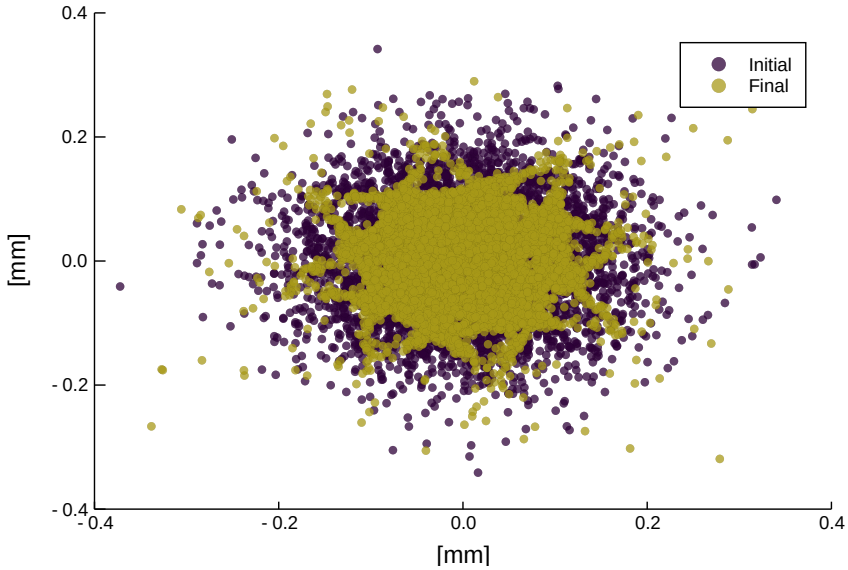

Figure 5.1: Transverse spatial profile for focusing of a neutron bunch through a narrow-aperture coaxial decapole. Pole-tip aperture: $r_0 = 0.3$ [mm]; decapole field strength $B_d = 0.83$ [T]; base dipole field strength $B_0 = 2.7$ [T] velocity 1 [mm/s]; longitudinal energy spread ∼5%; transverse momentum $p_r \approx 2.5\% \cdot p_z$; magnet length $L = 45$ [mm]. Initial distribution is Gaussian in all phase-space dimensions.

well-condensed such reserve bunches were, they could only reinject a fraction of the original spallation target's isotropic neutron cascade (though possibly enough to forestall a costly shutdown). Such a storage system would also be limited by the neutron lifetime (about 13.5 minutes). Skirting this limit by storing high-gamma neutrons would be ideal (possibly achievable by high-energy deuteron stripping;[10] though this would constitute an independent source).

In terms of collision experiments, probing the focusing limits of such high-energy neutrons may be also be fruitful in terms of luminosity enhancement. Further study of neutral-species beam physics may also shed light on the beam/bottle discrepancy in neutron lifetime measurements.[11] For example, it may be the case that extremely low transverse velocities or minimized spin-flip probabilities prolong the neutron lifetime.

[10] Serber, "The production of high energy neutrons by stripping"; Grand and Goland, "An intense neutron source based upon the deuteron-stripping reaction"; White, "Forward physics in PHENIX and ATLAS".

[11] Wietfeldt and Greene, "Colloquium: The neutron lifetime".

5.3 Emitted Fields

In general, applying beam-physics principles to neutral species seems to rest on the assumption their dynamics fall in a space-charge free domain. However, the basic retarded vector potential of a neutral particle should not be neglected:[12]

$$\begin{aligned}\vec{A} &= \frac{1}{R^3}\left[\vec{\mu}_{n_{\left(t-\frac{R}{c}\right)}}\cdot\vec{r}\right] + \frac{1}{cR^2}\left[\frac{\partial}{\partial t}\vec{\mu}_{n_{\left(t-\frac{R}{c}\right)}}\cdot\vec{r}\right] \\ &= \frac{\mu_n[\vec{n}\vec{r}]}{R^3} + \frac{\mu_n 2\pi[\vec{n}'\vec{r}]}{\lambda R^2} \\ &= \frac{\mu_n[\vec{n}\vec{r}]}{R^3} + \frac{\mu_n|\gamma_n\vec{B}|[\vec{n}'\vec{r}]}{cR^2}\end{aligned} \tag{5.9}$$

where R and $\vec{r}$ denote the source–objective separation vectors as with the Liénard–Wiechert potentials, and $\lambda = 2\pi c/\omega$ depends on the dipole's angular velocity ω. This we relate to the neutron's gyromagnetic ratio via $|\gamma_n| = \omega/|\vec{B}|$. The co-rotating unit vectors $\vec{n}$ and $\vec{n}'$ can then be defined in Cartesian terms as

$$\begin{aligned}\vec{n} &= \{\cos\left[\omega\left(t - r/c\right)\right]\hat{x} \quad , \quad \sin\left[\omega\left(t - r/c\right)\right]\hat{y} \quad , \quad \hat{z}\} \\ \vec{n}' &= \{-\sin\left[\omega\left(t - r/c\right)\right]\hat{x} \quad , \quad \cos\left[\omega\left(t - r/c\right)\right]\hat{y} \quad , \quad \hat{z}\}\end{aligned} \tag{5.10}$$

A check of where the $|\vec{B}|$ term becomes dominant requires values in the range of $|\vec{B}| = 10$ T and $r = 150$ mm. For an average interparticle spacing of 1 nm and $|\vec{B}| = 10$ T, the magnitude for the $|\vec{B}|$ dependent term is thus several orders of magnitude smaller.[†]

This discrepancy may leave one inclined to neglect the second term altogether. However, in a densely populated bunch a each particle will also *emit* a potential which augments the total magnetic field with an interaction term proportional to particle count N. Moreover, this potential neglects ω^2-dependent effects, which prove to be non-trivial.

[12] Sarychev, "Electromagnetic field of a rotating magnetic dipole and electric-charge motion in this field"; Tamm, *Fundamentals of the Theory of Electricity*.

[†] To briefly mention radiation: it is only dependent on the neutron's rotation orthogonal to direction of the magnetic moment. In other words, if the magnetic dipole axis is not orthogonal to the axis of rotation, then we can restate Eq. (5.9) as

$$\vec{A} = \mu_n\cos\alpha\frac{\vec{n}_z\vec{r}}{r^3} + \sin\alpha\left(\mu_n\frac{\vec{n}_\perp\vec{r}}{r^3} + \mu_n\frac{\omega}{cr^2}\vec{n}'_\perp\vec{r}\right) \tag{5.11}$$

where only the second term contributes to radiation. Thus, for a high-strength external field, dipole moments may be considered fully aligned according to the adiabatic approximation, and only the first term here is relevant. However, in a nonuniform field, the radiative effects should not be overlooked.

We will illustrate these effects shortly, but should first point out a distinguishing trait for neutrons: μ_n and γ_n both carry negative signs. This gives the two terms on the last line of Eq. (5.9) opposite signs, yeilding repulsive and attractive potentials for the left and right terms, respectively.[†] Thus, in general, a neutral particle with a positive magnetic dipole moment will behave quite differently from that of one with a negative moment if acting on a *charged* object. However, the forces between neutral particles are ultimately dependent on μ^2, and thus sign-agnostic.

For a more accurate approach, the Liénard–Wiechert-based pairwise fields can be used:[13,14]

$$\vec{B}_{ij} = \frac{|\vec{B}_{ext}\gamma_n|^2}{4\pi c^2 R(1-\vec{\beta}\cdot\hat{n})}\left[\vec{\mu}_n - (\vec{\mu}_n\cdot\hat{n})\hat{n}\right] + \frac{1}{R^3}\left[3(\vec{\mu}_n\cdot\hat{n})\hat{n} - \vec{\mu}_n\right] \tag{5.12}$$

where $\hat{n}$ is the unit vector $\vec{r}/R$ as usual, and we have re-introduced the requisite $\vec{\beta}$ dependence.[‡,15]

Here we must consequently assume that a particle witnesses a total field $\vec{B}_{tot} = \sum \vec{B}_{ij} + \vec{B}_{ext}$ (and that $|\vec{B}_{ext}|$ must remain greater than $|\sum \vec{B}_{ij}|$ for dipole moments to remain polarized along the beam axis).

This gives rise to a clear space-charge-like focusing limit. For example, if $|\vec{B}|$ is not explicitly dependent on r (as in the case of a coaxial dipole field) we can find a simple expression the force between two particles separated on the transverse axis with $\vec{\beta}$ also in the $\hat{n}$ direction

$$\begin{aligned}\vec{F}_{ij} &= \vec{\nabla}(\vec{\mu}_n\cdot\vec{B}_{ij}) \\ &= -\frac{\mu_n^2|\gamma_n\vec{B}_{ext}|^2}{R^2 4\pi c^2(1-\beta_n)}\hat{r} + 3\frac{\mu_n^2}{R^4}\hat{r}\end{aligned} \tag{5.13}$$

[†]Electrons share this trait, whereas these potentials are like-signed for protons. Of course, these potentials are negligible compared to space charge.

[13]Griffiths, "Dipoles at rest".

[14]Jackson, p413.

[‡]This expression can be derived from Jackson or Mognahan's works, not Tamm's, as was used above. We risk confusing the two on the grounds that for Tamm's is likely the more practical, but the others' are more robust.

Specifically, the Eq. (5.12) is the real part of an approximation about $e^{i\omega r/c}$, where we have assumed that this exponential term is approximately one. For greater distances and high magnet strengths (e.g. > 10 T and > 10 mm) this is not valid and the full expression should be used. Additionally, Heras and Mognahan's works (listed below) provide the most generalized models available.

[15]Heras, "Radiation fields of a dipole in arbitrary motion"; Monaghan, "The Heaviside-Feynman expression for the fields of an accelerated dipole".

where $\vec{\mu}_n \cdot \hat{n} = 0$. We can now complement our previous estimate for the potential shown above: for an external field strength of approximately 10 T these terms are balanced at a separation distance of 1.75 pm with each contributing a magnitude of roughly 10 pN, where the field-dependent term dominates at greater distances and we have ignored β_n. If, on the other hand, β_n were non-negligible in the $\hat{n}$ direction the force becomes asymptotically large (while attenuating to a factor of 1/2 if in the $-\hat{n}$ direction).

The second term in Eq. (5.13) thus gives us a fair estimate for a theoretical focusing limit for neutrons. What is perhaps more interesting is the resulting self-correcting nature of the first term: any outlier particle witnesses a bunch's total field $|\vec{B}_{tot}| \propto N \sum \vec{F}_{ij}$ where the attractive term can expected to have a substantial effect at average separation distances much greater than the repulsive term. Note that this is not the case for particles separated along the longitudinal axis (e.g. $\vec{\mu}_n \cdot \hat{n} = 1$): here there is a sole dependence on the repulsive term. This means the overall effect of a strong coaxial dipole $\vec{B}_{ext}\hat{z}$ for ultra-focused neutrons should be disk-like with sharp protuberances in the longitudinal directions.[†]

5.4 Remarks

While the theory and engineering for charged-particle acceleration is mature and well-suited for high-energy applications, neutral particles may provide a means for probing picoscale physics. Moreover, the acceleration of neutral particles, though not discussed here at length, is also feasible.[16] Although the accelerating gradients involved are several orders of magnitude weaker than those required for charged particles, the intra-bunch effects (analogous to space charge) are not only much weaker, but appear to be inherently self-stabilizing. Thus, for non-decaying neutral species (such as the hydrogen atom), experiments may be feasible on a timescale of days or weeks instead of hours.

Considering practical applications: given the renewed interest in spallation-driven reactors, a more robust theoretical framework for the spatial confinement and precision acceleration/deceleration of neutrons is wanting. A first-principles beam tracking approach is ideal, relying on the adiabatic approximation where necessary and using Liénard–Wiechert-based potentials for interparticle effects as in earlier chapters. Constructing a symplectic covariant integrator for the neutron

[†]Of course, this is a very simplified picture. For a neutron near the center of a densely populated bunch, it may be that $|\vec{B}_{ij}| \gg |\vec{B}_{ext}|$, in which case both spin-flipping and gradual changes to the direction of $\vec{\mu}_n$ must be accounted for.

[16]McChesney, "Neutron accelerator physics".

is non-trivial, however, especially considering that terms arising proportional to the change in dipole direction ($\partial\vec{\mu}_n/\partial\tau$) may not have an obvious solution and may become compounded with spin-flipping effects.

References

Alefeld, B., G. Badurek, and H. Rauch. "Observation of the neutron magnetic resonance energy shift". In: *Zeitschrift für Physik B Condensed Matter* 41.3 (1981), pp. 231–235. DOI: 10.1007/BF01294428.

Arimoto, Y. et al. "Demonstration of focusing by a neutron accelerator". In: *Phys. Rev. A* 86 (2 2012), p. 023843. DOI: 10.1103/PhysRevA.86.023843.

Bowman, C. et al. "Nuclear energy generation and waste transmutation using an accelerator-driven intense thermal neutron source". In: *Nuclear Instruments and Methods in Physics Research Section A: Accelerators, Spectrometers, Detectors and Associated Equipment* 320.1 (1992), pp. 336 –367. DOI: https://doi.org/10.1016/0168-9002(92)90795-6.

Grand, P. and A. Goland. "An intense neutron source based upon the deuteron-stripping reaction". In: *Nuclear Instruments and Methods* 145.1 (1977), pp. 49 –76. DOI: 10.1016/0029-554X(77)90557-2.

Griffiths, D. J. "Dipoles at rest". In: *American Journal of Physics* 60.11 (1992), pp. 979–987. DOI: 10.1119/1.17001.

Heras, J. A. "Radiation fields of a dipole in arbitrary motion". In: *American Journal of Physics* 62.12 (1994), pp. 1109–1115. DOI: 10.1119/1.17759.

Kügler, K.-J., W. Paul, and U. Trinks. "A magnetic storage ring for neutrons". In: *Physics Letters B* 72.3 (1978), pp. 422 –424. DOI: 10.1016/0370-2693(78)90154-5.

Kügler, K.-J. et al. "Nestor — a magnetic storage ring for slow neutrons". In: *Nucl. Instrum. Methods Phys. Res. A: Accelerators, Spectrometers, Detectors and Associated Equipment* 228.2 (1985), pp. 240–258. DOI: 10.1016/0168-9002(85)90266-9.

Lee, S. Y. *Final report - accelerator physics research at Indiana University in 2012–2016*. Tech. rep. Aug. 2017. DOI: 10.2172/1375754.

McChesney, P. "Neutron accelerator physics". English. PhD thesis. Indiana University, 2015, p. 203.

Monaghan, J. J. "The Heaviside-Feynman expression for the fields of an accelerated dipole". In: *Journal of Physics A: General Physics* 1.1 (1968), pp. 112–117. DOI: 10.1088/0305-4470/1/1/315.

Opat, G. I., S. J. Wark, and A. Cimmino. "Electric and magnetic mirrors and gratings for slowly moving neutral atoms and molecules". In: *Applied Physics B* 54.5 (1992), pp. 396–402. ISSN: 1432-0649. DOI: 10.1007/BF00325385.

Paul, W. et al. "Measurement of the neutron lifetime in a magnetic storage ring". In: *Zeitschrift für Physik C Particles and Fields* 45.1 (1989), pp. 25–30. ISSN: 1431-5858. DOI: 10.1007/BF01556667.

Sarychev, V. T. "Electromagnetic field of a rotating magnetic dipole and electric-charge motion in this field". In: *Radiophysics and Quantum Electronics* 52.12 (2009), pp. 900–907. ISSN: 1573-9120. DOI: 10.1007/s11141-010-9198-8.

Serber, R. "The production of high energy neutrons by stripping". In: *Phys. Rev.* 72 (11 1947), pp. 1008–1016. DOI: 10.1103/PhysRev.72.1008.

Summhammer, J., L. Niel, and H. Rauch. "Focusing of pulsed neutrons by traveling magnetic potentials". In: *Zeitschrift für Physik B Condensed Matter* 62.3 (1986), pp. 269–278. DOI: 10.1007/BF01313447.

Tamm, I. E. *Fundamentals of the Theory of Electricity*. Dec. 1966. URL: http://adsabs.harvard.edu/abs/1966fte..book.....T.

Vladimirskii, V. "Magnetc mirrors, channels and bottles for cold neutrons". In: *Soviet Phyiscs JETP* 12.4 (Apr. 1961), pp. 1062–1070.

Weinfurter, H. et al. "Inelastic action of a gradient radio-frequency neutron spin flipper". In: *Zeitschrift für Physik B Condensed Matter* 72.2 (1988), pp. 195–201. DOI: 10.1007/BF01312135.

White, S. "Forward physics in PHENIX and ATLAS". In: (2009). slides to be presented at QCD at Cosmic Energies IV which will be held in Trieste May 25-29 on 5/27 at 15:00. URL: http://cds.cern.ch/record/1178884.

Wietfeldt, F. E. and G. L. Greene. "Colloquium: the neutron lifetime". In: *Rev. Mod. Phys.* 83 (4 2011), pp. 1173–1192. DOI: 10.1103/RevModPhys.83.1173. URL: https://link.aps.org/doi/10.1103/RevModPhys.83.1173.

Appendix A: Proof for the Symplectic Condition

While the proof in the text for Liouville's theorem suffices to demonstrate that the determinant of the Jacobian matrix $|J| = 1$ for a Hamiltonian system, the more useful relation is the symplectic condition:

$$J^T S J = S \tag{A.1}$$

We first note that this leads immediately to $|J| = \pm 1$. The Pfaffian can then be used to explicitly rule out the -1 case

$$\begin{aligned} \mathrm{Pf(J^T SJ)} &= \det(J)\mathrm{Pf(S)} && \text{(A.2)} \\ \det(J) &= 1 && \text{(A.3)} \end{aligned}$$

To prove A.1 for any Hamiltonian system, we write J as

$$J = M\vec{\nabla} \tag{A.4}$$

Its time derivatives are then

$$\dot{J} = \frac{dM}{dt}\vec{\nabla}. \tag{A.5}$$

The time derivative of the n-th component of M is

$$\frac{d}{dt}M = \frac{\partial M}{\partial q_1}\frac{dq_1}{dt} + \cdots + \frac{\partial M}{\partial p_n}\frac{dp_n}{dt} \tag{A.6}$$

then we can write

$$\dot{M} = J\dot{\vec{s}} \tag{A.7}$$

and using $\dot{\vec{s}} = S \cdot \vec{\partial} H$ from Eqn. (1.15)

$$\dot{J} = J\dot{\vec{s}}\vec{\nabla} = JS\vec{\nabla}^T H\vec{\nabla} \tag{A.8}$$

Then we can calculate

$$\begin{aligned}\frac{d}{dt}\left(JSJ^T\right) &= \dot{J}SJ^T + JS\dot{J}^T \\ &= JS\vec{\nabla}^T H\vec{\nabla}SJ^T + JS\left(JS\vec{\nabla}^T H\vec{\nabla}\right)^T \\ &= JS\vec{\nabla}^T H\vec{\nabla}SJ^T + JS\vec{\nabla}^T\vec{\nabla}HS^TJ^T \\ &= 0 \end{aligned} \tag{A.9}$$

where we used $S^T = -S$ and $\vec{\nabla}^T\vec{\nabla}H = \vec{\nabla}^T H\vec{\nabla}$. Thus JSJ^T is a constant, and its value at time $t = 0$ must correspond to a matrix map $M = \mathbb{I}$ and in turn by Eq. (A.4) we have $J = \mathbb{I}$. Then

$$JSJ^T = S. \tag{A.10}$$

This is not quite the desired result, but the additional steps are fairly straightforward:

$$\begin{aligned} JSJ^T &= S \\ SJ^T &= J^{-1}S \\ J^T &= S^{-1}J^{-1}S \\ J^TS &= S^{-1}J^{-1}SS \\ J^TSJ &= S^{-1}J^{-1}SSJ \\ J^TSJ &= S \end{aligned} \tag{A.11}$$

where we have used $S^{-1} = -S$ and $S^2 = -\mathbb{I}$. This demonstrates that any solution of Hamilton's equations fulfills the symplectic condition.

References

Laface, E. *Accelerator recipes*. unpublished. 2018.

Appendix B: Liénard–Wiechert Potentials and Gravity

Having cited Hilborn's work[17] earlier in the text, the formalism developed throughout this thesis lends itself to generalizing his approach. In our notation (and ensuring all potentials remain energy-like in Gaussian units) $q_G = \sqrt{G}m$, with G being the gravitational constant, and assuming all A^α terms to be attractive. That is, for the static case $A^0(q_{EM}) = A^0(-q_G)$. Then, using $\partial^r A^0 = -\frac{\partial}{\partial r}A^0$ and $\mathcal{P}^\alpha = \mathcal{P}^0 = m_1 c + \frac{qA^0}{c}$ and Jackson's covariant equations of motion as throughout the main text, we have:

$$\frac{\partial \mathcal{P}^\alpha}{\partial \tau} = \frac{q_1}{m_o c} p_i (-\frac{\partial A^0}{\partial r}) = \frac{q_o q_s}{r^2}\hat{r} = -\frac{GM_s m_o}{r^2}\hat{r} \tag{B.1}$$

where the subscripts o and s denote objective and source particles, respectively.[†] Then, for the dynamic case $A^\alpha = \left(A^0(-q_G), \vec{A}(-q_G)\right)$ with $\hat{n} \cdot \beta_r = \pm\beta_r$ and $\beta_\phi = \beta_\theta = 0$ (i.e. perfectly linearly colliding/repelling masses with no spins) and reverting Eq. (2.4) to its simplified form via

$$\mathcal{P}^\alpha = p^\alpha + \frac{q}{c}A^\alpha = mV^\alpha + \frac{q}{c}A^\alpha \tag{B.2}$$

[17] Hilborn, "Gravitational waves from orbiting binaries without general relativity".

[†] In practice it can be helpful to remember that the momentum-dependent γ is affiliated with the objective while LW-dependent β belongs to the source. Then, in this formalism, the source "charge" is always negative, but the metric tensor and other dynamics are unaffected.

where $V^\alpha = (\gamma c, \gamma \vec{v})$, then one has

$$\begin{aligned}\frac{\partial \mathcal{P}^\alpha}{\partial \tau} &= \frac{q_1}{m_o c}(m_o V_\beta)\partial^\alpha A^\beta \\ &= \frac{q_1 q_2 \gamma}{r^2(1-\beta_r)}(1-\beta_r^2)\hat{r} = \frac{q_1 q_2}{r^2\gamma(1-\beta_r)}\hat{r} \\ &= \frac{-GM_s m_o}{r^2\gamma(1-\beta_r)}\hat{r} \end{aligned} \tag{B.3}$$

which implies an asymptotically increasing potential for relativistically colliding masses, and where $\hat{r} = \hat{n}$ (pointing *from* source to objective) is imposed by the Minkowski metric ($\hat{r} = -\hat{n}$ manifests a Euclidean metric).[†,18]

An interesting case arises for $\mathcal{P}^\alpha \approx qA^\alpha/c$ (i.e. p^α=0), since, by Eqs. (2.4) and (2.2)

$$\frac{\partial \mathcal{P}^\alpha}{\partial \tau} \to \frac{q_1^2}{m_o c^2} A_\beta \partial^\alpha A^\beta \tag{B.4}$$

This corresponds to—for the electromagnetic case—the potential witnessed by one bunch of 10^{11} protons at rest as another bunch approaches at 7 TeV to a distance of ∼20 cm. In the gravitational case, this corresponds to a potential witnessed by an equally populated 7 TeV proton bunch as it approaches a neutron star of 1 solar mass at a distance of 20,000 km (taken in the rest frame of the bunch, so that the neutron star appears to be the relativistically moving source term). Here, the surviving expressions are instead

$$\begin{aligned}\frac{\partial \mathcal{P}^\alpha}{\partial \tau} &\approx \frac{q_1^2 q_2^2}{r^3 m c^2 (1-\beta_r)^2}(1-\beta_r^2)\hat{r} \\ &= \frac{G^2 M_s^2 m_o}{c^2 r^3 (1-\beta_r)^2}(1-\beta_r^2)\hat{r} \end{aligned} \tag{B.5}$$

where in the latter case, an (instantaneous) repulsive gravitational potential occurs; this can be interpreted as a perturbative repulsive bump about $p^\alpha = 0$ in the bottom of the attractive gravitational potential well.

[†]Although the use of a Euclidean metric, and consequently Minkowski's original formulation $x_i = ict$ is typically treated as obsolete, here it has some pedagogical value, since for EM fields $\vec{E}_{x_i=ct} \to i\vec{E}_{x_i=ict}$, but $\vec{B}_{x_i=ct} \to \vec{B}_{x_i=ict}$. Then, instead of an assumed minus sign associated with A^α, we can use $q_G = \sqrt{G}im$. In this case, the gravitational fields are real in $\vec{E}$ and imaginary in $\vec{B}$, while the electromagnetic fields are the opposite. Such a metric may prove more convincing to the student by highlighting a fundamental disparity in the field-tensor definitions.

In any case, the potential-driven *dynamics*, are agnostic to these field definitions.

[18]Hehl, "Maxwell's equations in Minkowski's world: their premetric generalization and the electromagnetic energy-momentum tensor".

This zero-p^α condition is actually a limit, where $\beta_o \to -1$ (using an o subscript here for the object-mass velocity) while β_r is source velocity in the $\hat{n}$ direction.

We can also expect a singularity for $\frac{\partial \mathcal{P}^\alpha}{\partial \tau}$ at $\mathcal{P}^\alpha = p^\alpha + \frac{qA^\alpha}{c} = 0$. Here we can solve for r in the rest frame of an objective low-mass particle approaching a source mass ($p^\alpha = m_o c$, $A^\alpha = A^0 + A^\theta$). The spin-velocity $\beta_\theta \cdot \hat{n} = 0$ and the incoming particle then acquires a tangential velocity which approaches c but is attenuated by the spin of the source mass, such that $\beta_\theta \to \beta_o - \beta_s$. This yields

$$\begin{aligned} r &= -\frac{q_1 q_2 \left(1 + \beta_o - \beta_s\right)}{mc^2} \\ &= \frac{GM_s \left(1 + \beta_o - \beta_s\right)}{c^2} \end{aligned} \tag{B.6}$$

where $\beta_s = 0$ yields the Schwarzschild radius and $\beta_s \to 1$ yeilds the event-horizon radius for a rotating black hole. The classical proton/electron radius can then be found by the same method using the EM expressions for oppositely charged particles $q_1 = -q_2$, and where the *source* mass is not relevant.

The use of the LW potentials in this context should be limited to cases where the distance from the source is great enough to ensure negligible spacetime curvature (non-GR regime), but they may prove tractable in terms of predicting near- and far-field interactions for gravitational waves, particularly for many-body systems.

In the context of accelerator physics, it has been predicted that detection of gravitational waves may be possible at the 100 TeV scale.[19] However, in the case demonstrated in Fig. 3.7 and Eq. (3.21), charged particles traveling at near-parallel angles with $0.95 \leq \beta_z \leq 0.99$ do have a regime in which the electric and magnetic-dependent Lorentz forces stemming from the Liénard–Weichert potentials can be made to cancel (and thus electromagnetic space-charge effects are nullified). Under such conditions, the detection of gravitational velocity fields, whose total energy scales with γ^6, may be more feasible.

Moreoever, a noteworthy phenomenon occurs for the case of $\mathcal{P}^0 = -p^0/\gamma_o$. Recalling that $p^0 = \gamma_o mc = \mathcal{P}^0 - \frac{q_0 A^0}{c}$, and using the above definitions for q_G this results in the condition

$$r = \frac{GM_s}{c^2(\gamma_o^2 - \gamma_o)(1 - \beta_s)} \tag{B.7}$$

[19] Palazzi and Fargion, "On gravitational radiation emitted by circulating particles in high energy accelerators".

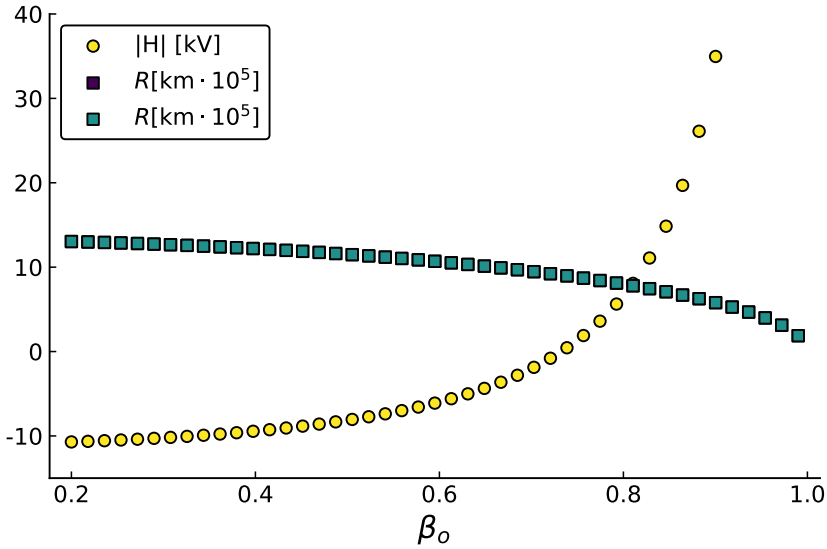

Figure B.1: Comparison of $R = |r|$ and H amplitudes via Eq. (B.9). Here the objective is a proton and the source is approximately one solar mass. Colinear velocity is taken in the proton's rest frame as $\beta_z = 0.99999956$, corresponding to an energy of $1\ \mathrm{TeV}$.

Building a Hamiltonian for this case is then straightforward:[†]

$$\begin{aligned}
H &= \frac{1}{m}\left((\mathcal{P}^0)^2 - (\vec{\mathcal{P}})^2 - 2\frac{q}{c}(\mathcal{P}^0 A^0 - \vec{\mathcal{P}}\vec{A}) + \frac{q^2}{c^2}\left((A^0)^2 - (A^n)^2\right)\right) - mc^2 \\
&= \frac{1}{m_o}\left((p^0)^2 - (\vec{p})^2 + 2\frac{q}{c}p^0 A^0 + \frac{q^2}{c^2}(A^0)^2\right) - m_o c^2 \\
&= -\gamma_o^2\beta_o^2 m_o c^2 + 2\frac{q}{\gamma_0 m_o c}p^0 A^0 + \frac{q^2}{m_o c^2}(A^0)^2 \\
&= -\gamma_o^2\beta_o^2 m_0 c^2 + \frac{q_o q_s}{R(1-\beta_s\cdot\hat{n})} + \frac{q_o^2 q_s^2}{c^2 R^2(1-\beta_s\cdot\hat{n})^2} \\
&= -\gamma_o^2\beta_o^2 m_o c^2 - \frac{G m_o M_s}{R(1-\beta_s\cdot\hat{n})} + \frac{G^2 m_o M_s^2}{c^2 R^2(1-\beta_s\cdot\hat{n})^2} \\
&= m_o c^2\left(\gamma_o^4 - 2\gamma_o^3 - \beta_o^2\gamma_o^2 + \gamma_o\right)
\end{aligned} \tag{B.9}$$

where we have used Eq. (B.7) with $R = |r|$ on the last line, and the objective-mass Lorentz factor β_o is relative to $\vec{p}$, *not* p^0.

[†]Here we re-use an approach similar to Eq. (4.11), building an LW-based Hamiltonian from Jackson's covariant Hamiltonian, as introduced in Eq. (2.1):

$$H = \frac{1}{m}\left(\mathcal{P}_\alpha - \frac{q}{c}A_\alpha\right)\left(\mathcal{P}^\alpha - \frac{q}{c}A^\alpha\right) - c\sqrt{\left(\mathcal{P}_\alpha - \frac{q}{c}A_\alpha\right)\left(\mathcal{P}^\alpha - \frac{q}{c}A^\alpha\right)} \tag{B.8}$$

where the second term reduces to $-mc^2$.

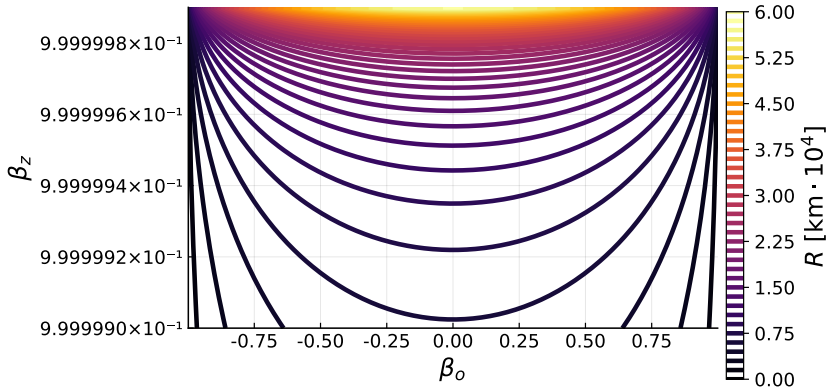

Figure B.2: $R = |r|$ scaling contours for Eq. (B.9) for high source and low objective (i.e. conlinear and non-colinear) velocites.

A zero-$|H|$ point can then be seen to occur at

$$r = \frac{GM_s\left(\sqrt{\beta_o^2\gamma_o^2} - 1\right)}{\beta_o^2 c^2 \gamma_o^2(\beta_s - 1)} \tag{B.10}$$

The utility of these Hamiltonians is demonstrated in Figs. B.1 and B.2, where a proton with a kinetic energy of 1 TeV approaches a solar mass with only orbital and colinear velocities, such that $\beta_s = \beta_z$. We calculate in the rest frame of the proton, and find that a repulsive region occurs for high transverse velocity β_o. In general, a zero-point magnitude H requires a fictitiously small r for any stellar objects (excluding extremely dense objects, such as neutron stars). However, as the proton's colinear kinetic energy exceeds 1 TeV, the threshold for H shifting from attractive to repulsive falls at r values exceeding the solar radius.

References

Hehl, F. "Maxwell's equations in Minkowski's world: their premetric generalization and the electromagnetic energy-momentum tensor". In: *Annalen der Physik* 17.9-10 (2008), pp. 691–704. DOI: 10.1002/andp.200810320.

Hilborn, R. C. "Gravitational waves from orbiting binaries without general relativity". In: *American Journal of Physics* 86.3 (Feb. 2018), pp. 186–197. ISSN: 0002-9505. DOI: 10.1119/1.5020984.

Palazzi, G. D. and D. Fargion. "On gravitational radiation emitted by circulating particles in high energy accelerators". In: *Physics Letters B* 197.1 (1987), pp. 302 –306. ISSN: 0370-2693. DOI: 10.1016/0370-2693(87)90388-1.

Appendix C: Covariant 3D Multipole Magnetic Potentials

We provide here a derivation for 3D magnetic multipole potentials based on Wolski's 2D potential,[20] starting from the cylindrical-coordinate version of Eq. (4.4):

$$A_z = -\frac{NIr^n e^{i\theta n}}{ncr_0^n} \tag{C.1}$$

where I and N are the respective coil current and number of turns, r_0 is pole-tip to center radius, r and θ are the respective radial and azimuthal position in the transverse plane, and we have set the alignment parameter ϕ_n to "normal" mode (0 or π) for simplicity. (Note that $r^n e^{i\theta n}$ reduces to $(x+iy)^n$.)

In Chapter 2, we posited Eq. (2.21) from Jackson's covariant vector-potential formalism.[21] We derive it in full here:

$$\begin{aligned}
\frac{\partial \mathcal{P}^\alpha}{\partial \tau} &= \frac{q}{mc}\left(\mathcal{P}_\beta - \frac{q}{c}A_\beta\right)\partial^\alpha A^\beta = \frac{q}{c}V_\beta \partial^\alpha A^\beta \\
&= \frac{q}{c}V^\alpha g_{\alpha\beta} g^{\beta\alpha}\partial_\beta A^\beta = \frac{q}{c}V^\alpha \delta^\alpha_\alpha \partial_\beta A^\beta \\
&= 4\frac{q}{c}V^\alpha \partial_\beta A^\beta \\
\therefore & \\
\partial_\beta A^\beta &= \frac{V_\alpha V_\beta}{4c^2}\partial^\alpha A^\beta
\end{aligned} \tag{C.2}$$

where we have used the identities $\mathcal{P}^\alpha = mV^\alpha + \frac{q}{c}A^\alpha$, $V^\beta V_\beta = c^2$, $V_\alpha = \gamma(c - \vec{v})$

[20] Wolski, *Beam dynamics: In High Energy Particle Accelerators*, p16.
[21] Jackson, *Classical Electrodynamics*, p583.

and $\delta^\alpha_\alpha = 4$. For the case of a z-only potential (i.e. $A^\alpha = A^z$), this becomes

$$\begin{aligned}\frac{\partial A_z}{\partial z} &= -\frac{\beta_z\gamma}{4}\left(\frac{\partial A_z}{\partial r}\beta_r + \frac{1}{r}\frac{\partial A_z}{\partial \theta}\beta_\theta + \beta_z\frac{\partial A_z}{\partial z}\right) \\ &= -\frac{\beta_z\gamma}{\beta^2\gamma + 4}\left(\frac{\partial A_z}{\partial r}\beta_r + \frac{1}{r}\frac{\partial A_z}{\partial \theta}\beta_\theta\right)\end{aligned} \tag{C.3}$$

where we assume no time dependence, and in cylindrical coordinates $\partial^\alpha A^z = -\left(\frac{\partial A_z}{\partial r} + \frac{1}{r}\frac{\partial A_z}{\partial \theta} + \frac{\partial A_z}{\partial z}\right)$. We can then guess that a z-dependent extension of Eq. (C.1) will have the form

$$A_z = -\frac{NIr^n e^{i\theta n}}{ncr_0^n}\exp\left[\frac{zn}{r}(\beta_r + i\beta_\theta)\right] \tag{C.4}$$

Thus, explicitly

$$\begin{aligned}\frac{\partial A_z}{\partial z} &= nr^{-1}(\beta_r + i\beta_\theta)A_z \\ \frac{1}{r}\frac{\partial A_z}{\partial \theta} &= inr^{-1}A_z \\ \frac{\partial A_z}{\partial r} &= nr^{-1}A_z - \frac{z}{r}\frac{\partial A_z}{\partial r}\end{aligned} \tag{C.5}$$

which can be reinserted into Eq. (C.3) to yield

$$r = \frac{\beta_r\beta_z\gamma z}{\beta_z^2\gamma + \beta_z\gamma + 4} \tag{C.6}$$

which, can then be inserted into Eq. (C.4) for equivalent r and z-dependent solutions

$$A_z(r,\theta) = -\frac{NIr^n e^{i\theta n}}{ncr_0^n}\exp\left[\frac{n\left(\beta_r + i\beta_\theta\right)\left(\beta_z^2\gamma + \beta_z\gamma + 4\right)}{\beta_r\beta_z\gamma}\right] \tag{C.7}$$

$$A_z(z,\theta) = -\frac{NIe^{i\theta n}}{ncr_0^n}\left(\frac{\beta_r\beta_z\gamma z}{\beta_z^2\gamma + \beta_z\gamma + 4}\right)^n\exp\left[\frac{n\left(\beta_r + i\beta_\theta\right)\left(\beta_z^2\gamma + \beta_z\gamma + 4\right)}{\beta_r\beta_z\gamma}\right] \tag{C.8}$$

where the predominant $\left(\frac{\beta_r}{\beta_z}z\right)^n$ dependence in the latter equation indicates a negligible z dependent contribution for $\beta_z \gg \beta_r$. The r dependent potential here remains the simpler option for building a covariant integrator; either choice frees us from violating the identity (in Gaussian units)

$$\partial_\alpha A^\alpha = \frac{1}{c}\frac{\partial\Phi}{\partial\tau} + \frac{\partial A_z}{\partial z} = 0 \tag{C.9}$$

when solving for $\underset{+1}{r}^{0}$ and $\underset{+1}{P}^{0}$ (as was done for brevity in the body text).

For completeness, we can take a new $\frac{\partial A_z}{\partial z}$ from Eq. (C.8) and equate it to its mate in Eq. (C.5) yields the alternative expression

$$r = -z(\beta_r + i\beta_\theta) \tag{C.10}$$

which can be used to simplify $A_z(z, \theta)$ to

$$A_z(z,\theta) = -\frac{NIr^n e^{i\theta n}}{ncr_0^n}\left(-z\left(\beta_r + i\beta_\theta\right)\right)^n \exp\left[-\frac{n\left(\beta_r + i\beta_\theta\right)\left(\beta_z^2\gamma + \beta_z\gamma + 4\right)}{4\beta_r\beta_z\gamma}\right] \tag{C.11}$$

We also now have definitions of all three β components which can be used with the *original* form of Eq. (C.4) to find

$$\begin{aligned}\frac{1}{c}\frac{\partial\Phi}{\partial\tau} = -\frac{\partial A_z}{\partial z} &= -\cancel{\frac{\partial A_z}{\partial\beta_z}}\cancel{\frac{\partial\beta_z}{\partial z}} - \frac{\partial A_z}{\partial\beta_r}\frac{\partial\beta_r}{\partial z} - \frac{\partial A_z}{\partial\beta_\theta}\frac{\partial\beta_\theta}{\partial z} - \frac{\partial A_z}{\partial r}\frac{\partial r}{\partial z} \\ &= -\frac{4\beta_r\beta_z\gamma n}{r\left(\beta_z^2\gamma + \beta_z\gamma + 4\right)}A_z\end{aligned} \tag{C.12}$$

which can be combined with the $\frac{\partial A_z}{\partial z}$ expression from Eqs. (C.5) to solve for a γ solely dependent on β components. This leads to the solution

$$\frac{1}{c}\frac{\partial\Phi}{\partial\tau} = -\frac{NIr^n e^{i\theta(n-1)}}{zcr_0^n} \tag{C.13}$$

or

$$\Phi = -\frac{\tau NIr^n e^{i\theta(n-1)}}{zr_0^n} \tag{C.14}$$

which is consistent with Gaussian units for electromagnetic potential. We now have a complete solution for A^α with a linearly time-dependent Φ component.

This solution has a practical weakness: Eq. (C.4) does not fall off with large z values, and assumes an unmoderated exponential growth/falloff in z. So without an additional scaling factor such as e^{-z_0}, it is primarily of use in calculating a particle or bunch as it approaches or exits from the aperture a multipole magnet. With a suitable scaling factor, one can also take $z \to |z|$ with the center of the magnet as a maximum.

Alternatively, to calculate the potential falloff near the center of a multipole magnet, we can change signs in the z dependent exponential term in our potiential:

$$A_z = -\frac{NIr^n e^{i\theta n}}{ncr_0^n}\exp\left[-\frac{zn}{r}(\beta_r + i\beta_\theta)\right] \tag{C.15}$$

which has less forgiving intermediate solutions, but ultimately yeilds

$$\Phi = -c\tau \left(\frac{n}{z} - \frac{2nr}{\beta_r} \right) A_z \tag{C.16}$$

In either case, a longitudinal scaling factor should also be introduced through the middle of the magnet.

References

Jackson, J. D. *Classical Electrodynamics*. New York, NY, USA: John Wiley & Sons Inc., 1999, pp. 579–585,661–663.

Wolski, A. *Beam dynamics: In High Energy Particle Accelerators*. London, UK: Imperial College Press, 2014. URL: `http://cds.cern.ch/record/1622200`.

Appendix D: Position–Momentum Decoupling Approximation

This appendix summarizes a non-covariant speedup approach presented in an earlier works.[22, †] It is similar to the covariant method stemming from Eq. (2.28); the results shown rely on a paraxial Hamiltonian and Lie-operator tracking, but compatibility with covariant integrators is also discussed.

The starting point for this method involves taking particle count N as an invariant as the position and momentum envelopes ρ_x and ρ_p evolve:

$$\int \rho_x^L dx_L = \int \rho_x^i dx_i = \int \rho_p^L dp_L = \int \rho_p^i dp_i = N \tag{D.1}$$

where ρ_x^L and ρ_x^i are the respective final and initial position densities, and likewise for the momentum densities.

To exploit this identity, ρ_x^L must be independent of p_i. This can be accomplished using the approximation[23]

$$p_i \approx -\frac{\alpha}{\beta} x_i \tag{D.2}$$

where α and β are the well-known Twiss parameters. Unfortunately, this approximation is only valid if the previous history of the beam is linear (thus

[22] Folsom and Laface, "Fast tracking of nonlinear dynamics in the ESS linac simulator via particle-count invariance"; Folsom and Laface, "Approximating nonlinear forces with phase-space decoupling".

[†] The usage of "decoupling" here is not to be confused with that in Section 4.3, and the sources cited therein, where it refers to eliminating terms with horizontal–vertical interdependence.

[23] Yuri et al., "Uniformization of the transverse beam profile by means of nonlinear focusing method"; Meot and Aniel, "Principles of the non-linear tuning of beam expanders".

maintaining elliptical phase-space densities). Since we want an algorithm that remains accurate for iterated nonlinear kicks (which develop irregular density profiles), a new approximation is needed.

Proceeding under the constraint that the initial distribution is Gaussian in both x and p, we can solve Eq. (D.1) for x_i and p_i.

$$\begin{aligned} \int \rho_x^0 dx_i &= \int \rho_p^i dp_i \\ \frac{1}{2}\,\mathrm{erf}\left(\frac{\sqrt{2}x_i}{2\,\sigma_{x_i}}\right) &= \frac{1}{2}\,\mathrm{erf}\left(\frac{\sqrt{2}p_i}{2\,\sigma_{p_i}}\right) \end{aligned} \tag{D.3}$$

which yields

$$p_i = \sqrt{2}\sigma_{p_i}\,\mathrm{erfinv}\left(\mathrm{erf}\left(\frac{\sqrt{2}x_i}{2\sigma_{x_i}}\right)\right) = x_i\frac{\sigma_{p_i}}{\sigma_{x_i}} \tag{D.4}$$

This solution does produce a bigaussian phase-space ellipse, so is still unsuitable for approximating p_i with distributions of an irregular shape. We retain it as a "naive" approximation for further comparison.

We continue by guessing that a solution exists for $p_i = f(x_i)$ for irregularly shaped distributions. Denoting these solutions as p^* and ρ_p^* for momentum and momentum density, respectively, we have

$$\int \rho_p^*(p_i)\; dp^*(x_i) = \int \rho_p^i dp_i \tag{D.5}$$

where it is critical to note that p^* is solely dependent on x_i, while ρ_p^* remains a function of p_i (and likewise for x^* and ρ_x^*). With the left-hand-side integrand and integration variables decoupled, it follows (for both x^* and p^*):

$$\begin{aligned} N = x^*\rho_x^* &= \int \rho_x^i dx_i \\ = p^*\rho_p^* &= \int \rho_p^i dp_i \end{aligned} \tag{D.6}$$

Exploiting particle-count invariance again, and squaring N, we can assert that

$$N^2 = \mathcal{C} = \rho_x^*\rho_p^* x^* p^* \tag{D.7}$$

and thus

$$\frac{d}{dx_i}\mathcal{C} + \frac{d}{dp_i}\mathcal{C} = 0 \tag{D.8}$$

We can then simplify, momentarily neglecting the $\frac{d}{dp_i}$ terms as $f(p_i)$:

$$\begin{aligned} 0 &= \frac{d}{dx_i}\mathcal{C} + \frac{d}{dp_i}\mathcal{C} \\ &= \frac{\partial \rho_x^*}{\partial x_i}\left(\rho_p^* x^* p^*\right) + \frac{\partial p^*}{\partial x_i}\left(\rho_x^* \rho_p^* x^*\right) + f(p_i) \\ &= \frac{\partial \rho_x^*}{\partial x_i}\left(\int \rho_p^i dp_i \; x^*\right) \\ &+ \frac{\partial p^*}{\partial x_i}\left(\int \rho_x^i dx_i \; \frac{\int \rho_p^i dp_i}{p^*}\right) + f(p_i) \end{aligned} \tag{D.9}$$

Then, dividing by $\int \rho_p^i dp_i$, the $f(p_i)$ terms become zero[†] and we have:

$$\begin{aligned} 0 &= \frac{\partial \rho^*}{\partial x_i}\; x^* + \frac{\partial p^*}{\partial x_i}\; \frac{1}{p^*} \int \rho_x^i dx_i \\ &= \frac{\rho_x^*}{\partial x_i}\; x^* + \frac{\partial p^*}{\partial x_i}\; \frac{1}{p^*} x^* \rho_x^* \\ &= \left(\frac{\partial \rho_x^*}{\partial x_i} + \frac{\partial p^*}{\partial x_i}\; \frac{1}{p^*} \rho_x^*\right) \end{aligned} \tag{D.11}$$

By reusing Eq. (D.6), all p_i dependence can be eliminated, leaving

$$\frac{\partial p^*}{\partial x_i} = -p^* \frac{\rho_x^i}{\int \rho_x^i dx_i} = -\frac{p^* \rho_x^i}{\Upsilon_x}, -\frac{2p^* \rho_x^i}{\Upsilon_x} \tag{D.12}$$

where the second solution can be obtained integrating by parts, and, in the case of a Gaussian initial distribution, the placeholder in the denominator is defined as

$$\Upsilon_x \equiv \frac{1}{2} \operatorname{erf}\left(\frac{\sqrt{2} x_i}{2\sigma_x}\right) \tag{D.13}$$

[†]This is done by selecting

$$\begin{aligned} \frac{\partial x^*}{\partial p_i} &= \frac{\partial}{\partial p_i}\left(\frac{\int \rho_x^i dx_i}{\rho_x^*}\right) = 0 \\ \frac{\partial p^*}{\partial p_i} = \frac{\partial}{\partial p_i}\left(\frac{\int \rho_p^i dp_i}{\rho_p^*}\right) &= \frac{\partial}{\partial p_i}\left(\frac{\int \rho_x^i dx_i}{\rho_p^*}\right) = 0 \end{aligned} \tag{D.10}$$

Thus, in contrast with Eq. (D.4), we have an expression where $\frac{\partial p}{\partial x}$ is no longer constant.

We now check the following approximation:

$$p^* \approx -2\sinh\left(\frac{\rho_x^i}{\Upsilon_x}x_i\right)\mathcal{D} \tag{D.14}$$

Where we normalize $\mathcal{D}$ using Eq. (D.4); setting to $p^* \approx -p_i$ near $|x_i| = 0$, leaving

$$p^* \approx 2\sinh\left(\frac{\rho_x^i}{\Upsilon_x}x_i\right)x_i\frac{\sigma_p}{\sigma_x} \tag{D.15}$$

which can be shown numerically to agree with Eq. (D.12) for $|x_i| \lesssim 6\,\sigma_x$.

At this point, the updated particle postition x_L can be calculated using our covariant approach, such that

$$\mathcal{P}^\alpha = \gamma mc + p^* + \frac{q}{c}A^\alpha \tag{D.16}$$

which, being independent of p_i, will be explicit for any potential when used in a symplectic integrator.

For brevity, the following results use the noncovariant exponential Lie-operator tracking (see Eq. (1.55):[24]

$$x_L(x_i, p^*) = \{\exp[\,-t : H(x_i, p_i) :]\, x_i\}|_{p_i \to p^*} \tag{D.17}$$

where t is elapsed time in the lab frame and the paraxial Hamiltonian for a normal multipole magnet in the transverse plane is

$$H = \frac{e}{p}\frac{k \cdot \mathfrak{Re}(x_i + iy_i)^n}{r_0^{n-1}\ n!} + \frac{(p_i)^2}{2m} \tag{D.18}$$

Here, e, p, m, and r_0 are the fundamental charge, reference longitudinal momentum, particle mass, and magnet-pole radius, respectively; $n = 3, 4, 5...$ for sextupoles, octupoles, decapoles, etc; and k (in SI units) is in Teslas.[†]

In the following analysis, longitudinal momentum is normalized to 1 GeV/c and r_0 is set to 20 mm unless otherwise noted.

[24] Dragt, *Lie Methods for Nonlinear Dynamics with Applications to Accelerator Physics*.

[†] We use Wolski's scaling convention here, where momentum p_i is also scaled by a cofactor of $\frac{q}{p}$, such that the Hamiltonian in Eq. (D.18) is unitless.

In implementing Eq. (D.17), H must be calculated symbolically first for each element. Then, $p^*(x_i)$ and x_i are substituted in at each step, reducing the bivariate $x_L(x_i, p_i)$ to a monovariate $x_L(x_i, \sigma_x, \sigma_p)$, where σ_x and σ_p remain constant for a given timestep.

Although an analogous $x^*(p_i)$ can be derived, it is not useful in practice. Specifically, in calculating Eq. (D.18) in 2D for position and momentum – $x_L(x_i, y_i, p_x^*, p_y^*)$ and $p_{xL}(x^*, y^*, p_{x0}, p_{y0})$ – the resulting x_L expression is dependent on σ_x and σ_{px}, while p_L is dependent on σ_x, σ_y, σ_{px}, and σ_{py}, rendering it computationally inefficient. Other schema involving alternate forms such as $p_L(x_i, p^*)$ have been checked, but the following is found to be most stable, with notable performance gains:

$$\begin{aligned} x_1, y_1, p_{x1}, p_{y1} \quad &\rightarrow \quad x_L(x_i, y_i, p_x^*, p_y^*), y_L(x_i, y_i, p_x^*, p_y^*) \\ &\qquad\quad p_{xL}(x_i, y_i, p_{xi}, p_{xi}), p_{yL}(x_i, y_i, p_{xi}, p_{yi}) \\ &\qquad\quad \downarrow \\ x_2, y_2, p_{x2}, p_{y2} \quad &\rightarrow \quad x_D(x_1, y_1, p_{x1}, p_{y1}), y_D(x_1, y_1, p_{x1}, p_{y1}) \\ &\qquad\quad p_{xD}(x_1, y_1, p_{x1}, p_{y1}), p_{yD}(x_1, y_1, p_{x1}, p_{y1}) \end{aligned} \tag{D.19}$$

where the D subscript denotes a drift space of at least five times the kick length. This effectively limits the technique to a thin-lens approximation. Such drift spaces can be reserved for incorporating space-charge effects, leading to a comparable number of calculation steps using Eq. (D.19) versus a standard nonlinear beam-physics code.

Figure D.1 compares the accuracy of multiparticle transformations following Eq. (D.19) with and without using p^*. Also shown are a baseline with $p^* = 0$ and a "naive" approximation, where $p^* \approx p_i$ from Eq. (D.4) is used in the low $|x_i|$ limit of Eq. (D.15):

$$p^* \approx -x_i \frac{\sigma_p}{\sigma_x} \tag{D.20}$$

To emphasize visible discrepancies, the results shown have their σ values updated after each timestep by taking a new standard deviation. However, if mean absolute deviations are taken instead, an improved matching with the baseline can be observed.

Both the naive and null-momentum approximations fail at $\sigma_p \gtrsim \sigma_x$. Figure D.2 illustrates such a case for 2D Gaussian proton distributions with a kinetic energy of 8 GeV passing through an octupole magnet. For this case, beam parameters were derived relativistically from Twiss parameters and B_0 by normalizing the

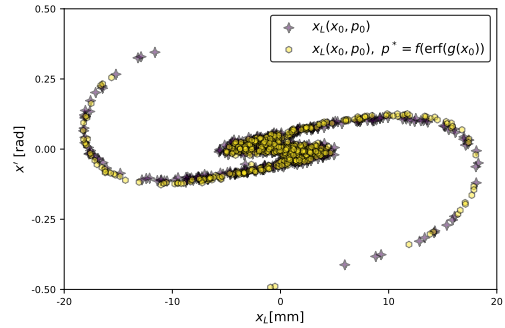

(a) Error-function Approximation

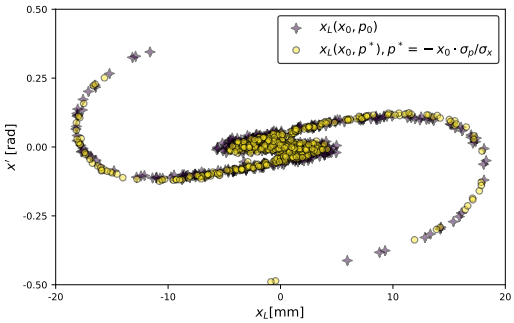

(b) Naive Approximation

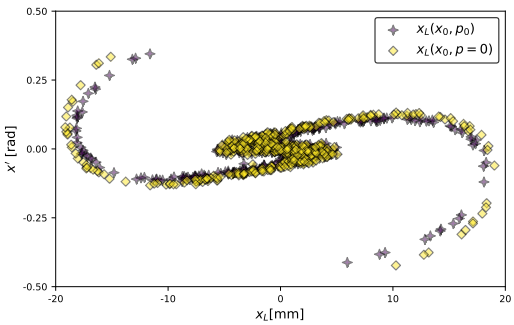

(c) Null-momentum Approximation

Figure D.1: Iterated use of Eq. (D.15) versus standard Lie transport results in 1D phase-space for 100,000 protons with initial Gaussian distributions of $\sigma_x = 10$ mm, $\sigma_p = 0.01$ rad (a). Also shown are two alternate p^* approximations: $p^* = x_i \frac{\sigma_p}{\sigma_x}$ in (b) and $p^* = 0$ in (c). The transport map consists of 200 octupole–drift sections: $B_0 = 10$ [T] (As earlier, this strength is exaggerated to visualize the tails of the distribution), $L_{oct} = 0.1$ [mm], $L_{drift} = 1.0$ [mm]. Lie transforms are truncated to fifth order.

kinetic term in Eq. (D.18) to the beam's average kinetic energy then verified against Tracewin.

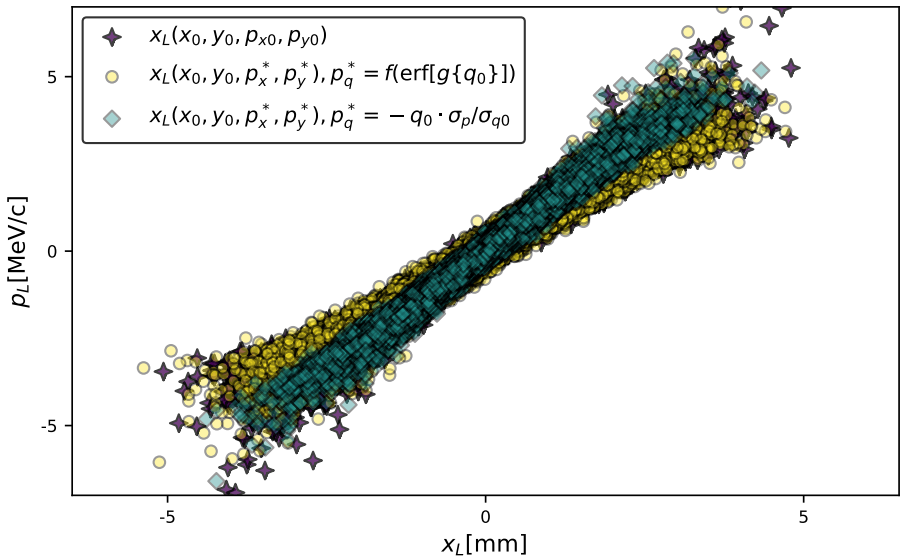

Figure D.2: Iterated octupole transforms for 2D Gaussian bunches of 100,000 protons at 8 GeV: $r_0 = 15$ [mm], $\epsilon_\perp = 0.25$ [$\pi \cdot$ mm $\cdot$ mrad], $\beta_\perp = 1$ [mm/($\pi \cdot$ mrad)]. The map consists of 400 kick–drift sections: $B_0 = 12$ T, $L_{oct} = 0.2$ [mm], $\mathrm{L_{drift}} = 2$ [mm], for an integrated field strength of 0.211 [T/m^2].

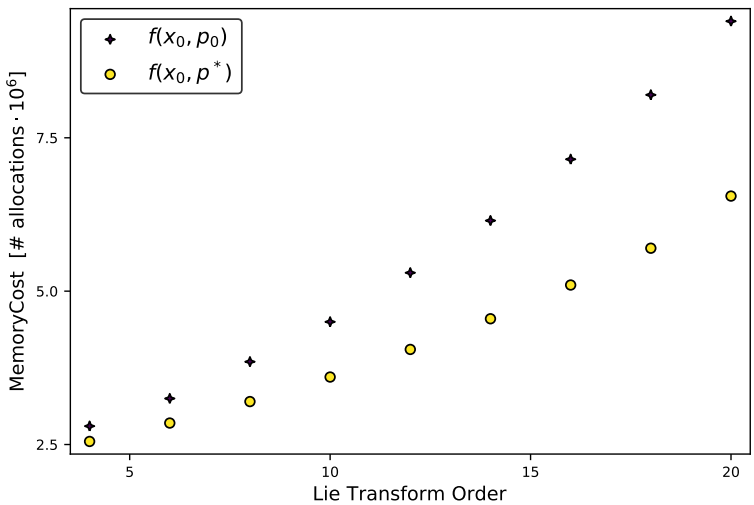

Figure D.3: Raw memory-allocation cost for multiparticle simulations with k and L parameters matching those of Fig. D.1. Number of particles: 10,000. Number of simulated segments: 5.

For the non-null p^* approximations, performance improves with increasing particle count, with increasing magnetic pole count, and particularly with increased order of Lie-transform series truncation (Fig. D.3). Since trajectory variations

are negligible beyond a 6th-order truncation in most cases, the average reduction in CPU overhead using Eq. (D.15) is roughly 15%.

Similar results were obtained for sextupoles, decapoles, and high-order magnets, as well as with waterbag distributions, despite the assumption of a Gaussian shape in deriving Eq. (D.15). At low energies (or specifically, any low $\frac{\sigma_p}{\sigma_x}$ ratio), all three approximations tested have essentially identical results, with performance improving in ascending order for $p^* = (f[\mathrm{erf}])$; $p^* = -x_i \cdot \sigma_p/\sigma_x$; and $p^* = 0$.

For all the approximations tested, trajectories only became unstable in cases where the momentum values exceeded $\sim 100\,\sigma_p$. This leaves only the necessarily large drift–kick ratio requirement as the major limitation of this method.

References

Dragt, A. J. *Lie Methods for Nonlinear Dynamics with Applications to Accelerator Physics*. College Park, MD, USA: University of Maryland, Forthcoming, 2019. URL: https://www.physics.umd.edu/dsat/dsatliemethods.html.

Folsom, B. and E. Laface. "Approximating nonlinear forces with phase-space decoupling". In: *Proc. of International Particle Accelerator Conference (IPAC'17), Copenhagen, Denmark, 14–19 May, 2017*. (Copenhagen, Denmark). International Particle Accelerator Conference 8. 10.18429/JACoW-IPAC2017-WEPIK084. Geneva, Switzerland: JACoW, 2017, pp. 3120–3123. ISBN: 978-3-95450-182-3. DOI: doi.org/10.18429/JACoW-IPAC2017-WEPIK084.

— "Fast tracking of nonlinear dynamics in the ESS linac simulator via particle-count invariance". In: *Proc. of International Particle Accelerator Conference (IPAC'16), Busan, Korea, May 8-13, 2016*. (Busan, Korea). International Particle Accelerator Conference 7. Geneva, Switzerland: JACoW, 2016, pp. 3080–3082. DOI: doi:10.18429/JACoW-IPAC2016-WEPOY041.

Meot, F and T Aniel. "Principles of the non-linear tuning of beam expanders". In: *Nuclear Instruments and Methods in Physics Research Section A: Accelerators, Spectrometers, Detectors and Associated Equipment* 379.2 (1996), pp. 196–205. DOI: 10.1016/0168-9002(96)00539-6.

Yuri, Y. et al. "Uniformization of the transverse beam profile by means of nonlinear focusing method". In: *Physical Review Special Topics-Accelerators and Beams* 10.10 (2007), p. 104001. DOI: 10.1103/PhysRevSTAB.10.104001.